



---

# Validation of Asphalt Mixture Pavement Skid Prediction Model and Development of Skid Prediction Model for Surface Treatments

Technical Report 0-6746-01-1

---

Cooperative Research Program

TEXAS A&M TRANSPORTATION INSTITUTE  
COLLEGE STATION, TEXAS

in cooperation with the  
Federal Highway Administration and the  
Texas Department of Transportation  
<http://tti.tamu.edu/documents/0-6746-01-1.pdf>



1. Report No. FHWA/TX-17/0-6746-01-1		2. Government Accession No.		3. Recipient's Catalog No.	
4. Title and Subtitle VALIDATION OF ASPHALT MIXTURE PAVEMENT SKID PREDICTION MODEL AND DEVELOPMENT OF SKID PREDICTION MODEL FOR SURFACE TREATMENTS				5. Report Date Published: April 2017	
				6. Performing Organization Code	
7. Author(s) Arif Chowdhury, Emad Kassem, Sand Aldagari, and Eyad Masad				8. Performing Organization Report No. Report 0-6746-01-1	
9. Performing Organization Name and Address Texas A&M Transportation Institute The Texas A&M University System College Station, Texas 77843-3135				10. Work Unit No. (TRAIS)	
				11. Contract or Grant No. Project 0-6746	
12. Sponsoring Agency Name and Address Texas Department of Transportation Research and Technology Implementation Office 125 E. 11 <sup>th</sup> Street Austin, Texas 78701-2483				13. Type of Report and Period Covered Technical Report: November 2012–December 2016	
				14. Sponsoring Agency Code	
15. Supplementary Notes Project performed in cooperation with the Texas Department of Transportation and the Federal Highway Administration. Project Title: Validation of TxDOT Flexible Pavement Skid Prediction Model URL: <a href="http://tti.tamu.edu/documents/0-6746-01-1.pdf">http://tti.tamu.edu/documents/0-6746-01-1.pdf</a>					
16. Abstract <p>Pavement skid resistance is primarily a function of the surface texture, which includes both microtexture and macrotexture. Earlier, under the Texas Department of Transportation (TxDOT) Research Project 0-5627, the researchers developed a method to predict asphalt pavement skid resistance based on inputs including aggregate texture before and after polishing, gradation of asphalt mixture, and traffic levels. In this study, the researchers validated and revised the skid prediction model for asphalt pavements and developed a skid prediction model for seal coat surfaces. The researchers investigated and examined the surface friction characteristics of 70 test sections of asphalt mixtures and surface-treated roads in Texas. The test sections covered a wide range of mixtures and aggregate types. The researchers measured pavement macrotexture and microtexture of these sections and revised the traffic calculation. Historical skid numbers were obtained from TxDOT's Pavement Management Information System database and measured using a skid trailer. Aggregate texture and angularity was quantified using the aggregate image measurement system.</p> <p>Statistical methods were used to develop a prediction model for skid numbers, and the predicted values were compared to the measured ones in the field. The revised model describes the skid resistance of asphalt pavements as a function of aggregate characteristics, mixture gradation, and traffic level. The researchers incorporated aggregate angularity as an additional parameter in the model. Similarly, the researchers developed a skid prediction model for seal coat surfaces using the same parameters. A Microsoft Access–based Visual Basic desktop application was developed to automatically calculate the predicted skid numbers by incorporating the skid prediction models. Using this standalone application, one can input the basic aggregate characteristics and traffic data to predict the pavement's skid resistance during its service life.</p>					
17. Key Words Skid Resistance, Asphalt Mixture, Surface Treatment, Aggregate Texture, Aggregate Angularity			18. Distribution Statement No restrictions. This document is available to the public through NTIS: National Technical Information Service Alexandria, Virginia, <a href="http://www.ntis.gov">http://www.ntis.gov</a>		
19. Security Classif. (of this report) Unclassified		20. Security Classif. (of this page) Unclassified		21. No. of Pages 168	22. Price



**VALIDATION OF ASPHALT MIXTURE PAVEMENT SKID  
PREDICTION MODEL AND DEVELOPMENT OF SKID PREDICTION  
MODEL FOR SURFACE TREATMENTS**

by

Arif Chowdhury, DoE, P.E.  
Assistant Research Engineer  
Texas A&M Transportation Institute

Emad Kassem, PhD  
Assistant Professor  
Department of Civil Engineering  
University of Idaho

Sand Aldagri  
Graduate Student  
Department of Civil Engineering  
University of Idaho

and

Eyad Masad, PhD, P.E.  
Professor  
Zachry Department of Civil Engineering  
Texas A&M University

Report 0-6746-01-1

Project 0-6746

Project Title: Validation of TxDOT Flexible Pavement Skid Prediction Model

Performed in cooperation with the  
Texas Department of Transportation  
and the  
Federal Highway Administration

Published: April 2017

TEXAS A&M TRANSPORTATION INSTITUTE  
College Station, Texas 77843-3135



## **DISCLAIMER**

This research was performed in cooperation with the Texas Department of Transportation (TxDOT) and the Federal Highway Administration (FHWA). The contents of this report reflect the views of the authors, who are responsible for the facts and the accuracy of the data presented herein. The contents do not necessarily reflect the official view or policies of FHWA or TxDOT. This report does not constitute a standard, specification, or regulation. This report is not intended for construction, bidding, or permit purposes. The engineer in charge of the project was Arif Chowdhury, P.E. #90891.

## **ACKNOWLEDGMENTS**

This project was conducted in cooperation with TxDOT and FHWA. Many personnel made possible the coordination and accomplishment of the work presented herein. Ms. Caroline Heinen, P.E., was the project director for this research project. Mr. Edward Morgan and Mr. Phillip Hemphill were members of the Project Monitoring Committee (PMC). Mr. Kevin Pete was the project manager. The authors are thankful to the PMC members for their guidance and directions. Numerous engineers, laboratory supervisors, and inspectors at the TxDOT districts and Pavement Division assisted by providing information, traffic control, and material samples, and by helping in some field testing. Without their cordial cooperation, it would not have been possible to complete this project. The authors are thankful to Mohamad Al-Assi, a graduate student of the University of Idaho, for helping in analyses; to Jerry Le of the Texas A&M Transportation Institute (TTI) for his contribution in developing the skid prediction software application; and to Mr. Tom Freeman of TTI for assisting with obtaining historical skid data from TxDOT's Pavement Management Information System database.



# TABLE OF CONTENTS

	<b>Page</b>
<b>List of Figures</b> .....	<b>ix</b>
<b>List of Tables</b> .....	<b>xii</b>
<b>Chapter 1: Introduction</b> .....	<b>1</b>
Background.....	1
Problem Statement .....	2
Objectives .....	3
Research Tasks .....	3
Task 1: Conduct Literature Search.....	3
Task 2: Design Experiment and Select Field Test Sections .....	3
Task 3: Conduct Field and Laboratory Testing .....	4
Task 4: Refine and Validate Skid Prediction Model for HMA.....	4
Task 5: Develop a Skid Prediction Model for Seal Coat Surfaces .....	4
Task 6: Modify Desktop Application for Skid Prediction .....	5
Task 7: Document Findings .....	5
Report Organization.....	5
<b>Chapter 2: Literature Review</b> .....	<b>7</b>
Introduction.....	7
Definition of Skid Resistance .....	7
Pavement Surface Characteristics.....	8
Effects of Pavement Surface Characteristics on Skid Resistance.....	10
Asphalt Seal Coat Treatment .....	11
Aggregate Properties Affecting Pavement Friction.....	12
Hardness and Mineralogy .....	12
Polish Resistance .....	12
Abrasion Resistance.....	13
Angularity, Texture, and Form .....	13
Soundness .....	14
Friction/Skid Resistance Measuring Devices .....	14
Locked-Wheel Skid Trailer.....	14
Side Force Devices .....	15
Fixed Slip Devices .....	16
Variable Slip Devices .....	16
Dynamic Friction Tester .....	17
The International Friction Index .....	17
Pavement Texture Measurements.....	18
CTMeter Device.....	18
Sand Patch Method .....	19
Stereo Photogrammetric Technique.....	20
Aggregate Resistance to Polishing .....	21
Effect of Pavement Deterioration on Skid Resistance.....	22
Developing Skid Resistance Models .....	22
Masad et al.'s (2007) Model .....	22
Masad et al.'s (2010) Model .....	25

Wu et al.'s (2012) Model .....	29
Kassem et al.'s (2013) Model .....	30
Summary .....	33
<b>Chapter 3: Testing and Data Collection .....</b>	<b>35</b>
Selection of the Field Sections.....	35
Measurements of Friction Characteristics .....	39
Aggregate Characterization .....	46
Aggregate Gradation Parameters .....	49
Skid Number Measurements.....	49
Data Collection .....	51
Skid from PMIS .....	51
Construction Data .....	52
Traffic Data.....	52
Summary .....	53
<b>Chapter 4: Data Analysis and Results for Hot Mix Asphalt Test Sections .....</b>	<b>55</b>
Analysis of Aggregate Gradation .....	55
Analysis of Aggregate Texture and Angularity .....	57
Development of Predictive Model for IFI .....	64
Analysis of Mean Profile Depth .....	66
Skid Number Analysis.....	67
HMA Skid Resistance Model Sensitivity Analysis .....	69
Effect of Mixture Gradation.....	69
Effect of Traffic Level .....	70
Effect of Aggregate Type.....	71
Summary .....	72
<b>Chapter 5: Data Analysis and Results for Seal Coat Test Sections.....</b>	<b>73</b>
Analysis of Aggregate Gradation .....	73
Analysis of Aggregate Texture and Angularity .....	74
Development Predictive Model for IFI for Seal Coat.....	79
Analysis of Mean Profile Depth .....	81
Skid Number Analysis .....	82
Seal Coat Skid Resistance Model Sensitivity Analysis .....	84
Effect of Seal Coat Size .....	84
Effect of Traffic Level .....	85
Effect of Aggregate Type.....	86
Summary .....	87
<b>Chapter 6: A System for Predicting Skid Number Using Desktop Application .....</b>	<b>89</b>
Aggregate Classification System Based on Proposed Model.....	103
<b>Chapter 7: Conclusions and Recommendations .....</b>	<b>107</b>
Conclusions.....	107
Recommendations.....	108
<b>References.....</b>	<b>111</b>
<b>Appendix A: Asphalt Mixture Test Section Results .....</b>	<b>117</b>
<b>Appendix B: Seal Coat Test Section Results .....</b>	<b>129</b>
<b>Appendix C: SAAP Flow Chart for Asphalt Mixture .....</b>	<b>139</b>
<b>Appendix D: SAAP Flow Chart for Surface Treatment .....</b>	<b>147</b>

## LIST OF FIGURES

	<b>Page</b>
Figure 1. Friction Force and Surface Characteristics (Noyce et al. 2005).....	7
Figure 2. Schematic of Microtexture and Macrottexture (Henry 2000). ....	9
Figure 3. Key Mechanisms of Tire-Pavement Friction (Hall et al. 2009). ....	10
Figure 4. Change in Pavement Friction with Speed (after Hogervorst 1974). ....	11
Figure 5. Effect of Microtexture/Macrottexture on Pavement Friction (Hall et al. 2006).....	11
Figure 6. AIMS Aggregate Shape Characteristics.....	13
Figure 7. Locked-Wheel Skid Trailer. ....	15
Figure 8. Side Force Device (Hall et al. 2009). ....	15
Figure 9. Fixed Slip Device (Putov et al. 2016). ....	16
Figure 10. Variable Slip Friction Testing Device (Putov et al. 2016). ....	17
Figure 11. Dynamic Friction Tester.....	17
Figure 12. CTMeter Device. ....	19
Figure 13. Sand Patch Method (Sarsam et al. 2015).....	20
Figure 14. 3D Pavement Surface from Stereo Photogrammetric Technique (Mustaffar et al. 2004). ....	21
Figure 15. AIMS Texture Index versus Time in the Micro-Deval Test for (A) Texture Level 4, (B) Texture Level 5, and (C) Texture Level 6. ....	23
Figure 16. Laboratory Experiments in the TxDOT (Masad et al. 2010). ....	26
Figure 17. Aggregate Texture before and after Micro-Deval and Percent Change (Masad et al. 2010). ....	26
Figure 18. An Example of IFI vs. Polishing Cycles (Kassem et al. 2013). ....	27
Figure 19. Steps Needed to Predict Skid Number SAAP in TxDOT Project No. 0-5627.....	29
Figure 20. Test Slabs Preparation and Polishing (Kassem et al. 2013). ....	31
Figure 21. Texture Index and Weight Loss Results (Kassem et al. 2013).....	31
Figure 22. AIMS System (Kassem et al. 2013). ....	32
Figure 23. Texture Index and Weight Loss Results (Kassem et al. 2013).....	33
Figure 24. Layout of Measurement Section.....	40
Figure 25. Collecting Field Measurements. ....	40
Figure 26. DFT Measurements for Seal Coat Test Section (IH-35-LRD-NP-COT-S_SealCoat).....	41
Figure 27. DFT Measurements for Type D Asphalt Mix Test Section (SH-36-HMA_TypeD).....	41
Figure 28. Correlation between MPD and Coefficient of Friction at 80 km/h (DFT <sub>80</sub> ) for Seal Coat Test Sections. ....	42
Figure 29. Correlation between IFI and Coefficient of Friction at 80 km/h (DFT <sub>80</sub> ) for Seal Coat Test Sections. ....	43
Figure 30. Correlation between MPD and Coefficient of Friction at 80 km/h (DFT <sub>80</sub> ) for Hot Mix Asphalt Test Sections. ....	43
Figure 31. Correlation between IFI and DFT <sub>80</sub> for Hot Mix Asphalt Test Sections. ....	44
Figure 32. Correlation between IFI and DFT <sub>80</sub> for Hot Mix Asphalt and Seal Coat Test Sections and Pavement Surface Condition for Seal Coat Test Sections.....	45

Figure 33. Correlation between IFI and DFT <sub>80</sub> for Hot Mix Asphalt and Seal Coat Test Sections and Pavement Surface Condition for Asphalt Mixture Test Sections.....	46
Figure 34. Procedure for Measuring Aggregate Texture and Its Resistance to Polishing.....	48
Figure 35. Loss in Aggregate Texture and Angularity as a Result of Micro-Deval Abrasion and Polishing of Virgin Aggregates.....	49
Figure 36. Locked-Wheel Skid Trailer.....	51
Figure 37. Flow Chart of the Research Methodology.....	56
Figure 38. Weibull Distribution Function for Different Aggregate Sizes.....	56
Figure 39. Texture Indices of Sections in San Antonio.....	59
Figure 40. Angularity Indices of Sections in San Antonio.....	59
Figure 41. Regression Constants for Aggregate Texture.....	60
Figure 42. Regression Constants for Aggregate Angularity.....	60
Figure 43. Relationship between Predicted and Measured IFI.....	66
Figure 44. Relationship between Measured and Calculated MPD Values.....	67
Figure 45. Relationship between the Measured and Predicted SN.....	68
Figure 46. Measured Skid Numbers in Terms of Traffic Level.....	69
Figure 47. Effect of Mixture Gradation on the Skid Number.....	70
Figure 48. Effect of AADT on the Skid Number.....	71
Figure 49. Effect of Aggregate Texture on the Skid Number.....	72
Figure 50. Weibull Distribution Function for Different Aggregate Sizes.....	74
Figure 51. Texture Indices of Sections in Odessa.....	75
Figure 52. Angularity Indices of Sections in Odessa.....	76
Figure 53. Regression Constants for Aggregate Texture.....	76
Figure 54. Regression Constants for Aggregate Angularity.....	77
Figure 55. Relationship between Predicted and Measured IFI.....	81
Figure 56. Relationship between Measured and Calculated MPD Values.....	82
Figure 57. Relationship between Measured and Predicted SN.....	83
Figure 58. Measured Skid Numbers at Different Traffic Level.....	84
Figure 59. Effect of Seal Coat Aggregate Size on the Skid Number.....	85
Figure 60. Effect of AADT on the Skid Number.....	86
Figure 61. Effect of Aggregate Texture on the Skid Number.....	87
Figure 62. Initial Window of the Program.....	90
Figure 63. Project Name Input.....	90
Figure 64. Pavement Surface Type Input.....	91
Figure 65. Choice of Mixture Type.....	91
Figure 66. Manual Aggregate Gradation Input.....	92
Figure 67. Selection of AIMS Test Data Points.....	93
Figure 68. Aggregate Texture Input for Two Data Points.....	93
Figure 69. Aggregate Texture Input for Three Data Points.....	94
Figure 70. Aggregate Angularity Input for Two Data Points.....	94
Figure 71. Aggregate Angularity Input for Three Data Points.....	95
Figure 72. Mean Profile Depth Input.....	96
Figure 73. Highway Type and Traffic Data Input.....	97
Figure 74. Output Data Display Options.....	98
Figure 75. Skid Prediction Chart for 15 Years.....	99
Figure 76. Selection of Thresholds or Aggregate Classification.....	100

Figure 77. Sample Aggregate Classification Based on Skid Performance.....	101
Figure 78. Saving Input and Output Spreadsheet Files.....	102
Figure 79. Sample Input Spreadsheet. ....	102
Figure 80. Sample Output Spreadsheet.....	103

## LIST OF TABLES

	<b>Page</b>
Table 1. Classification of Pavement Texture (Henry 2000). .....	8
Table 2. Aggregate Texture Regression Coefficients. ....	24
Table 3. HMA Test Sections. ....	36
Table 4. Selected Sections for Seal Coat. ....	38
Table 5. Aggregate Classification Based on the SN. ....	50
Table 6. Scale and Shape Parameters of the Weibull Distribution. ....	58
Table 7. Regression Parameters of Aggregate Texture and Angularity. ....	63
Table 8. Traffic Groups Based on TMF. ....	69
Table 9. Scale and Shape Parameters of the Weibull Distribution. ....	73
Table 10. Regression Parameters of Aggregate Texture and Angularity. ....	79
Table 11. Traffic Groups Based on TMF. ....	84
Table 12. Skid Number Threshold Values after Five Years of Service. ....	104
Table 13. Aggregate Classification for Different Roads. ....	105
Table 14. Combined Mixture Gradation. ....	117
Table 15. Combined Mixture Gradation (Former Sieve Sizes) .....	118
Table 16. Aggregate Texture and Angularity Data. ....	118
Table 17. Traffic Data. ....	119
Table 18. Beaumont CTMeter Data. ....	120
Table 19. Odessa CTMeter Data. ....	120
Table 20. Atlanta CTMeter Data. ....	120
Table 21. Pharr and San Antonio CTMeter Data. ....	121
Table 22. Laredo CTMeter Data. ....	121
Table 23. Lufkin, Houston, and YKM CTMeter Data. ....	122
Table 24. Austin CTMeter Data. ....	122
Table 25. Bryan CTMeter Data. ....	123
Table 26. Beaumont DFT Data. ....	123
Table 27. Odessa DFT Data. ....	124
Table 28. Atlanta DFT Data. ....	124
Table 29. Pharr and San Antonio DFT Data. ....	125
Table 30. Laredo DFT Data. ....	125
Table 31. Lufkin, Houston, and YKM DFT Data. ....	126
Table 32. Austin DFT Data. ....	126
Table 33. Bryan DFT Data. ....	127
Table 34. Aggregate Gradation (Cumulative Percent Retained). ....	129
Table 35. Aggregate Texture and Angularity Data. ....	130
Table 36. Traffic Data. ....	131
Table 37. Beaumont and Odessa CTMeter Data. ....	132
Table 38. Atlanta CTMeter Data. ....	132
Table 39. Pharr CTMeter Data. ....	133
Table 40. San Antonio CTMeter Data. ....	133
Table 41. YKM and Brownwood CTMeter Data. ....	134
Table 42. Dallas-FW CTMeter Data. ....	134

Table 43. Lufkin CTMeter Data. ....	135
Table 44. Beaumont and Odessa DFT Data.....	135
Table 45. Atlanta DFT Data.....	136
Table 46. Pharr DFT Data.....	136
Table 47. San Antonio DFT Data. ....	137
Table 48. YKM and Brownwood DFT Data. ....	137
Table 49. Fort Worth DFT Data. ....	138
Table 50. Lufkin DFT Data. ....	138





# CHAPTER 1: INTRODUCTION

## BACKGROUND

Traffic-related accidents are detrimental to the U.S. economy. The National Highway Traffic Safety Administration (NHTSA 2014) indicated that the total cost due to traffic crashes in 2014 was estimated at \$242 billion. Traffic-related accidents occur due to three major factors—road conditions, driver behavior, and vehicle factors (Noyce et al. 2005). In 2014, more than 6 million traffic collisions occurred in the United States, and the number of fatalities was 32,675, in addition to 2.338 million traffic-related injuries (NHTSA 2014). Previous research showed that 15 to 18 percent of total crashes occurred on wet pavements (Smith 1977; Federal Highway Administration [FHWA] 1990). The crashes on wet pavements are related to inadequate pavement skid resistance, which causes vehicles to skid. Henry and Wambold (1992) found a good correlation between skid numbers and wet-pavement crashes when tested with smooth tires. The number of wet-pavement accidents can be greatly reduced by conducting frequent skid measurements in order to ensure an adequate level of skid resistance of pavements (Rizenbergs et al. 1972).

The friction between pavement surface and vehicle tires is related to the macrotexture and microtexture of pavement surface. The macrotexture of asphalt pavement is dependent on aggregate gradation, while the microtexture is dependent on aggregate shape characteristics (Masad et al. 2010; Kassem et al. 2012, 2013). Aggregates with angular shape and rough texture provide a higher level of skid resistance compared to aggregates with a smooth surface (Kassem et al. 2012, 2013). In addition, pavement surfaces with high macrotexture provide higher skid resistance than do those with low macrotexture (Masad et al. 2010; Kassem et al. 2012, 2013).

Henry (1986) studied the effect of vehicle speed on pavement friction. The results showed that skid resistance decreases with speed. Aggregates are polished with frequent traffic applications. Some aggregates become smoother than others, resulting in low skid resistance. Shafii (2009) discussed the effect of rubber temperature on skid resistance of asphalt pavement. The results showed that the skid resistance decreases as the temperature of the rubber increases. Other factors that affect skid resistance include pavement surface grooving and bleeding. The

skid resistance decreases with the bleeding of asphalt binders on the surface (Sullivan 2005), while it is improved with surface grooving (Pasindu et al. 2010).

There are several studies that attempted to develop prediction models for skid resistance of asphalt pavements. Ahammed and Tighe (2007) developed procedures to estimate skid resistance of concrete pavements as a function of concrete compressive strength, traffic level, and pavement texture. Kowalski (2007) developed a laboratory testing procedure to characterize pavement friction by determining the polishing rate and terminal friction value. Researchers at the Texas A&M Transportation Institute (TTI) developed prediction models for skid resistance of asphalt pavement (Masad et al. 2010; Kassem et al. 2012, 2013). These models describe the skid resistance of asphalt pavements as a function of aggregate characteristics, mixture gradation, and traffic levels.

## **PROBLEM STATEMENT**

Pavement skid resistance is primarily a function of the surface texture, which includes both microtexture and macrotexture. Macrotexture is an overall asphalt mixture characteristic that provides surface drainage paths for water to drain from the contact area between the tire and pavement. Microtexture is primarily an aggregate surface characteristic that provides a rough surface, which in turn disrupts the continuity of the water film and produces frictional resistance between the tire and pavement by creating intermolecular bonds. In the Texas Department of Transportation (TxDOT) Research Project 0-5627, researchers (Masad et al. 2010) developed a method to predict asphalt pavement skid resistance based on inputs including aggregate texture before and after polishing, gradation of asphalt mixture, and traffic levels. Although the 0-5627 research team conducted extensive field testing on hot mix asphalt (HMA) surfaces, the evaluation of surface-treatment skid resistance was limited to the analyses of corresponding data from the Pavement Management Information System (PMIS) database. There is need for further testing so that the HMA asphalt prediction model can be tailored to the skid prediction model of surface treatment so that the skid prediction model can be validated at a wide variety of conditions and for more asphalt mixture types.

TxDOT sponsored a follow-up study, Research Project 0-6746, for TTI to further investigate the results from the previous research study, Research Project 0-5627. There was also

a need for revising the traffic model to incorporate the effect of truck traffic and lane distribution of traffic at different highway configurations.

## **OBJECTIVES**

The objectives of this study were to:

1. Investigate and examine surface and friction characteristics of about 35 test sections of asphalt mixtures and 35 test sections of surface-treated roads in Texas. The test sections covered a wide range of mixtures and aggregate types used in Texas.
2. Validate and revise the skid prediction model for HMA; develop a prediction model for skid resistance of seal coat surfaces; and incorporate an improved method of traffic analysis, lane distribution of traffic data, and the effect of the percentage of truck traffic.

## **RESEARCH TASKS**

The above objectives were achieved by conducting the following tasks.

### **Task 1: Conduct Literature Search**

A literature search was conducted to develop an up-to-date documentation of the following topics:

- Pavement surface characteristics that affect skid resistance.
- Methods used to measure macrotexture and microtexture of asphalt pavements.
- Test methods used to measure pavement friction.
- Methods used to measure aggregate resistance to abrasion and polishing.
- Attempts to predict friction or skid resistance of flexible pavements.

### **Task 2: Design Experiment and Select Field Test Sections**

The objective of Task 2 was to develop an experimental design to validate and revise the existing skid model for HMA pavements and expand the existing model or develop a new skid model for seal coat surfaces. Under this task, the researchers selected HMA and seal coat test sections for field testing. These test sections covered a wide range of asphalt mixture types, seal coat sizes, aggregate sources, traffic levels, and environmental conditions.

### **Task 3: Conduct Field and Laboratory Testing**

Under this task, the measurements of pavement macrotexture and microtexture were collected on the selected sections using the circular texture meter (CTMeter) and dynamic friction tester (DFT). Also, the skid number was measured using a skid trailer. In the laboratory, the aggregate texture and angularity was quantified at different time durations of polishing in the Micro-Deval test using the aggregate image measurement system (AIMS). Additionally, the information about the mix design of HMA and seal coat size was obtained. Seal coat slabs from three different highways were cut from the roadway and were subjected to polishing at the lab using a three-wheel polisher and taking periodic measurements of texture and friction.

### **Task 4: Refine and Validate Skid Prediction Model for HMA**

Under this task, the skid prediction model for HMA developed by Masad et al. (2010) was revised to accommodate a wide range of conditions. The skid prediction model describes the skid resistance of asphalt pavements as a function of aggregate characteristics, mixture gradation, and traffic level. The aggregate texture and angularity were quantified using AIMS, and parameters were developed to describe the resistance of aggregates to abrasion and polishing. Also, parameters were developed to describe aggregate gradation. Researchers used statistical methods to develop a prediction model for skid number, and the predicted values were compared to the measured ones in the field.

### **Task 5: Develop a Skid Prediction Model for Seal Coat Surfaces**

Under this task, researchers developed a skid prediction for seal coat surfaces. The skid resistance of seal coat depends on the same parameters as that of HMA, including aggregate size, aggregate shape characteristics (angularity and texture), and traffic level. Three seal coat grades (Grade 3, Grade 4, and Grade 5) were used and examined in the seal coat test sections. Each grade stands for a different aggregate size, with Grade 3 being the coarsest. As with HMA, researchers developed parameters to describe aggregate shape characteristics and its resistance to abrasion and polishing. In addition, analytical tools were used to describe the macrotexture of the seal coat test sections. Statistical methods were used to develop a prediction skid model for the skid number of seal coat, and the predicted skid values were compared to the measured ones in the field.

### **Task 6: Modify Desktop Application for Skid Prediction**

Under this task, a previously developed Excel-based macros tool called Skid Analysis of Asphalt Pavement (SAAP) was modified in order to (a) accommodate improved asphalt mix skid prediction model, (b) accommodate new seal coat prediction model, and (c) make the application more user friendly. SAAP was originally developed as an Excel-based macros tool. Researchers extracted some of the codes and wrote new codes in an Access-based application using Visual Basic Application (VBA) language. Using the inputs from the user, this standalone Windows-based application is capable of calculating the predicted skid numbers automatically. The output of the program, charts, and data will be presented to the user, and the user can print, save, or modify the information.

### **Task 7: Document Findings**

This task entailed the documentation of research efforts, results, and recommendations of this study.

## **REPORT ORGANIZATION**

Research efforts and outcomes are documented in seven chapters and four appendices of this report. Chapter 1 provides an introduction and background of the research project, including the problem statement and objectives, research tasks, and report organization. Chapter 2 provides a literature review on skid resistance, including factors affecting skid resistance, pavement frictional surface characteristics, test methods used to measure pavement friction, and previous attempts to predict friction or skid resistance of flexible pavements. Chapter 3 discusses the research plan and describes various tests conducted in the field and laboratory. Chapter 4 presents the model development of the skid resistance of HMA based on the collected data from the field and laboratory. Chapter 5 presents the model development of the skid resistance of seal coat surfaces. Chapter 6 documents the effort to automate the calculation of skid numbers using a desktop application. It also shows the step-by step procedures of how to use the software. Finally, Chapter 7 summarizes the main findings of this study and provides recommendations for future studies. Appendices document the laboratory and field test results and the flow charts used in the automated calculation of skid numbers for both surface types.



## CHAPTER 2: LITERATURE REVIEW

### INTRODUCTION

Skid resistance is a key component in road safety. Skid resistance depends on several factors, including pavement surface characteristics, tire material properties, and environmental conditions. Several laboratory and field methods are used to characterize the parameters that affect the skid resistance of asphalt pavements and determine the skid level in the field (Kennedy et al. 1990). These methods and parameters are discussed in this section.

### DEFINITION OF SKID RESISTANCE

Pavement friction is the force that resists the relative motion between a vehicle tire and a pavement surface. Skid resistance is an essential factor that prevents vehicles from sliding and reduces the stopping distance (Noyce et al. 2005). Figure 1 shows the friction force and the surface characteristics affecting skid resistance.

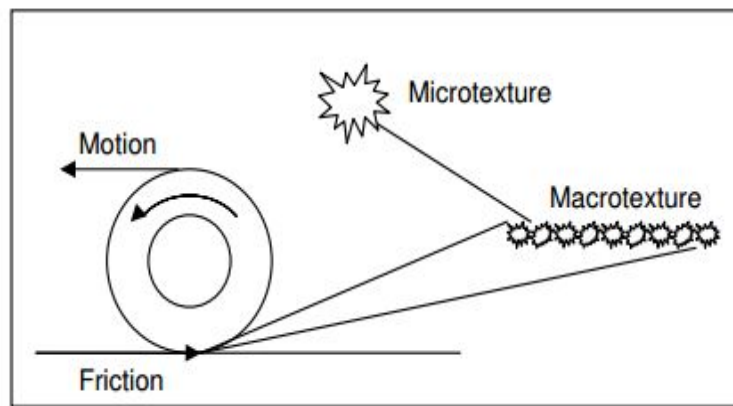


**Figure 1. Friction Force and Surface Characteristics (Noyce et al. 2005).**

Pavement skid resistance may slightly increase right after construction due to wearing of asphalt binders that coat the rocks at the pavement surface. Skid resistance decreases as the surface aggregates are polished under traffic. The polishing action affects the microtexture and macrotexture of pavement surface (Flintsch et al. 2005; Forster 1989).

## PAVEMENT SURFACE CHARACTERISTICS

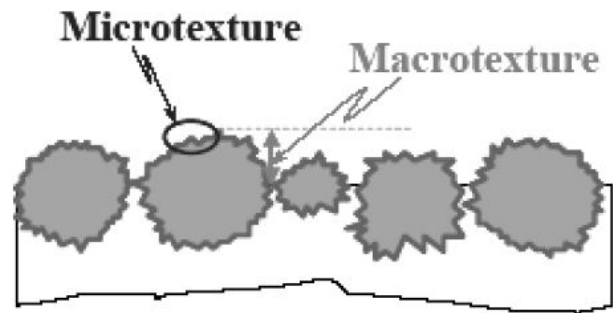
Pavement texture and its friction is a key component of road safety (Mahone 1975). The skid resistance of asphalt pavements is affected by the macrotexture and microtexture of the pavement surface. In wet conditions, water acts as a lubricant between the tires and pavement surface, leading to reduced friction (Dahir 1978). The macrotexture of pavement is dependent on aggregate gradation, compaction level, and mixture design, while the microtexture is dependent on aggregate shape characteristics (Crouch et al. 1995). The texture is a property related to the surface that describes the interaction between the tires and pavement surface (Henry 2000). Texture is classified into several categories based on its wavelength, as presented in Table 1.

**Table 1. Classification of Pavement Texture (Henry 2000).**

<b>Texture Classification</b>	<b>Relative Wavelength</b>
Microtexture	$\lambda < 0.5 \text{ mm}$
Macrotexture	$0.5 \text{ mm} < \lambda < 50 \text{ mm}$
Megatexture	$50 \text{ mm} < \lambda < 500 \text{ mm}$
Roughness/Smoothness	$500 \text{ mm} < \lambda < 50 \text{ m}$

Henry (2000) demonstrated the distinction between macrotexture and microtexture, as shown in Figure 2. Macrotexture describes the irregularities of pavement surface. It is important in assisting water drainage from a pavement's surface. In addition, it contributes to the hysteresis component of the friction (Dahir 1979). Pavement macrotexture is affected by the nominal maximum aggregates size. Mixtures with a nominal aggregate size of 9.5 mm or 12.5 mm provide a macrotexture below 0.5 mm (Wagner et al. 2004). Asphalt mixtures with coarse aggregate gradation usually have a higher macrotexture than asphalt mixtures with fine aggregate gradation. Rough surface texture contributes to a high level of skid resistance; however, it may increase noise and vibration (Ivey et al. 1992). Microtexture is dependent on aggregate characteristics and contributes to skid resistance on both wet and dry conditions (Crouch et al. 1995; Dunford 2013; Flintsch et al. 2005).

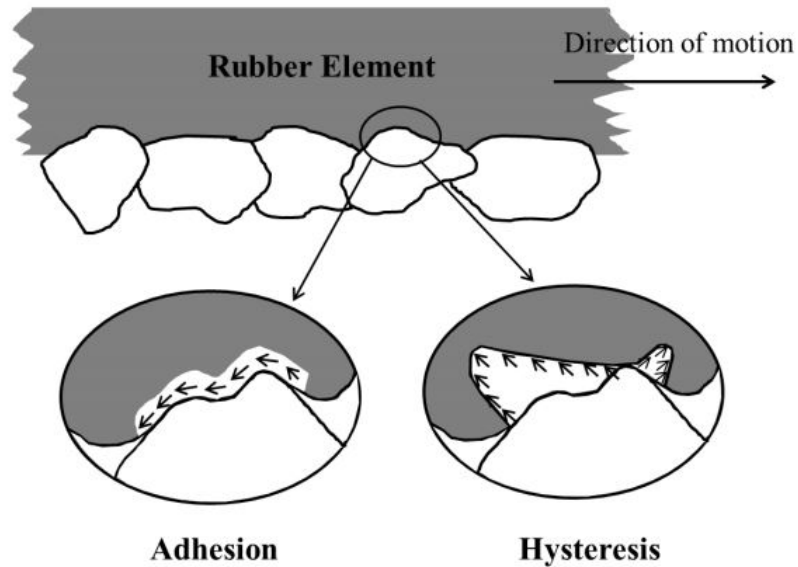




**Figure 2. Schematic of Microtexture and Macrotexture (Henry 2000).**

Megatexture is associated with the noise and rolling resistance and is affected by pavement surface deformation such as potholes and ruts. The roughness is caused by the deformation due to traffic loading and has adverse effects on the ride and drainage quality (Dunford 2013). Megatexture and roughness adversely affect pavement ride quality, while macrotexture and microtexture are considered significant factors affecting the skid resistance of asphalt pavements (Descornet 1989).

Skid resistance has two mechanisms—adhesion and hysteresis— as shown in Figure 3. These two mechanisms are highly affected by pavement macrotexture and microtexture (Tang et al. 2016). Adhesion develops due to the direct contact between the tires and pavement surface, especially in areas with high local pressure (Cairney 1997). Pavement microtexture is significant to the adhesion component that originates from molecular bonds between stone and rubber. In addition, pavement macrotexture contributes to the hysteresis component of the friction (Ivey et al. 1992). Hysteresis develops due to energy dissipation caused by the deformation of the tire's rubber around bulges and depressions in the pavement surface (Cairney 1997).



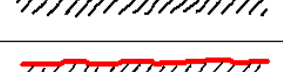
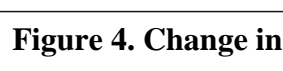


**Figure 3. Key Mechanisms of Tire-Pavement Friction (Hall et al. 2009).**

### **EFFECTS OF PAVEMENT SURFACE CHARACTERISTICS ON SKID RESISTANCE**

Adhesion and microtexture affect skid resistance at all speeds, and they have prevalent influence at speeds below 30 mph. Hysteresis and macrotexture have little significance at low speeds; however, macrotexture is an essential factor for safety in wet conditions as speed increases (Galambos et al. 1997).

Hogervorst (1974) has shown that the reduction in skid resistance is associated with vehicle speed, and it depends on pavement microtexture and macrotexture (Figure 4). Results of that study showed that skid resistance decreased with an increase in vehicle speed, and pavements with coarse and rough surface provide better skid resistance than ones with fine and polished surfaces.

	Road Surface	Surface Texture	
		macro	micro
A		coarse	rough
B		coarse	polished
C		fine	rough
D		fine	polished

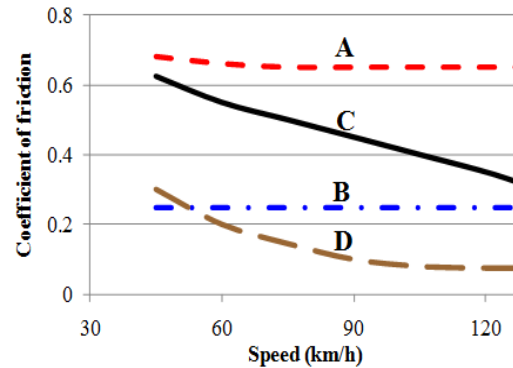


**Figure 4. Change in Pavement Friction with Speed (after Hogervorst 1974).**

Hall et al. (2009) indicated that microtexture locates the magnitude of skid resistance, while macrotexture controls the slope of the skid resistance reduction as the speed increases (Figure 5). Macrotexture affects the pavement friction at high speed by reducing the friction-speed slope, but it has little influence on friction at low speed. On the other hand, microtexture defines the level of friction (Hall et al. 2009; Rose et al. 1970; Gallaway et al. 1972).

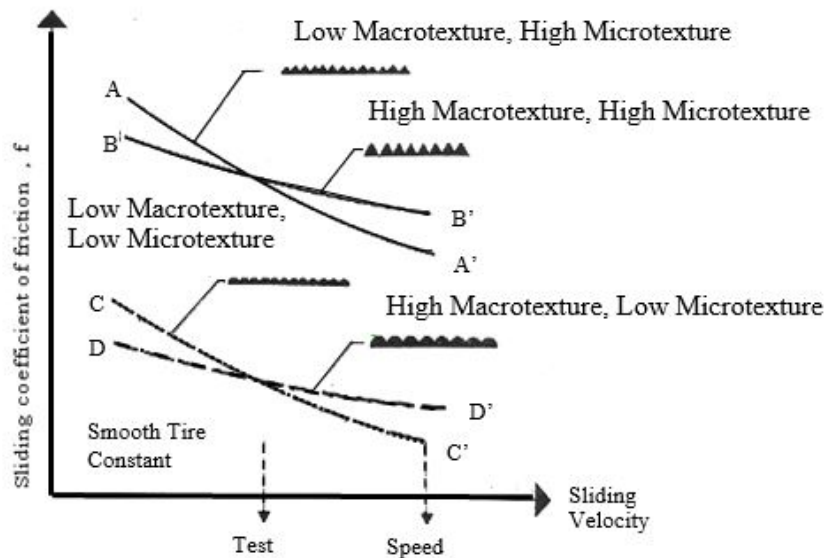


**Figure 5. Effect of Microtexture/Macrotexture on Pavement Friction (Hall et al. 2006).**

### ASPHALT SEAL COAT TREATMENT

The seal coat, or chip seal, is widely used as a preventive maintenance treatment and is considered a relatively inexpensive pavement surface treatment. It can be used effectively on

roads with both high and low traffic levels (TxDOT 2003). Similar to HMA surfaces, the macrotexture and microtexture of seal coat surface have significant contributions to the skid resistance. The macrotexture of pavement surface is affected by the aggregate size and its embedment into the binder. Immoderate embedment may reduce the skid resistance of seal coat (Krugler et al. 2012; Roque et al. 1991). In addition, aggregate polishing due to traffic reduces the skid resistance, and the rate of skid reduction depends on the aggregate shape characteristics (Masad et al. 2010; Rezaei et al. 2011). The seal coat surface treatments (Grade 3 and Grade 4) provided higher skid resistance compared to asphalt concrete-surfaced pavements (Type C), but the skid resistance of the surface treatments may decrease significantly once its macrotexture decreases (Masad et al. 2010).

## **AGGREGATE PROPERTIES AFFECTING PAVEMENT FRICTION**

This section discusses the aggregate properties that affect pavement friction.

### **Hardness and Mineralogy**

The hardness of aggregate affects the aggregate resistance to wear, and it can be measured using the hardness test. This test measures the resistance of aggregate surface to scratching on a scale from 1 to 10. Hardness values higher than 6 for hard minerals and 3 to 5 for soft minerals are recommended to ensure acceptable pavement frictional performance (Dahir and Henry 1978).

### **Polish Resistance**

This term refers to the ability of the aggregate to maintain its microtexture after it is subjected to repeated traffic loadings. The most common methods used to evaluate the polish resistance include the polished stone value (PSV) test and the acid insoluble residue (AIR) test (Hall et al. 2009). In the PSV test, the aggregate is polished by an accelerated polishing machine, and then the aggregate surface friction is measured using a British pendulum (Masad et al. 2007). The AIR test is performed to measure the noncarbonate ingredients of the aggregates, which contribute to aggregate resistance. Values of 30 to 35 for the PSV test and 50 to 70 percent for the AIR test are recommended to ensure sufficient frictional resistance (Hall et al. 2009).

## **Abrasion Resistance**

Abrasion resistance refers to the ability of aggregates to resist mechanical degradation. The Micro-Deval and Los Angeles (LA) abrasion tests are used to evaluate the abrasion resistance of the aggregates (Hall et al. 2009). The Micro-Deval test consists of a container with small steel balls, and the aggregate, with the presence of water, is polished in the rotating container (Kassem et al. 2012). Also, the LA abrasion test is used to measure the coarse aggregate resistance to degradation by inserting the aggregate into the LA abrasion device and when the large still ball impacts the aggregates inside the rotating drum (American Association of State Highway and Transportation Officials [AASHTO] T96). Values of losses less than 17 to 20 percent for the Micro-Deval test and 35 to 45 percent for the LA abrasion test are recommended to provide sufficient frictional resistance (Hall et al. 2009).

## **Angularity, Texture, and Form**

Aggregate shape characteristics, including angularity, texture, and form (Figure 6), are essential parameters in pavement skid resistance. The coarse and angular aggregates provide higher pavement friction than flat and elongated aggregates (Prowell et al. 2005). Also, an aggregate with a rough surface provides higher friction than an aggregate with a smooth surface (Kassem et al. 2013). The AIMS is used to quantify aggregate shape characteristics (Masad et al. 2010). Also, there are other methods, including laser-based aggregate analysis systems, computer particle analyzers, multiple ratio shape analyses, and VDG-40 video graders, that are used to perform the same function.

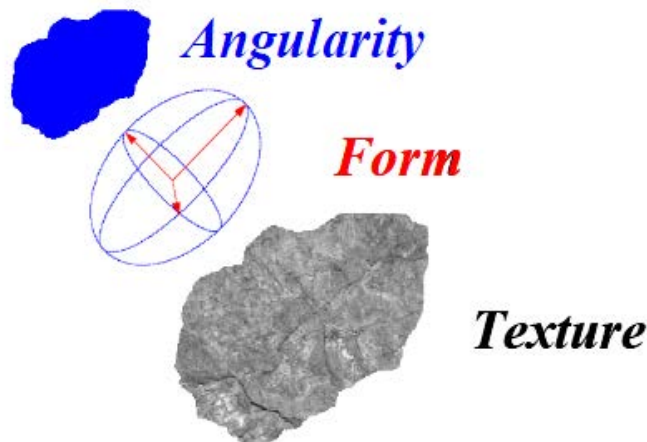


**Figure 6. AIMS Aggregate Shape Characteristics.**

## **Soundness**

Soundness of aggregates can be defined as the ability of aggregates to resist degradation due to climatic and environmental factors such as thawing, freezing, wetting, and drying. The soundness is quantified using the magnesium sulfate soundness test by quantifying the loss percentage of aggregates after cycles of hydration-dehydration. Loss percentages ranging from 10 percent to 20 percent are typical and provide sufficient frictional performance (Hall et al. 2009).

## **FRICITION/SKID RESISTANCE MEASURING DEVICES**

There are several devices that are used to measure skid resistance in the field, and some of them can be used in the field and laboratory. These devices rely on different measuring principles, and some of them measure peak friction while others measure values close to peak friction (Henry 2000). This section discusses common devices used in measuring friction and the skid resistance of pavements.

### **Locked-Wheel Skid Trailer**

A locked-wheel skid trailer can be used to measure pavement friction (Burchett and Rizenbergs 1980). The coefficient of friction is measured by the locked-wheel device and reported as a skid number (SN) (Gargett 1990). The SN is calculated using Equation 2.1.

$$SN = (F / N) * 100 \quad (2.1)$$

where

SN = skid number.

F = friction force.

N = normal (vertical) load on the test tire.

The skid trailer (Figure 7) is an appropriate method in terms of accuracy and safety. However, the data cannot be collected continuously, and the skid trailer does not have the ability to measure the low friction accurately (Burchett et al. 1980). When using the skid trailer, water is sprayed in front of the left wheel, and the left wheel is locked while the truck is traveling at a certain speed (e.g., 50 mph for Texas). The friction force that resists the rotation of the tire is measured (Masad et al. 2010).



**Figure 7. Locked-Wheel Skid Trailer.**

### **Side Force Devices**

Side force devices are used to measure pavement side friction on runways and highways. Figure 8 shows an example of the side device. As in the skid trailer test, a small amount of water is sprayed in front of the wheel, and the side force at 40 mph is recorded (Gargett 1990). The side force method is used to determine the ability of vehicles to maintain control, especially on curves (Henry 2000).



**Figure 8. Side Force Device (Hall et al. 2009).**

## Fixed Slip Devices

The fixed slip system is used to measure the friction between tires and pavements, and anti-lock brakes are considered. Figure 9 shows a fixed slip device. This method is used essentially at airports (Putov et al. 2016). The device can maintain at most 20 percent of firm slip, and the friction force between the surface and tire can be calculated after subjecting a vertical load to the tire. The advantage of using the fixed slip device is that it can be operated continuously without excessive wear on the tires (Henry 2000).



**Figure 9. Fixed Slip Device (Putov et al. 2016).**

## Variable Slip Devices

The variable slip device is another device that measures the frictional force when the tire is taken through a predetermined set of slip ratios (Figure 10). The result of dividing the longitudinal force by the vertical force is the slip friction number (SFN). The SFN is reported by using slip speeds between zero and the assigned speed (Henry 2000).





**Figure 10. Variable Slip Friction Testing Device (Putov et al. 2016).**

### **Dynamic Friction Tester**

The dynamic friction tester (DFT) is used to measure the coefficient of friction. This device consists of a circular disk with three rubber pads (Figure 11). The circular disk rotates up to 100 km/h. Once the disk reaches the specified speed, the disk is lowered to the pavement surface, and the coefficient of friction is measured as the speed of the rotating disk gradually decreases (Saito et al. 1996; Henry 1986). The pavement microtexture is quantified by the value of the coefficient of friction at 20 km/h (DFT<sub>20</sub>).



**Figure 11. Dynamic Friction Tester.**

### **THE INTERNATIONAL FRICTION INDEX**

The Permanent International Association of Road Congress (PIARC) developed a unified equation for the international friction index (IFI) to determine the surface friction of a pavement (Rado et al. 1995). It incorporates parameters that describe the microtexture and macrotexture of

a pavement, as presented in Equation 2.2. The macrotexture is described by mean profile depth (MPD) measured by CTMeter, while the microtexture is quantified by the coefficient of friction measured using DFT at 20 km/h (DFT<sub>20</sub>) (Wambold et al. 1995; Henry 2000).

$$\text{IFI} = 0.081 + 0.732 * \text{DFT}_{20} * \exp\left(\frac{-40}{S_p}\right) \quad (2.2)$$

$$S_p = 14.2 + 89.7\text{MPD} \quad (2.3)$$

where

IFI = international friction index.

$S_p$  = speed constant parameter.

MPD = mean profile depth.

## **PAVEMENT TEXTURE MEASUREMENTS**

There are several methods used for quantifying the macrotexture of asphalt pavements. These methods include the CTMeter, the sand patch method, the outflow meter, and laser-based (or electro-optic) technique (Hall et al. 2009).

### **CTMeter Device**

This device is used to measure the MPD in the field and laboratory (Figure 12). The device has a charge-coupled, laser displacement sensor attached to an arm mounted to the device. The arm rotates in a circle with a diameter of 28.4 cm. The laser sensor can collect 1,024 data points per round. The average MPD is calculated and reported according to the American Society for Testing and Materials (ASTM) E2157.



**Figure 12. CTMeter Device.**

### **Sand Patch Method**

The sand patch test is used to quantify the macrotexture of pavement surface by measuring the mean texture depth (MTD) in accordance with ASTM E1845. The sand patch method includes a brush for cleaning the surface, a cup and spreading tool to distribute the sand, and a scale tape (Figure 13). An amount of 100 grams of sand is used in each test. The sand sample should pass through a No. 30 sieve and be retained in a No. 50 sieve (Sarsam and Al Shareef 2015). The sand is spread in a circle on the pavement surface, and the diameter of the circle is measured. The MTD is measured using Equation 2.4 as a function of sand volume and the diameter of the sand patch (ASTM 2009).

$$MTD = \frac{4V}{3.14 D^2} \quad (2.4)$$

where

MTD = mean texture depth (mm).

D = average diameter of sand patch circle (cm).

V = sand volume (cm<sup>3</sup>), (weight of sand / density of sand).



**Figure 13. Sand Patch Method (Sarsam et al. 2015).**

### **Stereo Photogrammetric Technique**

This technique is based on a three-dimensional (3D) measurement of pavement surface texture. The 3D images provide an indication of physical changes to the pavement surface that cannot be accurately quantified using two-dimensional (2D) profiles. The changes in the aggregate surface due to the polishing process can be observed and quantified using 3D measurements (Dunford 2013). Stereo photogrammetry relies on taking various images from different angles in order to estimate the 3D coordinates of a point. The close range photogrammetry is a version of stereo photogrammetry that uses an ordinary camera to take various images from different angles to construct the 3D profile. Previous research demonstrated that this technique can be used to quantify the macrotexture, microtexture, and megatexture (McQuaid et al. 2014). Figure 14 shows the pavement 3D image obtained from stereo photogrammetric techniques.

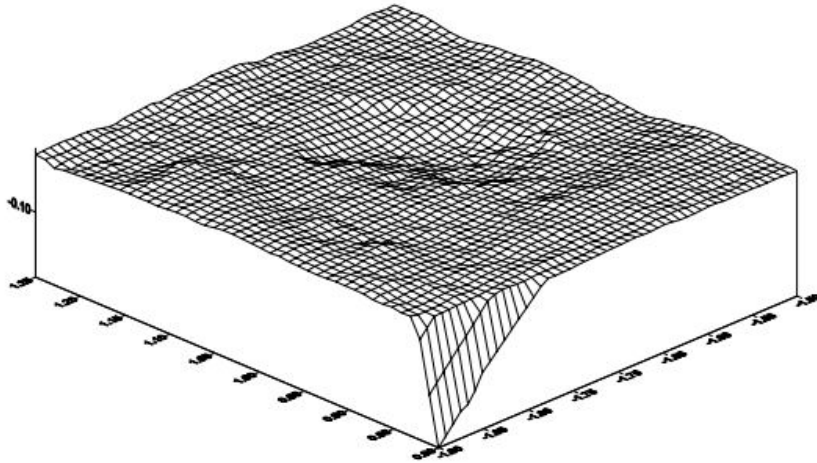


**Figure 14. 3D Pavement Surface from Stereo Photogrammetric Technique (Mustaffar et al. 2004).**

### **AGGREGATE RESISTANCE TO POLISHING**

Aggregates with good resistance to polishing retain their microtexture for a longer period of time than do aggregates with poor resistance to polishing and abrasion. The LA abrasion test is used to measure the coarse aggregate resistance to degradation (West et al. 2001; Fülöp et al. 2000). Despite the British pendulum test being widely used to predict the frictional properties of aggregates, researchers indicated that this test has a high level of variability (Dahir and Henry 1979; Fwa et al. 2004).

The Micro-Deval polishing device was found to be a good alternative to the LA abrasion test (Prowell et al. 2005). The aggregates are typically polished in the Micro-Deval for 105 min and 180 min (Al Rousan 2005). Another study (Mahmoud and Masad 2007) recommended using the AIMS to measure the aggregate characteristics after subjecting the aggregates to polishing in the Micro-Deval test. Although there were some developments regarding new tests, there was only slight progress in terms of developing models that can estimate the skid resistance of pavement (Mahmoud et al. 2007).

Polishing the pavement surface due to frequent traffic applications is the main cause of skid resistance reduction. Using aggregates with good resistance to polishing and abrasion provides pavements with higher friction (Kassem et al. 2013).

## **EFFECT OF PAVEMENT DETERIORATION ON SKID RESISTANCE**

Luis and Hess (2010) conducted a study to evaluate the correlation between pavement roughness and skid resistance. They used a skid trailer to measure the skid number of different pavement test sections. These test sections were selected to have comparable surface characteristics in terms of macrotexture and microtexture but different levels of roughness. The analytical investigation demonstrated that sections with comparable surface characteristics but different roughness levels had different skid numbers. The researchers concluded that a high level of roughness provides low skid numbers; in addition, the roughness should be considered in pavement safety evaluation. Conversely, Fuentes (2009) studied the correlation between the international roughness index and skid resistance, and the results did not provide enough evidence on the effect of roughness on skid resistance.

The excessive binder in the mixture reduces the void content and causes bleeding. Bleeding is defined as excessive asphalt film on the road surface. Skid resistance decreases due to the loss of macrotexture and microtexture caused by bleeding and coating the aggregate particles with excessive asphalt binders. Surface treatments may increase the asphalt binder at the surface, causing bleeding and hence reducing skid resistance (Kane et al. 2009).

## **DEVELOPING SKID RESISTANCE MODELS**

There have been several attempts for developing prediction models for friction and skid resistance of asphalt pavements. This section discusses some of these attempts.

### **Masad et al.'s (2007) Model**

Masad et al. (2007) developed a new method to evaluate the change in the asphalt pavement skid resistance depending on aggregate texture, properties of mixtures, and environmental conditions. This method relies on the use of the Micro-Deval test and AIMS to evaluate the resistance of aggregates to polishing and abrasion. Aggregates retained in a No. 4 sieve (4.75 mm) were considered due to the significant effects of coarse aggregates on skid resistance compared to fine aggregates. The measurements of aggregate texture were obtained using AIMS at different time durations of polishing in the Micro-Deval (15, 30, 60, 75, 90, 105,

and 180 min), as shown in Figure 15. Figure 15 demonstrates the change in aggregate texture at three different levels (4, 5, and 6). Each level stands for a different aggregate size.

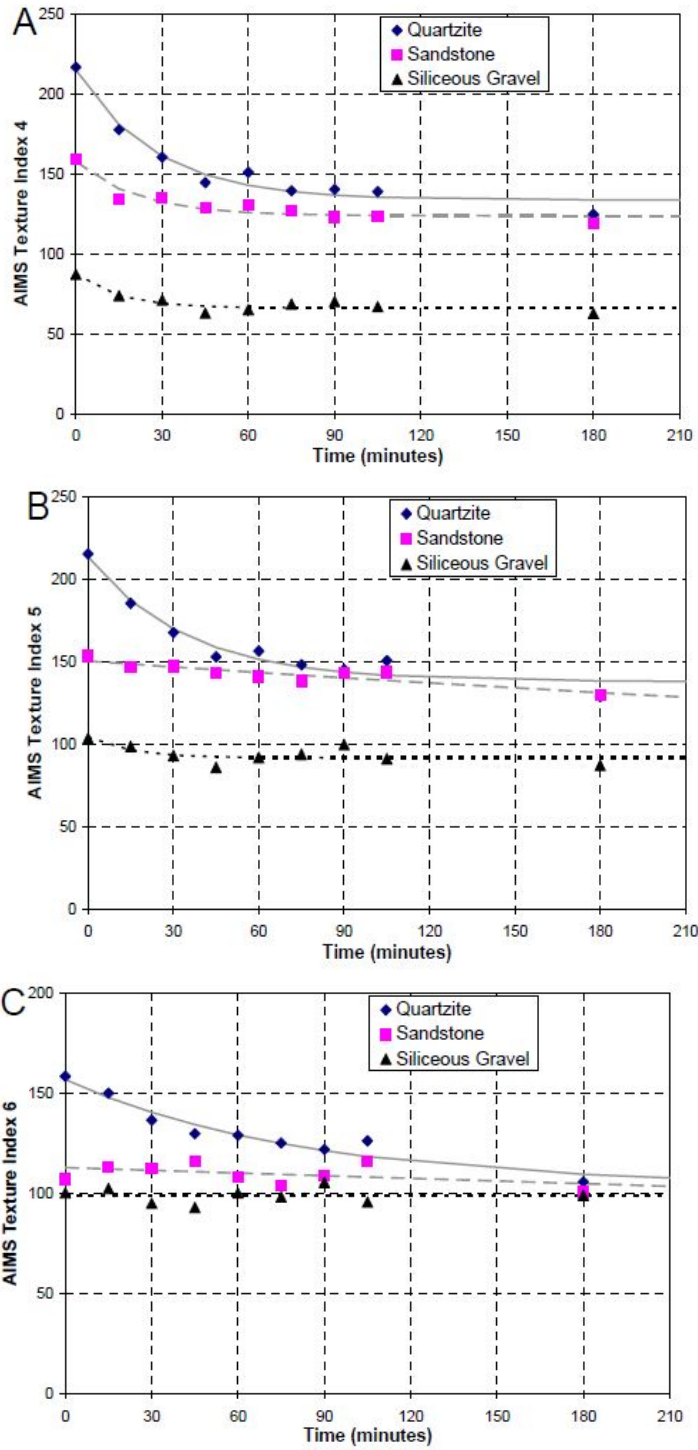


**Figure 15. AIMS Texture Index versus Time in the Micro-Deval Test for (A) Texture Level 4, (B) Texture Level 5, and (C) Texture Level 6.**



In the field, they examined nine pavement sections. These selected sections had different aggregate types (siliceous, sandstone, and quartzite) and mix design (CMHB-C, Superpave, and Type C). The skid number was measured on the shoulder and on the outside lane. In the laboratory, test slabs were prepared using different aggregate types and different mixture types. The analysis of variance (ANOVA) was conducted at a significance level of 0.05 to investigate the effect of both aggregate and mix type on the skid number. The results demonstrated that the aggregate type was a significant factor (P-value < 0.05), while the mix type was not statistically significant (P-value = 0.089). The mix type had been considered an essential factor affecting the skid resistance; however, the mixes used in this study did not significantly contribute to skid resistance. The SPSS software was used to fit Equation 2.5 in order to quantify the change in texture due to polishing in the Micro-Deval tests. Table 2 presents an example of the obtained regression coefficients.

$$\text{Texture (t)} = a + b \times \exp(-c \times t) \quad (2.5)$$

**Table 2. Aggregate Texture Regression Coefficients.**

Aggregate	Texture Level	a	b	c
Siliceous Gravel	Level 4	66.19	21.04	0.06738
	Level 5	91.70	12.45	0.06687
	Level 6	49.38	49.54	0.00000
Sandstone	Level 4	123.70	33.69	0.04641
	Level 5	58.66	91.60	0.00130
	Level 6	0.21	112.77	0.00041
Quartzite	Level 4	133.54	81.17	0.03632
	Level 5	137.90	75.32	0.02875
	Level 6	103.67	53.18	0.01219

The results showed that aggregate type has a significant effect on skid resistance. Gravel provided less skid resistance than sandstone and quartzite. Pavement sections constructed with sandstone provided higher skid resistance than quartzite. The aggregate gradation was not found to have a significant effect on skid resistance.



### **Masad et al.'s (2010) Model**

Masad et al. (2010) conducted a study that included measurements in the field and laboratory. In the laboratory, several slabs with different asphalt mixtures and aggregate types were prepared and tested. Three mixture designs (Type C, Type D, and porous friction course [PFC]) were evaluated. These mix designs were found to provide different frictional performance in the field. The mixtures were prepared and compacted in a special metal mold using a vibrator roller compactor, as shown in Figure 16a. The minimum slab size required to conduct the skid resistance measurements by the CTMeter and DFT was 17.75 inches by 17.75 inches. The slabs' dimensions were 60 inches by 26 inches. The researchers evaluated the friction at three different locations on a single test slab (Figure 16b). A three-wheel polisher (Figure 16c) was used to polish the test slabs, and the measurements of the friction and mean profile depth were collected using the DFT and the CTMeter (Figure 16d) after different polishing cycles (5,000, 10,000, 20,000, 35,000, 50,000, 75,000, and 100,000). The British pendulum test and the sand patch method were also used in this study in a similar fashion.

Aggregate texture and angularity were measured before and after different time intervals of polishing in the Micro-Deval. Figure 17 shows the change in the texture index before and after subjecting the aggregates to polishing and abrasion in the Micro-Deval. It shows that the selected aggregates provided different resistance to polishing. The effect of aggregate type on the pavement skid resistance was investigated among the prepared slabs. The results demonstrated a high correlation between the aggregate properties and the mixture frictional characteristics. The aggregate characteristics affecting the skid resistance were the British pendulum value, the initial texture measured by AIMS, the terminal texture after Micro-Deval measured by AIMS, and the coarse aggregate acid insolubility value.

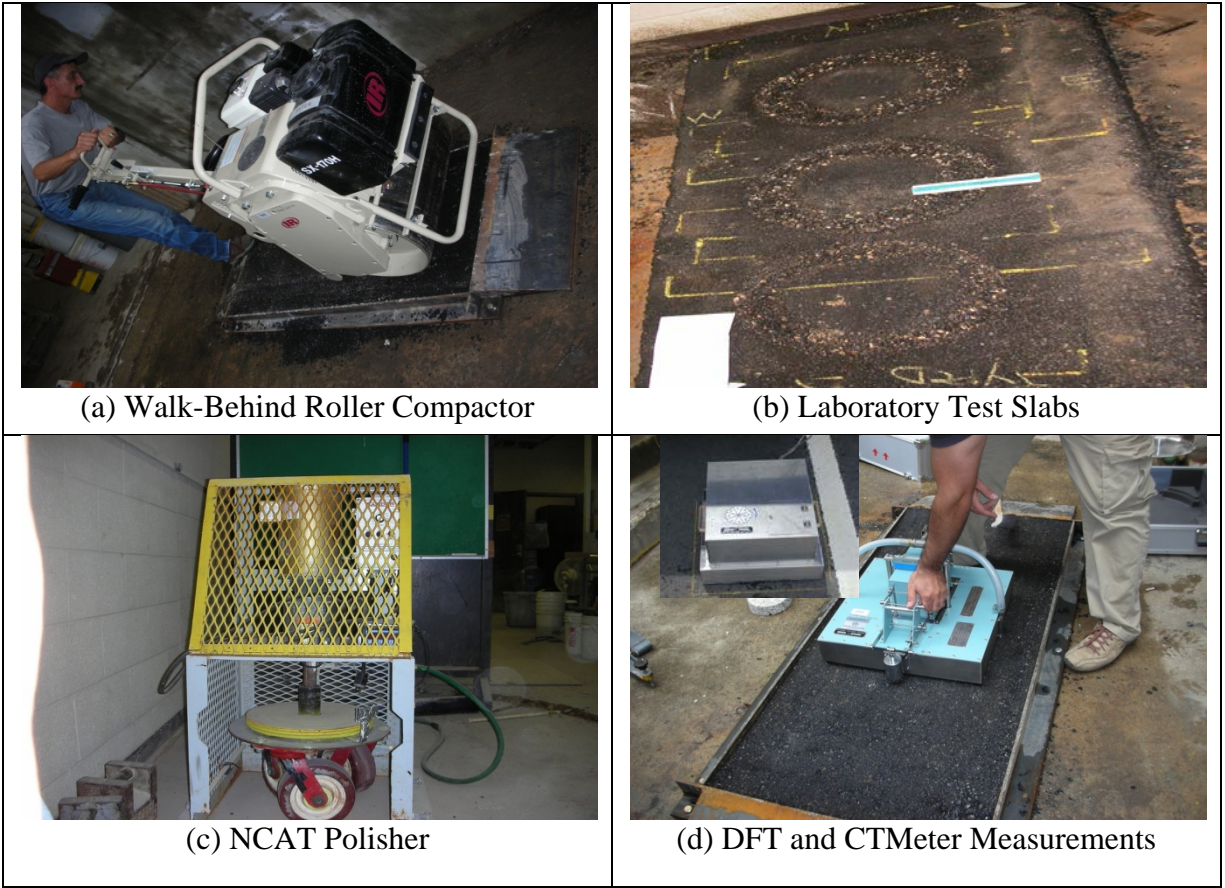


**Figure 16. Laboratory Experiments in the TxDOT (Masad et al. 2010).**

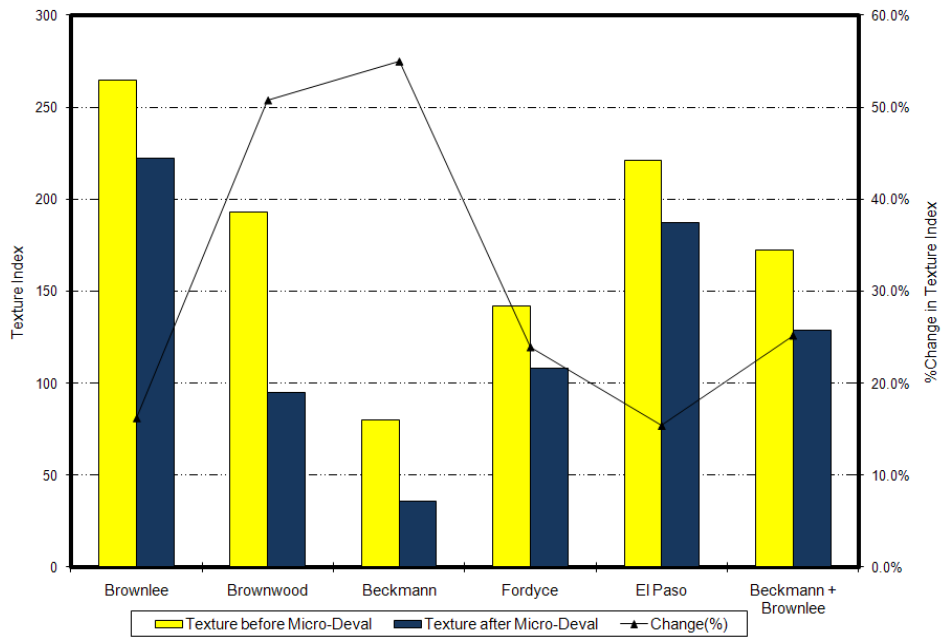


**Figure 17. Aggregate Texture before and after Micro-Deval and Percent Change (Masad et al. 2010).**

Masad et al. (2010) found that the change in the calculated IFI (Equation 2.2) with the polishing cycles based on the MPD and DFT<sub>20</sub> measurements can be described by Equation 2.6.

$$IFI(N) = a_{mix} + b_{mix} * e^{(-c_{mix}*N)} \quad (2.6)$$

where

$a_{mix}$ : terminal IFI value for the mix.

$a_{mix} + b_{mix}$ : initial IFI value for the mix.

$c_{mix}$ : rate of change in IFI for the mix.

$N$ : number of polishing cycles in the laboratory.

Figure 18 shows an example of the change in IFI with polishing cycles and the regression constants of Equation 2.6. Based on the laboratory stage, Masad et al. (2010) developed a model to predict the initial friction, terminal friction, and rate of change in IFI as a function of aggregate characteristics measured with the AIMS system and aggregate gradation parameters. This model can be used to select the proper aggregate type to provide adequate skid resistance. Equations 2.7 to 2.9 represent the developed model.

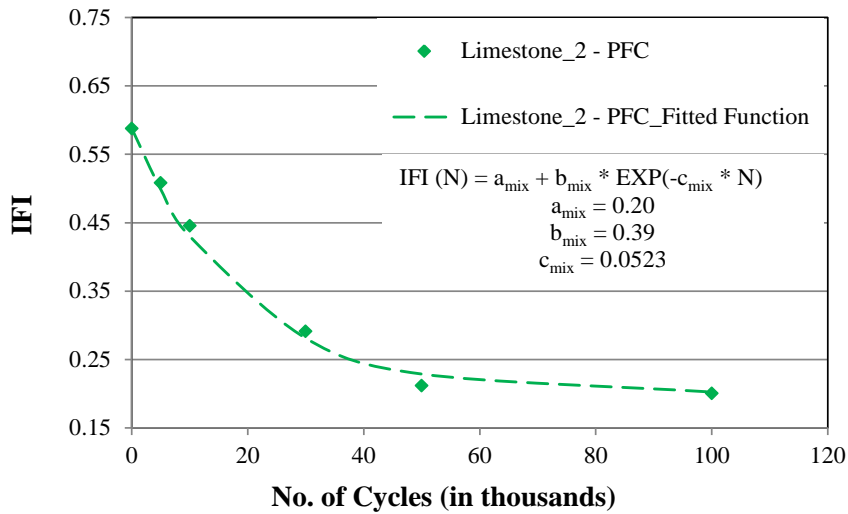


**Figure 18. An Example of IFI vs. Polishing Cycles (Kassem et al. 2013).**

$$a_{mix} = \frac{18.422 + \lambda}{118.936 - 0.0013(AMD)^2} \quad (2.7)$$

$$a_{mix} + b_{mix} = 0.4984 * \ln(5.656 * 10^{-4}(a_{agg} + b_{agg}) + 5.846 * 10^{-2}\lambda - 4.985 * 10^{-2}k) + 0.8619 \quad (2.8)$$

$$C_{mix} = 0.765 * e^{\left(-7.297 * \frac{10^{-2}}{C_{agg}}\right)} \quad (2.9)$$

where

$a_{mix}$  = terminal IFI value for the mix.

$a_{mix} + b_{mix}$  = initial IFI value for the mix.

$c_{mix}$  = rate of change in IFI for the mix.

AMD = aggregate texture after Micro-Deval.

$a_{agg} + b_{agg}$  = aggregate initial texture using texture model.

$c_{agg}$  = aggregate texture rate of change using texture model.

$\kappa$  = shape factor of Weibull distribution used to describe aggregate gradation.

$\lambda$  = scale factor of Weibull distribution used to describe aggregate gradation.

The data collected in the laboratory were compared to skid values measured in the field for the same asphalt mixtures. Masad et al. (2010) developed a system to predict the skid number of asphalt mixtures as a function of traffic level. Input parameters required for this model included aggregate texture measured using AIMS before and after polishing in Micro-Deval, aggregate gradations, and traffic data. A computer program called SAAP was developed to execute the steps needed to calculate the skid resistance of asphalt pavements as a function of time (or cumulative traffic). Figure 19 summarizes the steps needed to predict the skid number according to Masad et al. (2010).

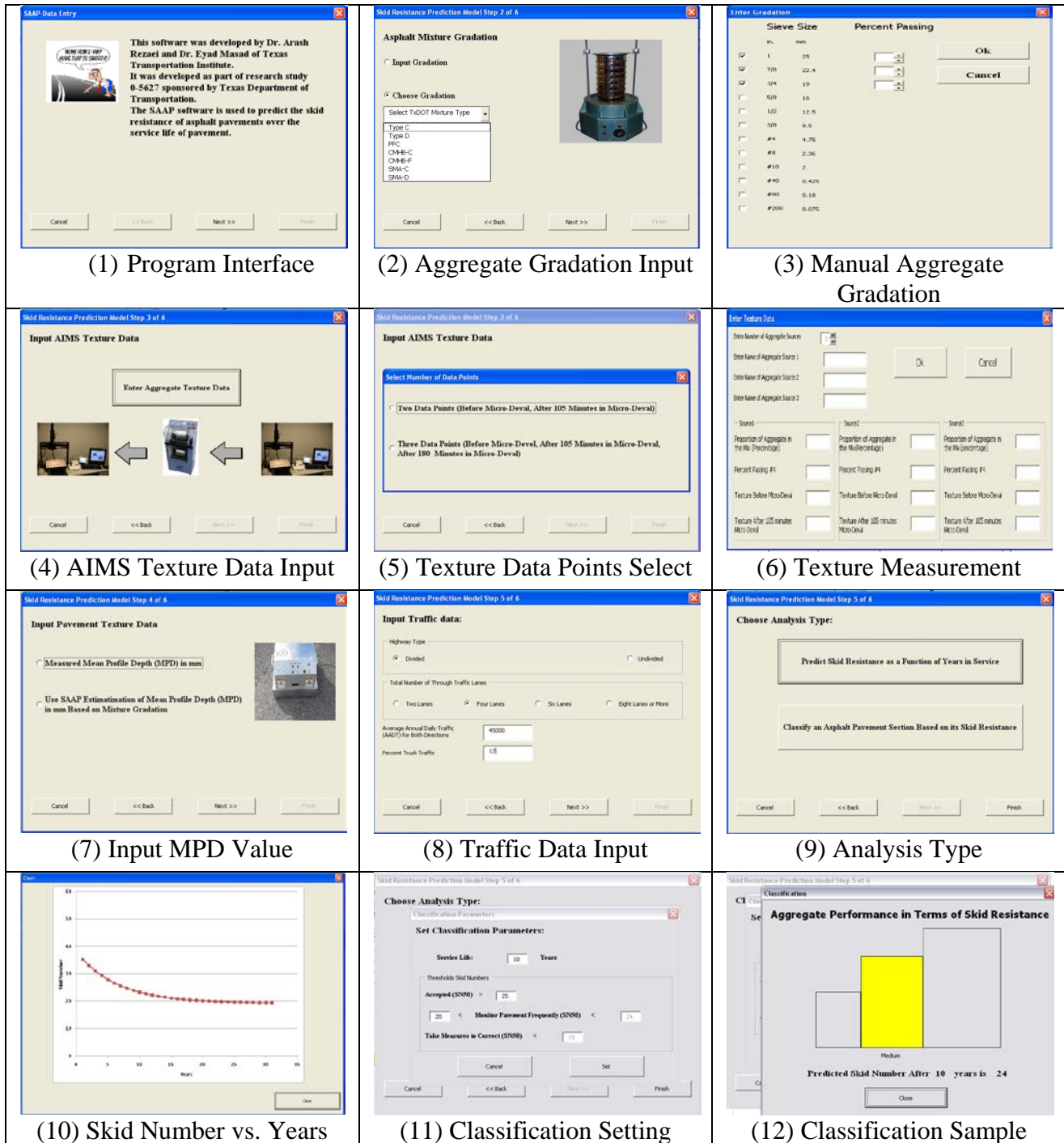


**Figure 19. Steps Needed to Predict Skid Number SAAP in TxDOT Project No. 0-5627.**

### Wu et al.'s (2012) Model

Wu et al. (2012) developed a new model to estimate skid resistance based on 12 mixtures with various mix types and aggregate analysis. The aggregates included sandstone and siliceous limestone, and four mix types were evaluated (19-mm Superpave Level 2 mix, 12.5-mm

Superpave Level 2 mix, stone mastic asphalt [SMA], and PFC. The selection of the aggregates was based on the mixture construction in Louisiana. The Micro-Deval was used to polish the prepared slabs according to AASHTO T327-05. Also, the British pendulum number was measured according to AASHTO T278 and T279. Additionally, the macrotexture and microtexture of the prepared slabs were measured using the CTMeter and DTF after different polishing cycles. The model presented in Equation 2.10 was developed as a function of the MPD and the DFT at 20 km/h. The model estimates the friction number at 60 km/h. The researchers also demonstrated that aggregates with low skid resistance can be blended with good quality aggregates in order to achieve adequate skid resistance.

$$F60 = 0.081 + 0.732 \text{DFN}_{20} * \exp \frac{-40}{14.2+89.7\text{MPD}} \quad (2.10)$$

where

F60 = friction number at 60 km/h.

MPD = mean profile depth.

DFN<sub>20</sub> = friction at 20 km/h.

### **Kassem et al.'s (2013) Model**

Kassem et al. (2013) conducted a study to validate the IFI models developed by Masad et al. (2010). Squared-shaped slabs were prepared in the laboratory using three different types of aggregates (Limestone 1, Limestone 2, and sandstone), and four asphalt mixture designs (Type F, Type C, SMA, and PFC) were evaluated. A total number of 12 asphalt mixtures were prepared, and two slabs of each mixture were tested. A total number of 24 slabs were tested in this study. The laboratory slabs were prepared using a linear kneading compactor (Figure 20a). The size (20 inches by 20 inches) of the prepared slabs was adequate for friction and mean profile depth measurements. A three-wheel polishing device was used to polish the test slabs at 5,000, 10,000, 30,000, 50,000, and 100,000 cycles (Figure 20b).

Aggregate texture and angularity were measured using the AIMS system at different time durations of polishing in the Micro-Deval. Figure 21 shows the percent weight loss of test aggregates. Sandstone had the highest texture index and lowest weight loss, while Limestone 1 had the lowest texture index and highest percent weight loss. The AIMS (Figure 22) was used to

measure the texture and angularity before and after polishing time durations of the Micro-Deval test.

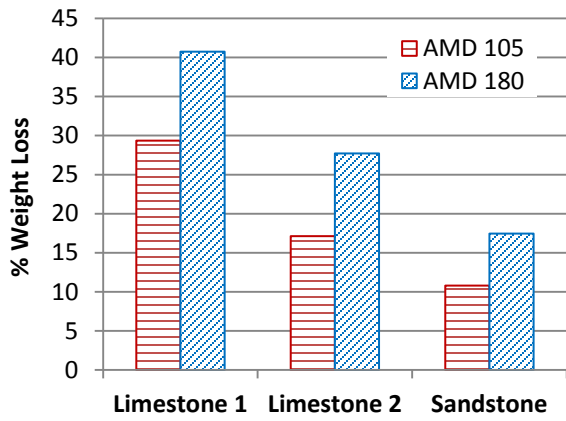


(a) Preparing Slabs using Linear Kneading Compactor

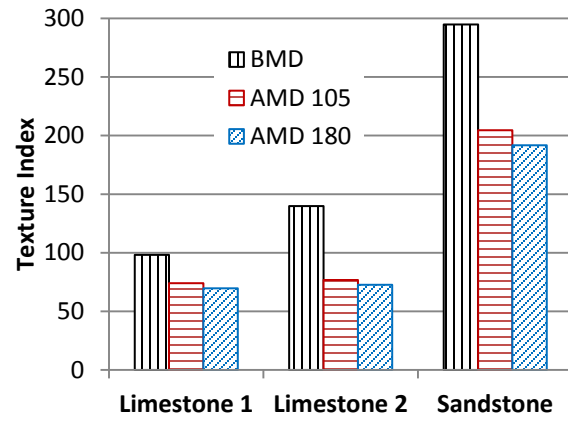


(b) Polishing Test Slabs using TTI Polisher

**Figure 20. Test Slabs Preparation and Polishing (Kassem et al. 2013).**



(a) Weight Loss of Micro-Deval Abrasion Test



(b) Texture Index Measured using AIMS

**Figure 21. Texture Index and Weight Loss Results (Kassem et al. 2013).**





**Figure 22. AIMS System (Kassem et al. 2013).**

The measurements of friction and macrotexture were conducted using the DFT and CTMeter after different polishing cycles. Then, the IFI was calculated based on the measured MPD and DFT at 20 km/h. Figure 23 shows the IFI versus polishing cycles. The IFI of Limestone 1 test slabs reached the terminal value after only 30,000 cycles, while the sandstone reached the terminal value after 100,000 cycles. Also, the terminal IFI value of the sandstone is higher than the terminal value of Limestone 1. The sandstone had rough texture with better abrasion resistance than Limestone 1. The findings also indicated that the coarse mixtures had better friction than the fine mixtures. The results demonstrated a high correlation between the measured and predicted IFI after considering aggregate texture and angularity indices in the developed model. Equations 2.11, 2.12, and 2.13 present the developed models.



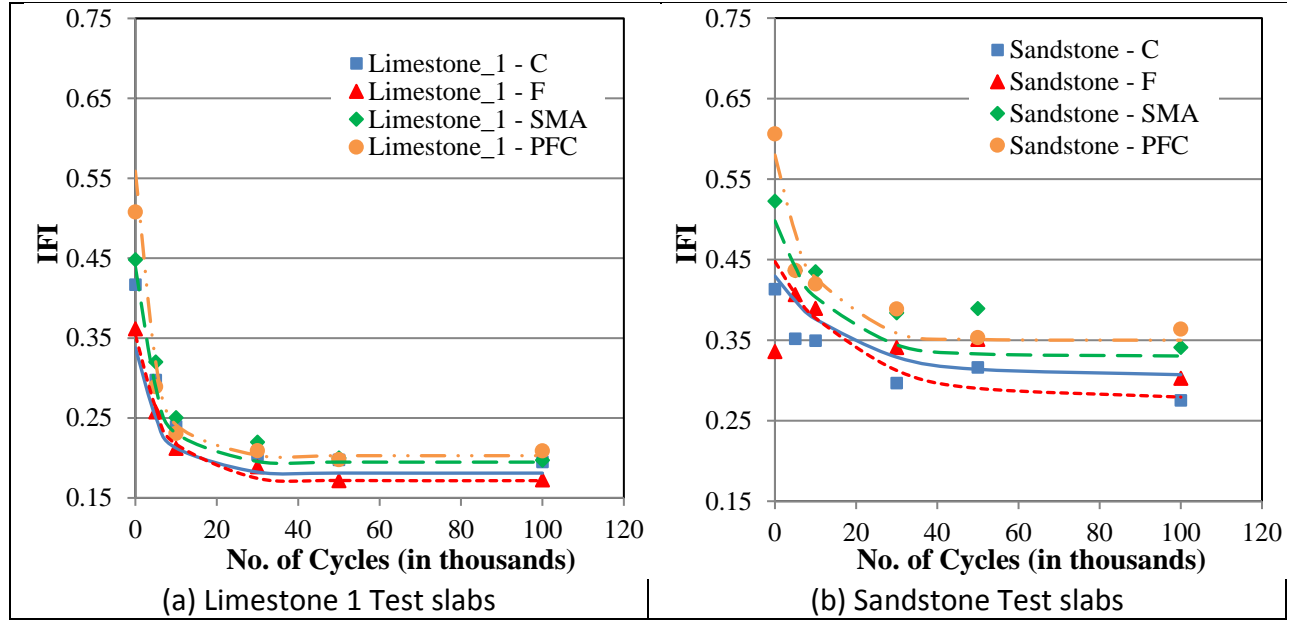


**Figure 23. Texture Index and Weight Loss Results (Kassem et al. 2013).**

$$a_{mix} = \frac{47.493 + \lambda}{307.071 - 0.003(AMD)^2} \quad (2.11)$$

$$a_{mix} + b_{mix} = 0.308 * \ln \left( \frac{1.438 * (a_{TX} + b_{TX}) + 46.893 * \lambda + 333.491 * k}{2.420 * (a_{GA} + b_{GA})} \right) + 1.008 \quad (2.12)$$

$$C_{mix} = 0.052 + 2.284 * 10^{-14} * e^{\left(\frac{0.523}{C_{TX}}\right)} + 2.008 * 10^{-47} * e^{\left(\frac{1.708}{C_{GA}}\right)} \quad (2.13)$$

where

$a_{mix}$  = terminal IFI.

$a_{mix} + b_{mix}$  = initial IFI.

$C_{mix}$  = rate of change in IFI.

$\lambda, k$  = scale and shape parameters of Weibull distribution.

AMD = the texture after 150 min in Micro-Deval.

$a_{TX}, b_{TX}$  = regression constants for texture.

$a_{GA}, b_{GA}$  = regression constants for angularity.

## SUMMARY

The skid resistance of pavement surface is affected by its surface texture properties. Providing adequate macrotexture and microtexture are essential requirements for pavement to ensure high skid resistance at all speeds. Skid resistance is mainly associated with aggregate

characteristics and gradation. Additionally, recent studies showed that the Micro-Deval and AIMS are proper test methods for measuring the resistance of aggregates to abrasion and polishing. In order to improve the safety on highway pavements, the researchers have developed several models to predict the skid resistance as a function of aggregate characteristics, mix design, and traffic level. These models need to be validated with additional data that cover a wide range of variables and parameters. In addition, these models should be extended to predict the skid resistance of surface treatments such as seal coat.

## **CHAPTER 3: TESTING AND DATA COLLECTION**

The researchers measured the frictional characteristics and skid numbers on a number of HMA and seal coat test sections in Texas. All field measurements were made by the researchers at TTI. In addition, the aggregate shape characteristics were either measured in the laboratory or obtained from the TxDOT database by the researchers. In this study, 35 test sections of HMA and 35 seal coat test sections were examined. Four seal coat test sections were excluded due to excessive bleeding. This chapter discusses the research plan and the field and laboratory testing.

### **SELECTION OF THE FIELD SECTIONS**

The researchers identified and selected 35 test sections of HMA and 35 test sections with seal coat. During the selection of test sections, the research team made an effort to include surfaces with wide varieties of mixture gradations, aggregate sources, and climatic zones of Texas. Focus was given to identifying test sections with higher traffic levels so that the team could observe higher polishing within a relatively short time. Another important criterion of test sections' selection was to find existing sections with a history of skid measurement under TxDOT's annual network-level pavement evaluation program. TxDOT does not collect network-level skid data for all the roads every year. Typically, major highways (i.e., interstate highways) with higher traffic level are tested more frequently than other highways (i.e., farm-to-market roads). The annual skid testing frequency varies among different districts of TxDOT. Table 3 provides detailed information about the HMA test sections. This information includes the location of the test sections, section identification (ID), construction date, testing date, and number of lanes. The test sections of asphalt mixtures included different mixture types (SMA-C, SMA-D, SMA-F, CMHB-F, Type C, Type D, TOM, PFC, CMHB-C, and CAM), different aggregate types (limestone, gravel, granite, sandstone, dolomite, rhyolite, traprock, and quartzite), different years of construction (2004 to 2013), and were distributed across Texas (ATL, AUS, BMT, BRY, ODA, SAT, YKM, HOU, LRD, PHR, and LFK districts of TxDOT).

Table 4 provides the same information for the seal coat test sections. The test sections of seal coat included different grade types (Grade 3, Grade 4, and Grade 5), different aggregates (limestone, gravel, traprock, sandstone, dolomite, rhyolite, LRA, and lightweight), different

coating conditions (pre-coated and virgin), different years of construction (2009 to 2013), and also were distributed across Texas (ATL, BMT, ODA, SAT, YKM, LRD, PHR, LFK, BRY).

**Table 3. HMA Test Sections.**

District	Section ID	CTM DFT Test Date	Construction Date	Days between Construction and Field Testing	Lane Description
Atlanta	IH 30_ATL_SMA_	12/20/2013	7/1/2010	1268	Two lanes each way, divided
	US 59_ATL_CMHB-F_FM 2792	12/18/2013	8/1/2005	3061	Two lanes each way, divided
	US 59_ATL_TY D_TRM 310	12/18/2013	6/1/2011	931	Two lanes each way, divided
	US 59_ATL_TY D_SHELBY CO LINE	12/18/2013	4/1/2011	992	Two lanes each way, divided
	US 271_ATL_CMHB-F_CAMP	12/20/2013	6/1/2008	2028	Undivided, two lanes each way with turn lane
Austin	IH 35 TOM Mix_AUS	8/28/2014	7/1/2011	1154	Three lanes each way, divided
	RM 3238_AUS_TOM	8/28/2014	7/1/2013	423	Undivided, one lane each way
	US71_AUS_TOM	8/27/2014	7/1/2013	422	Two lanes each way, divided
Beaumont	IH10_BMT_SMA-D	9/30/2013	7/1/2009	1552	Two lanes each way, divided
	SH 82_BMT_SMA-D	9/30/2013	4/1/2013	182	Undivided, two lanes each way with turn lane
	SL 207_BMT_TY D	10/2/2013	5/1/2013	154	Undivided, one lane each way
	US 69_BMT_PFC	9/30/2013	9/1/2011	760	Two lanes each way, divided
	US 90_BMT_SMA-D	9/30/2013	5/1/2013	152	Undivided, two lanes each way with turn lane
Bryan	IH 45_BRY_TY C	10/2/2014	8/25/2008	2229	Two lanes each way, divided
	IH 45_BRY_PFC	10/2/2014	8/17/2009	1872	Two lanes each way, divided
	SH 6_BRY_NEW PFC	10/2/2014	9/28/2011	1100	Two lanes each way, divided
	SH 6_BRY_OLD PFC	10/2/2014	6/21/2007	2660	Two lanes each way, divided
Laredo	IH 35_LRD_SMA_WEBB	7/24/2013	6/1/2008	1879	Three lanes each way, divided
	IH 35_LRD_SMA-C_LASALLE	7/24/2013	6/1/2004	3340	Two lanes each way, divided
Lufkin	US 59_LFK_PFC_Nacodoches	8/16/2013	6/1/2013	76	Two lanes each way, divided
	SH 7_LFK_TY D_Houston	8/16/2013	5/1/2013	107	Undivided, one lane each way

**Table 3. HMA Test Sections (Continued)**

District	Section ID	CTM DFT Test Date	Construction Date	Days between Construction and Field Testing	Lane Description
Odessa	IH 20_ODA_SP-C_Martin	10/8/2013	9/1/2012	402	Two lanes each way, divided
	IH 20_ODA_SP-D_Midland_2012	10/8/2013	6/1/2012	494	Two lanes each way, divided
	IH 20_ODA_SP-D_Midland_2013	10/8/2013	6/1/2013	129	Two lanes each way, divided
	US 385_ODA_CMHB-F	10/7/2013	10/1/2005	2928	Two lanes each way, divided
	IH 20_ODA_PFC_2004	10/8/2013	6/1/2004	3416	Two lanes each way, divided
San Antonio	IH 10_SAT_SMA-D_BEXAR	3/10/2014	4/1/2012	708	Two lanes each way, divided
	IH 10_SAT_TY C_BEXAR	3/10/2014	3/1/2009	1835	Two lanes each way, divided
	IH 37_SAT_PFC_BEXAR	3/10/2014	6/1/2013	282	Two lanes each way, divided
YKM	IH 10_YKM_TY D_AUSTIN	5/23/2013	7/1/2011	692	Two lanes each way, divided
	SH 36_YKM_TY D_AUSTIN	5/23/2013	7/1/2006	2518	Undivided, one lane each way
PHARR	US 77_PHR_TY D_Kennedy	2/20/2014	2/1/2013	384	Two lanes each way, divided
	US 281_PHR_TY D_Hidalgo	2/20/2014	8/1/2011	934	Two lanes each way, divided
Houston	SH 6 Bwp 2-1, Wp 2-1 Middle	6/20/2013	7/1/2005	2911	Two lanes each way, divided
	SH 6 Bwp 2-1 Bottom	6/20/2013	7/1/2005	2911	Two lanes each way, divided

**Table 4. Selected Sections for Seal Coat.**

District	Section ID	CTM DFT Test Date	Construction Date	Days between Construction and Field Testing
Pharr	US 77_PHR_GR3_Cameron	2/20/2014	5/1/2013	295
	US 281_PHR_GR3_Hidalgo	2/21/2014	5/1/2011	1027
	US 281_PHR_GR3_Brooke_TRM 752	2/21/2014	5/1/2011	1027
	US 281_PHR_GR3_Brooke_TRM 722	2/21/2014	9/1/2011	904
Dallas-FW	US 377_FTW_GR3_Hood	11/18/2014	7/1/2010	1601
	US 377_FTW_GR3_Tarrant	11/18/2014	7/1/2011	1236
	SH 199_FTW_GR3_Parker	11/18/2014	7/1/2010	1601
Brownwood	US 67_BWD_GR4_Coleman	10/9/2014	7/1/2010	1561
	US 67_BWD_GR4_Brown	10/9/2014	7/1/2011	1196
	US 183_BWD_GR4_Eastland	10/9/2014	7/1/2012	830
	US 377_BWD_GR4_Brown	10/9/2014	7/1/2012	830
San Antonio	US 90_SAT_GR4_Bexar	3/11/2014	6/1/2013	283
	FM 1518_GR3_Bexar	3/11/2014	6/1/2013	283
	SH 16_SAT_GR4_Atascosa_TRM 626	3/12/2014	6/1/2012	649
	SH 16_SAT_GR 4_Atascosa_TRM 642	3/12/2014	6/1/2012	649
YKM	SH 36_YKM_GR 3_Austin	5/23/2013	8/1/2008	1756
Lufkin	US 59_LFK_GR3_Angelina	8/5/2013	6/1/2010	1161
	US 69_LFK_GR4_Angelina	8/5/2013	6/1/2012	430
	US 287_LFK_GR4_Trinity	8/16/2013	6/1/2013	76
	FM 2213_LFK_GR5_San Augustine	8/26/2014	6/1/2012	816
	US 59_LFK_GR4_Shelby	8/26/2014	6/1/2012	816
Odessa	LP 338_ODA_GR4_Ector	10/7/2013	6/1/2012	493
	US 385_ODA_GR4_Crane	10/7/2013	6/1/2009	1589
	US 385_ODA_GR4_Ector	10/7/2013	6/1/2010	1224
Beaumont	SH 82_BMT_GR4_Jefferson	10/1/2013	9/1/2010	1126
	FM 365_BMT_GR4_Jefferson	10/1/2013	7/1/2013	92
	FM 105_BMT_GR4_Orange	10/2/2013	7/1/2013	93
Atlanta	US 80_ATL-GR4_Harrison	12/19/2013	6/1/2012	566
	US 59_ATL_GR3_Cass_RG_TRM238	12/19/2013	6/1/2013	201
	SH 77_ATL_GR4_Cass_TRM 745_SS	12/19/2013	6/1/2012	566
	SH 77_ATL_GR4_Cass_TRM 720_RG	12/19/2013	6/1/2013	201

## MEASUREMENTS OF FRICTION CHARACTERISTICS

Field testing primarily included measurements of friction using the DFT, MPD using the CTMeter, and skid numbers using the TxDOT's skid trailer. Figure 24 shows a layout of the test section used by the TTI researchers when taking CTMeter and DFT measurements in the field. The CTMeter device was used to measure the MPD, while the DFT was used to measure the coefficient of friction at different speeds (20, 40, 60, and 80 km/h). During testing, the CTMeter and DFT devices were always positioned in the left wheel path of the outside lane. Six locations were tested in each section. Two locations were on the shoulder, and four locations were on the outer lane. Two DFT and six CTMeter readings were performed at each location. In some cases, where there was no shoulder, the researchers took CTMeter and DFT measurements between the wheel path to represent the initial skid values.

Figure 25 shows typical field operations at different locations and districts in Texas. Figure 26 shows an example of DFT measurements on a seal coat test section. One can notice, as expected, that the shoulder had a higher coefficient of friction ( $\mu$ ) compared to wheel path (WP) and between wheel paths (BWP). Note that the area between wheel paths also experiences some polishing due to vehicle lane changes and wheel wandering. The coefficient of friction between wheel paths was close to the coefficient of friction at the shoulder. Figure 27 shows an example of DFT measurements for a Type D asphalt mixture test section. The shoulder had higher friction value compared to the wheel path because the latter experienced frequent polishing under traffic.

Measurements of macrotexture and friction were conducted on the outer lane since the skid number was measured by the skid trailer at the outside lane (in case of multiple lanes) on the left wheel path. Also, the outer lane experiences a higher polishing rate because most trucks and more vehicles use this lane.

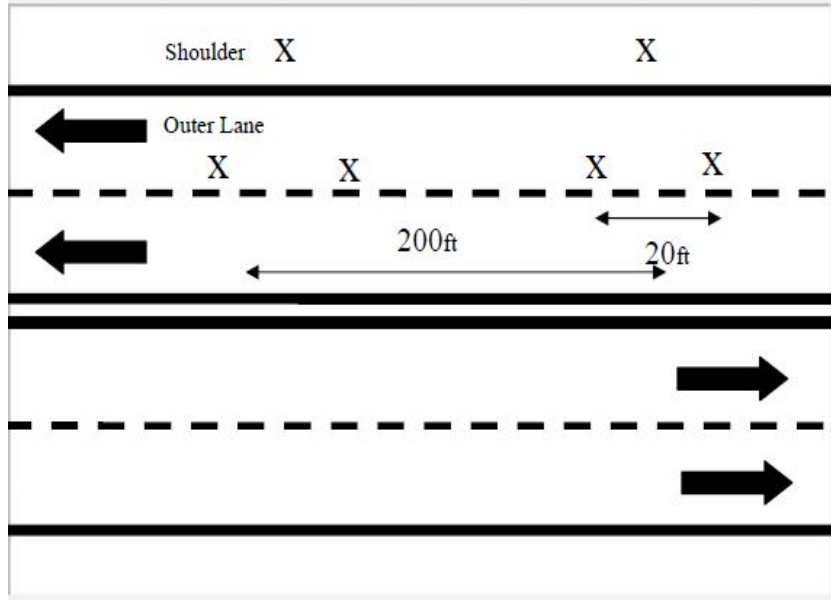


**Figure 24. Layout of Measurement Section.**



**Figure 25. Collecting Field Measurements.**



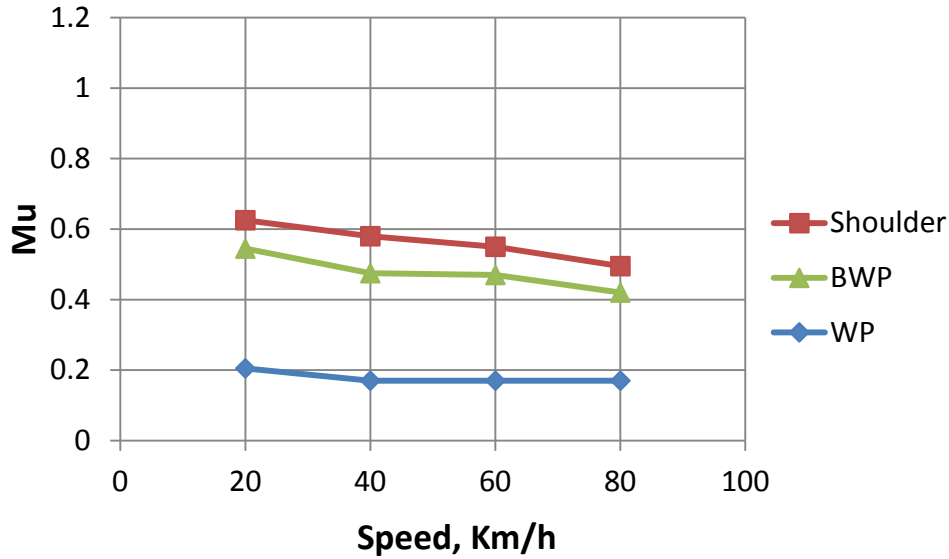


**Figure 26. DFT Measurements for Seal Coat Test Section (IH-35-LRD-NP-COT-S\_SealCoat).**

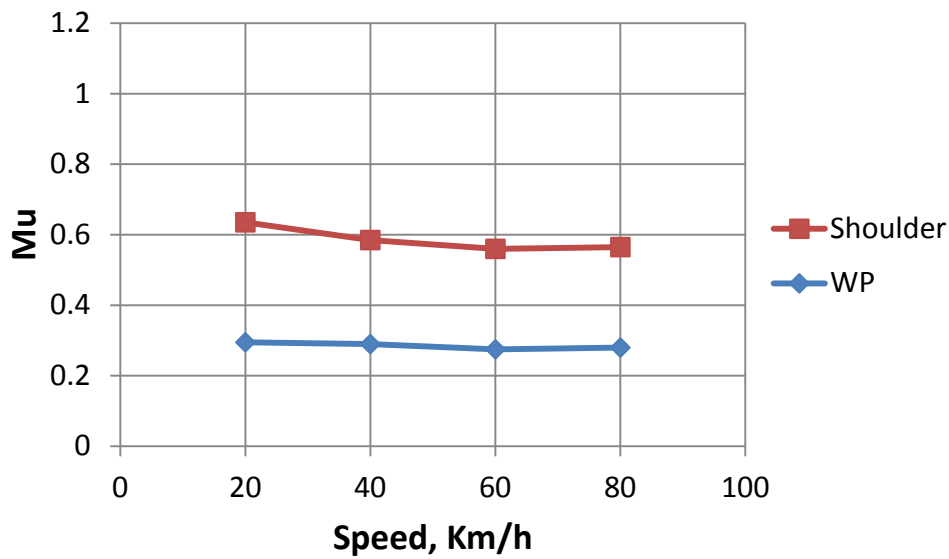


**Figure 27. DFT Measurements for Type D Asphalt Mix Test Section (SH-36-HMA\_TypeD).**

The results of the field testing on seal coat showed fair correlation between the MPD measured using the CTMeter and the coefficient of friction at 80 km/h ( $DFT_{80}$ ) measured using DFT, as shown in Figure 28. This relationship demonstrates that higher macrotexture (higher seal coat grade) would provide better friction. The researchers calculated the IFI using the mean profile depth and friction obtained from the field according to Equation 3.1.

$$IFI = 0.081 + 0.732 DFT_{20} \exp\left(\frac{-40}{S_p}\right) \quad (3.1)$$

$$S_p = 14.2 + 89.7 MPD \quad (3.2)$$

where

MPD = mean profile depth measured using the CTMeter.

DFT<sub>20</sub> = coefficient of friction at 20 km/h measured using DFT.

The researchers found good correlation between the IFI (Equation 3.1) and DFT<sub>80</sub> measured using the DFT, as shown in Figure 29.

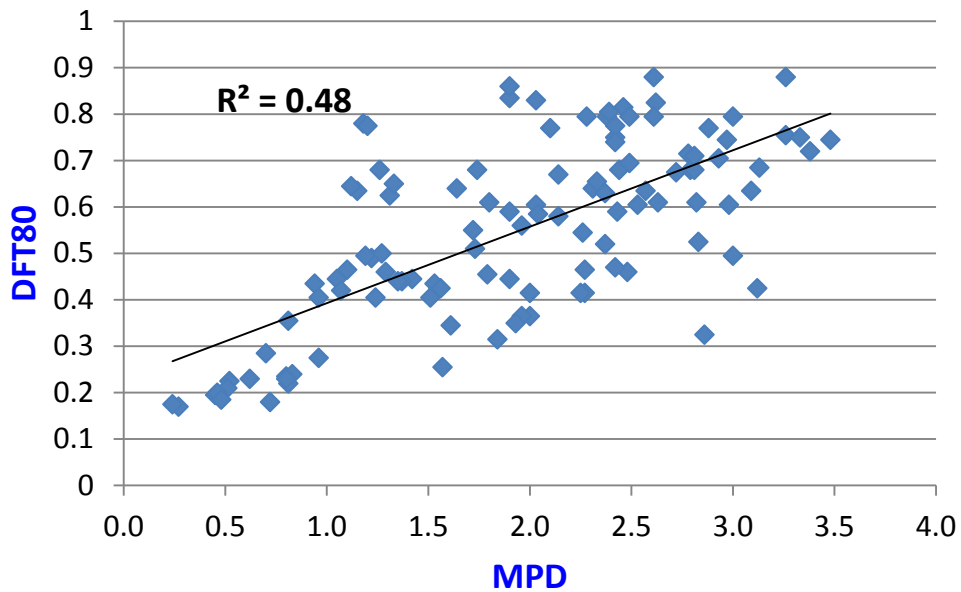


**Figure 28. Correlation between MPD and Coefficient of Friction at 80 km/h (DFT<sub>80</sub>) for Seal Coat Test Sections.**

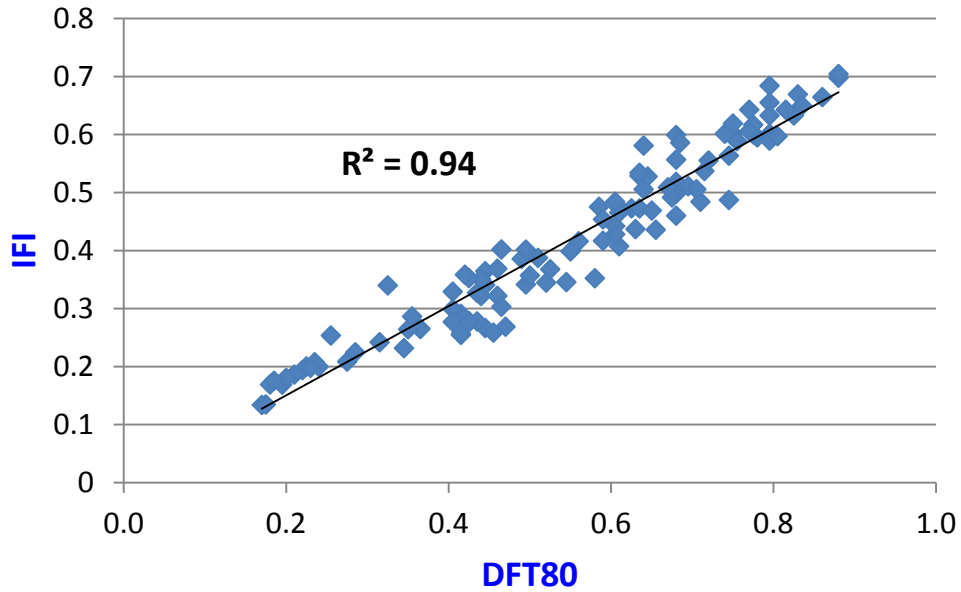


**Figure 29. Correlation between IFI and Coefficient of Friction at 80 km/h (DFT<sub>80</sub>) for Seal Coat Test Sections.**

The results of the field testing on asphalt mixture test sections showed no correlation between MPD measured using the CTMeter and DFT<sub>80</sub> measured using DFT, as shown in Figure 30. However, fair correlation was found between IFI and DFT<sub>80</sub>, as shown in Figure 31.

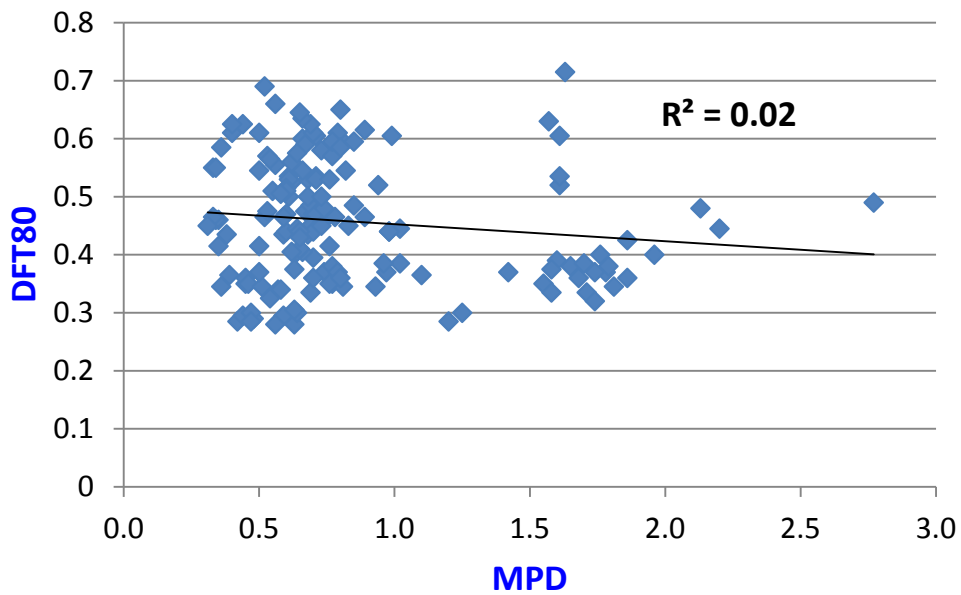


**Figure 30. Correlation between MPD and Coefficient of Friction at 80 km/h (DFT<sub>80</sub>) for Hot Mix Asphalt Test Sections.**

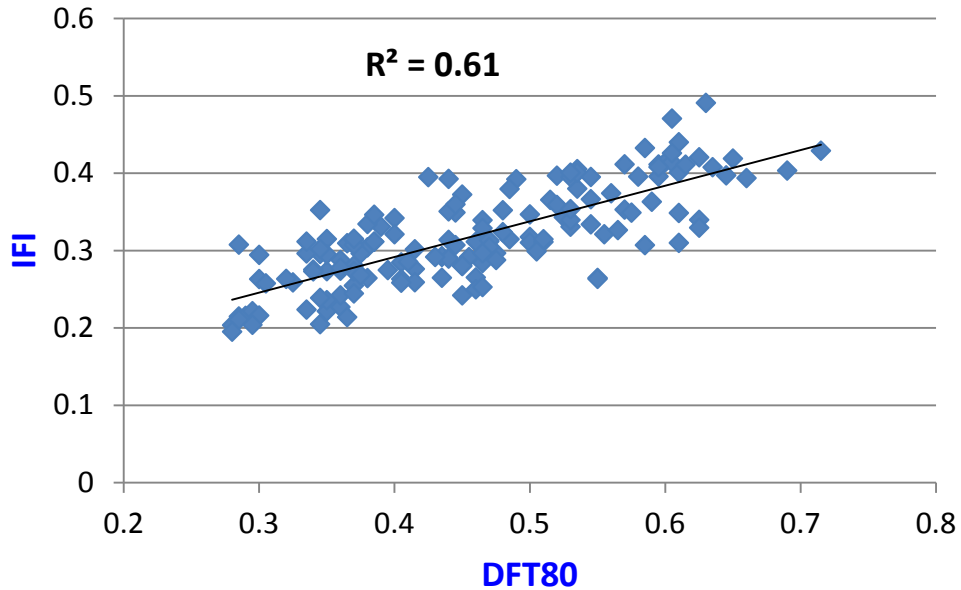


**Figure 31. Correlation between IFI and DFT<sub>80</sub> for Hot Mix Asphalt Test Sections.**

The fair correlation observed between IFI and DFT<sub>80</sub> is expected since the IFI is a function of DFT<sub>20</sub>, and DFT<sub>20</sub> has typically good correlation with DFT<sub>80</sub>. The main purpose of presenting Figure 29, Figure 31, Figure 32, and Figure 33 is to demonstrate the range of values for both IFI and DFT<sub>80</sub> in HMA and seal coat surfaces. Figure 32 shows the IFI versus DFT<sub>80</sub> measured using DFT for some seal coat test sections (blue data points) and asphalt mixture test sections (red data points) examined in this project. It can be seen from Figure 32 that, in general, the seal coat had higher friction compared to asphalt mixtures. However, the seal coat had a wider range of friction values compared to asphalt mixtures. Figure 33 shows the surface conditions of some of the examined asphalt mixture. The PFC had higher macrotexture and friction than the Type D mixture.



Pavement surface at the shoulder of a seal coat test section



Pavement surface at the wheel path of a seal coat test section

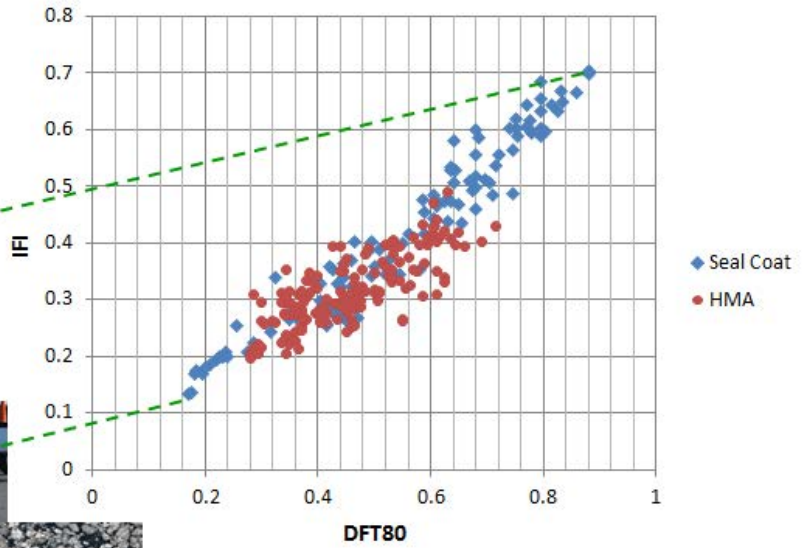


**Figure 32. Correlation between IFI and  $DFT_{80}$  for Hot Mix Asphalt and Seal Coat Test Sections and Pavement Surface Condition for Seal Coat Test Sections.**

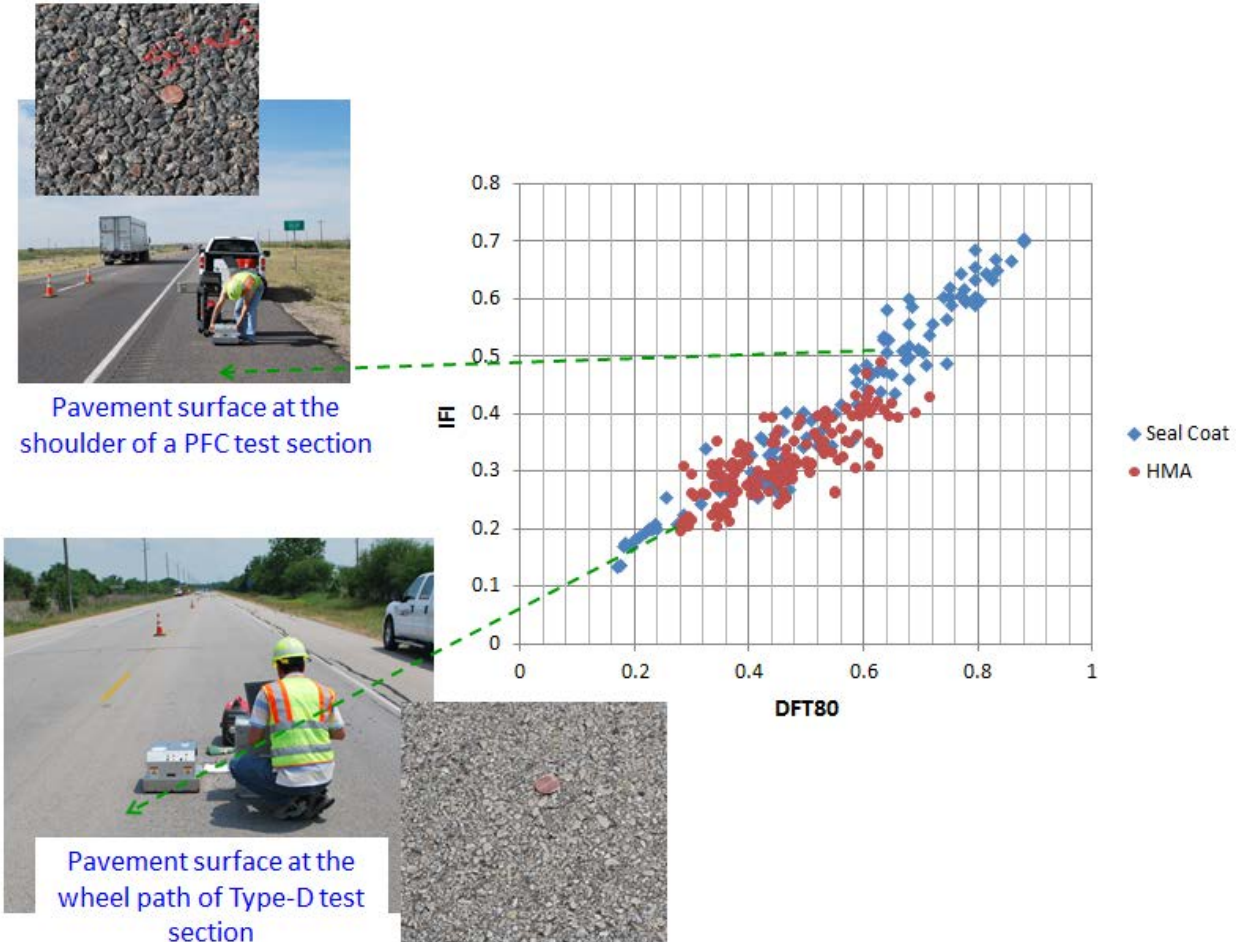


**Figure 33. Correlation between IFI and  $DFT_{80}$  for Hot Mix Asphalt and Seal Coat Test Sections and Pavement Surface Condition for Asphalt Mixture Test Sections.**

## AGGREGATE CHARACTERIZATION

Under this subtask, the researchers used the AIMS and Micro-Deval devices to measure an aggregate's resistance to polishing and abrasion. The AIMS was used to quantify the aggregate's texture and angularity before and after polishing by the Micro-Deval apparatus. Figure 34 illustrates the procedure followed in this study for measuring aggregate texture and angularity and its resistance to polishing and abrasion. Both the texture and angularity of aggregates decrease over time when polished in the Micro-Deval test. The loss of texture can be described using only three data points: texture measured before the Micro-Deval test, texture measured after 105 min, and texture measured after 180 min of polishing in the Micro-Deval test. Figure 35 shows an example of loss in aggregate texture and angularity as a result of Micro-Deval abrasion and polishing of virgin aggregates.

Mahmoud et al. (2007) and Kassem et al. (2013) suggested using Equations 3.3 and 3.4 to describe the change in aggregate texture and angularity as a function of polishing time in Micro-Deval:

$$TX(t) = a_{TX} + b_{TX} * e^{(-C_{TX}*t)} \quad (3.3)$$

$$GA(t) = a_{GA} + b_{GA} * e^{(-C_{GA}*t)} \quad (3.4)$$

where

TX (t) = change in texture as a function of time (min).

$a_{TX}, b_{TX}, C_{TX}$  = aggregate texture regression constants.

t = polishing time in Micro-Deval.

GA (t) = change in angularity as a function of time (min).

$a_{TX}, b_{TX}, C_{TX}$  = aggregate angularity regression constants.

t = polishing time in Micro-Deval.

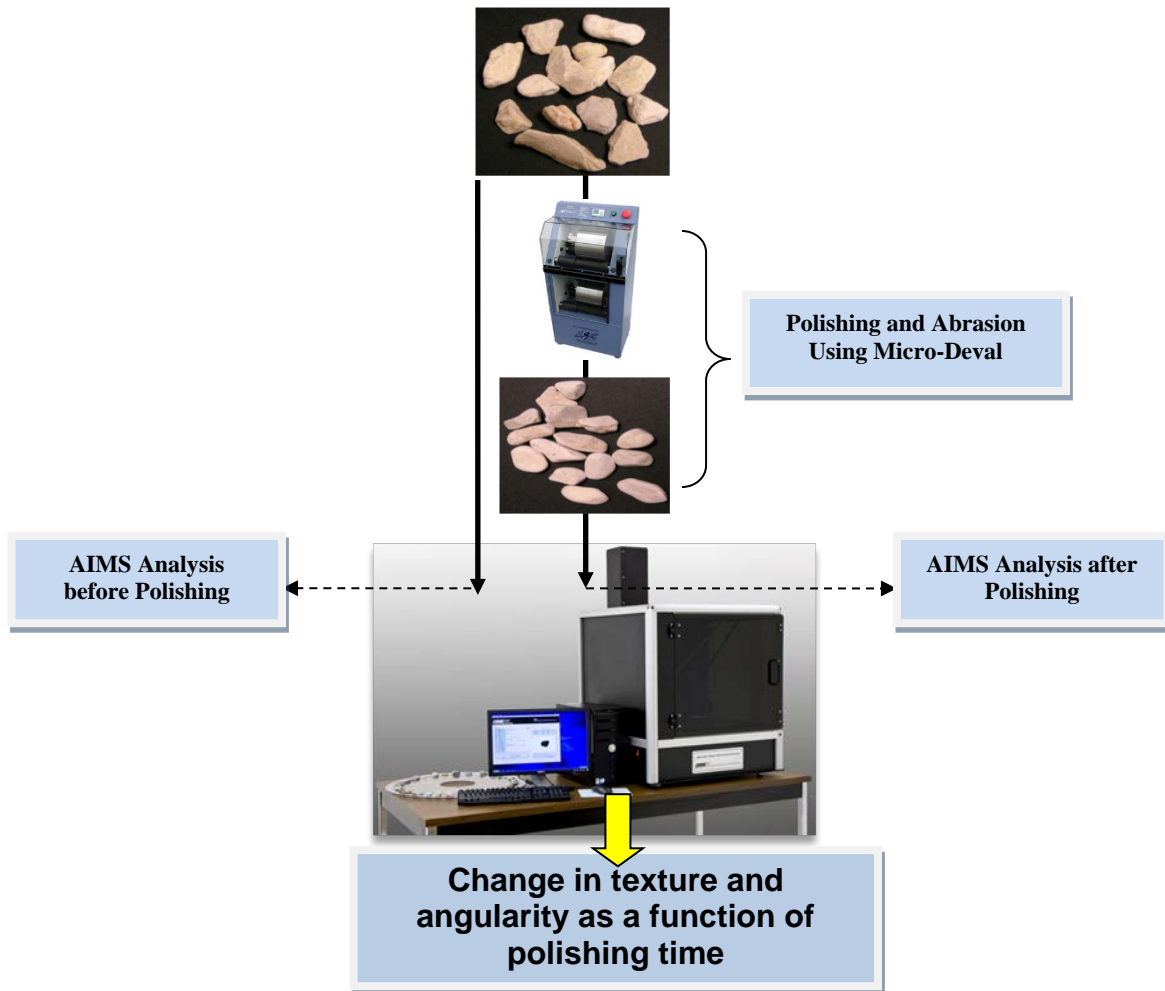


**Figure 34. Procedure for Measuring Aggregate Texture and Its Resistance to Polishing.**



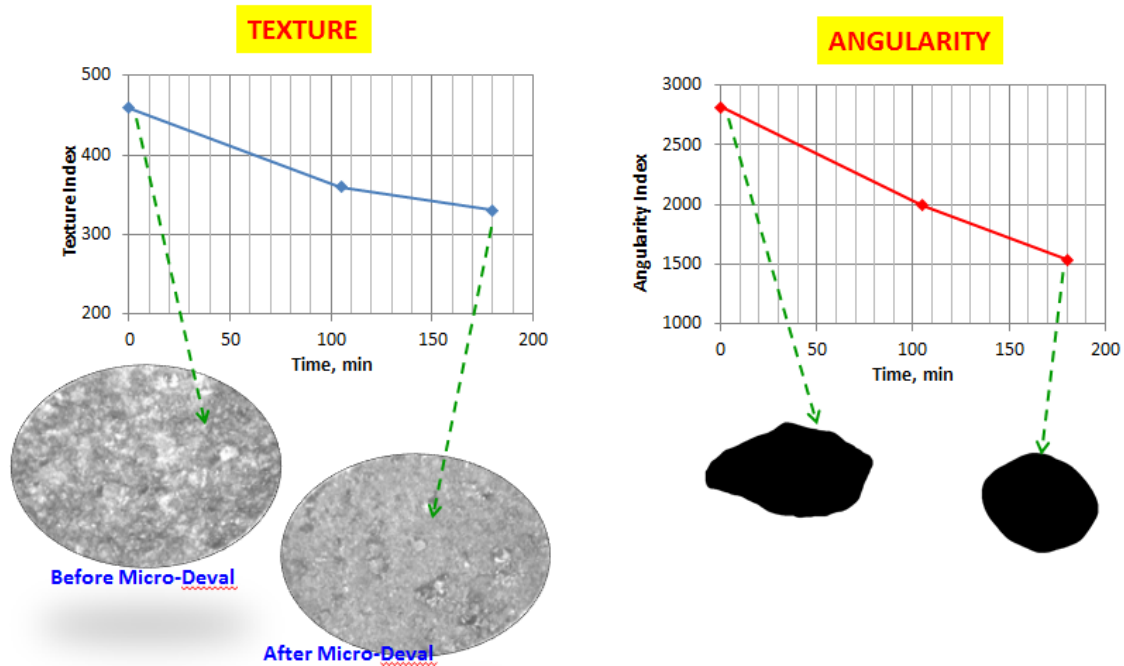


**Figure 35. Loss in Aggregate Texture and Angularity as a Result of Micro-Deval Abrasion and Polishing of Virgin Aggregates.**

### AGGREGATE GRADATION PARAMETERS

Masad et al. (2010) indicated that aggregate gradation is a fundamental factor that affects skid resistance. Masad et al. (2010) and Kassem et al. (2013) used the cumulative two-parameter Weibull distribution (Equation 3.5) to describe the aggregate gradation. The Weibull distribution function (Equation 3.5) is used to fit the aggregate size distribution, and both scale ( $\lambda$ ) and shape ( $\kappa$ ) parameters were used to quantify the aggregate gradation.

$$F(x, \lambda, \kappa) = 1 - e^{-\left(\frac{x}{\lambda}\right)^\kappa} \quad (3.5)$$

where

$x$  = aggregate size in millimeters.

$\lambda, \kappa$  = scale and shape parameters of Weibull distribution.

### SKID NUMBER MEASUREMENTS

Skid number data used in this study were obtained from two sources: TxDOT's annual network-level data collection and TTI's project level measurement. Each year, TxDOT periodically measures the skid number for all its highways, although at different intervals for

different highways. The research team obtained the data from TxDOT’s PMIS database. TxDOT’s PMIS database typically stores the skid number data for each of the PMIS sections, which are typically 0.5 mile long. The length of test sections included in this study varied from 2 miles to a little over 15 miles. TxDOT measures the skid number using a skid trailer with a smooth tire according to ASTM E 274’s “Standard Test Method for Skid Resistance of Paved Surfaces Using a Full-Scale Tire.” The left tire is locked to measure the skid number at 50 mph (80 km/h). The skid number is measured at the outside lane (in case of multiple lanes) on the left wheel path. The pavement sections are typically classified after 5 years of service based on the measured skid number by a skid trailer at 50 mph, as presented in Table 5.

**Table 5. Aggregate Classification Based on the SN.**

Aggregate Class	SN Values
High	$SN(50) \geq 30$
Medium	$21 \leq SN(50) < 30$
Low	$SN(50) < 21$

The SN can be measured as a function of IFI and speed constant parameter, according to Equation 3.6 (ASTM E 274).

$$IFI = 0.045 + 0.925 \times 0.01 \times SN(50)e^{\frac{20}{S_p}} \quad (3.6)$$

where

SN(50) = skid number measured by a smooth tire at 50 mph (80 km/h).

IFI = international friction index.

$S_p$  = speed constant parameter.

Figure 36 shows measuring the skid number using the skid trailer. When using the skid trailer, water is sprayed in front of the left wheel and the left wheel is locked while the truck is traveling at a certain speed (e.g., 50 mph in Texas). The friction force that resists the rotation of the tire is measured (Masad et al. 2010).



**Figure 36. Locked-Wheel Skid Trailer.**

## **DATA COLLECTION**

Besides the field testing, the researchers made significant effort in collecting relevant data from different districts, divisions, and databases. Some of the data collection efforts were made during the selection of test sections and others were made throughout the duration of this research project. Following paragraphs will briefly describe the data collection process for the three major components of data used in this study.

### **Skid from PMIS**

Majority of the skid data used in this study was obtained from TxDOT's PMIS database. TxDOT collects the skid data of its entire highway network annually, albeit at different frequencies based on highway types. Some districts collect skid data more often than others. The research team made an effort to gather and record the date of skid testing accurately. Based on the length of the test section (limits of the project), test section has somewhere 4 to 30 PMIS sections. So, for a given year, test sections had 4 to 30 skid data points. Most cases, the research team used the median of these available skid numbers as that section's skid value for that particular year. Careful study of this skid data resulted in the exclusion of some numbers due to their obvious irregularities. Besides obtaining skid data from the PMIS database, the researchers also measured the skid value using TTI's own equipment to supplement the historical data.

## **Construction Data**

During the selection of test sections the research team made sure that the selected sections have necessary information available. The major construction related data gathered included data of construction (paving of surface layer), location, project limits, mixture type and gradations, seal coat grade, aggregate sources. Sometimes approximate date was determined when the exact month of paving was not known. For Example, if the paving was done in Fall of 2011, the research team entered the date of construction as September 01, 2011. The research team also obtained and recorded relevant other construction data from the respective district personnel.

## **Traffic Data**

Traffic data obtained for the test sections include AADT, percent truck traffic for the entire duration of its service life starting from the year of construction. Other relevant data included the number through lanes, whether the highway was divided or undivided, and characterization of highway segment whether it was located predominantly rural or urban area. AADT obtained from TxDOT's PMIS database was considered as number of AADT per roadbed. Accordingly, AADT for undivided highway was considered as summation of traffic on all the lanes in both directions. Whereas, AADT for divided highway was considered as summation of traffic for all the lanes in each direction. Average AADTs over the years during the test sections' service life was used for the calculation.

Most challenging aspect of traffic calculation was the distribution of traffic on design lane. Lane distribution factors for both passenger vehicles and truck traffic were considered as 0.5 for undivided highway with one lane in each direction. There are no available data in literature to show the distribution of passenger vehicles and truck traffic on design lane based on different multi-lane highway configurations (e.g. number of lanes in one direction) and its location in urban or rural area. The research team came with following lane distribution factors based on some internal studies done by TxDOT, and some traffic data collected by weigh-in-motion device under different research projects.

## **SUMMARY**

Chapter 3 discusses the research plan and selection of HMA and seal coat test sections. About 35 HMA and 35 seal coat test sections were selected, which were distributed across Texas. These test sections, which were in the field, were constructed using different materials and mix design and were subject to different traffic levels. The researchers measured the surface frictional characteristics of the test sections using DFT and CTMeter; in addition, a skid trailer was used to measure the skid number. In the laboratory, the researchers used methods to characterize the resistance of test aggregates to abrasion and polishing and quantify the aggregate shape characteristics (texture and angularity). These data were used for model developments, as discussed in Chapters 4 and 5. This chapter also documents data collection effort.



## **CHAPTER 4: DATA ANALYSIS AND RESULTS FOR HOT MIX ASPHALT TEST SECTIONS**

Researchers in this study developed a skid prediction model for HMA and seal coat surfaces. The prediction models were developed using aggregate properties, field measurements, and traffic data. This chapter focuses on the development and validation of a prediction model for HMA pavements. Figure 37 shows the flowchart used for developing the predictive models for the skid resistance of HMA and seal coat surfaces. This effort included laboratory measurements of aggregate shape characteristics and their resistance to abrasion and polishing. The researchers used relationships to describe the change in aggregate texture and angularity due to abrasion and polishing. They also used mathematical models to describe the aggregate gradations for asphalt mixture and seal coat. Statistical methods were used to develop prediction models for friction and the skid resistance of HMA. The following subchapters describe how model parameters were obtained/measured and how they were used to develop the prediction models.

### **ANALYSIS OF AGGREGATE GRADATION**

The cumulative two-parameter Weibull distribution was used to describe the aggregate gradation, as shown in Equation 3.5. The MATLAB program was used to fit the Weibull function to aggregate size distribution. Figure 38 shows an example of Weibull functions for various aggregate gradations. The x-axis represents the aggregate size in millimeters, and the y-axis represents the cumulative percent passing of the aggregate. The scale ( $\lambda$ ) and shape parameters ( $\kappa$ ) were calculated by fitting the aggregate gradation to the cumulative two-parameter Weibull distribution. Table 6 presents the scale ( $\lambda$ ) and shape ( $\kappa$ ) parameters for the aggregate gradations for all the mixtures used in developing the HMA skid prediction model. The  $\lambda$  parameter varied from 10.95 to 2.899, while the  $\kappa$  parameter varied from 4.30 to 0.69. The r-squared values for fitting the Weibull function to the aggregate gradations were between 0.92 to 0.99. Higher values of  $\lambda$  were associated with coarser aggregate gradations, as presented in Figure 38. The research team also calculated these two parameters to describe the shape factor for all common mixture gradations used in Texas. Typically, the aggregate gradations running

through the middle of the bands (allowed by TxDOT), for given mixture type, was used to calculate the default shape parameters.

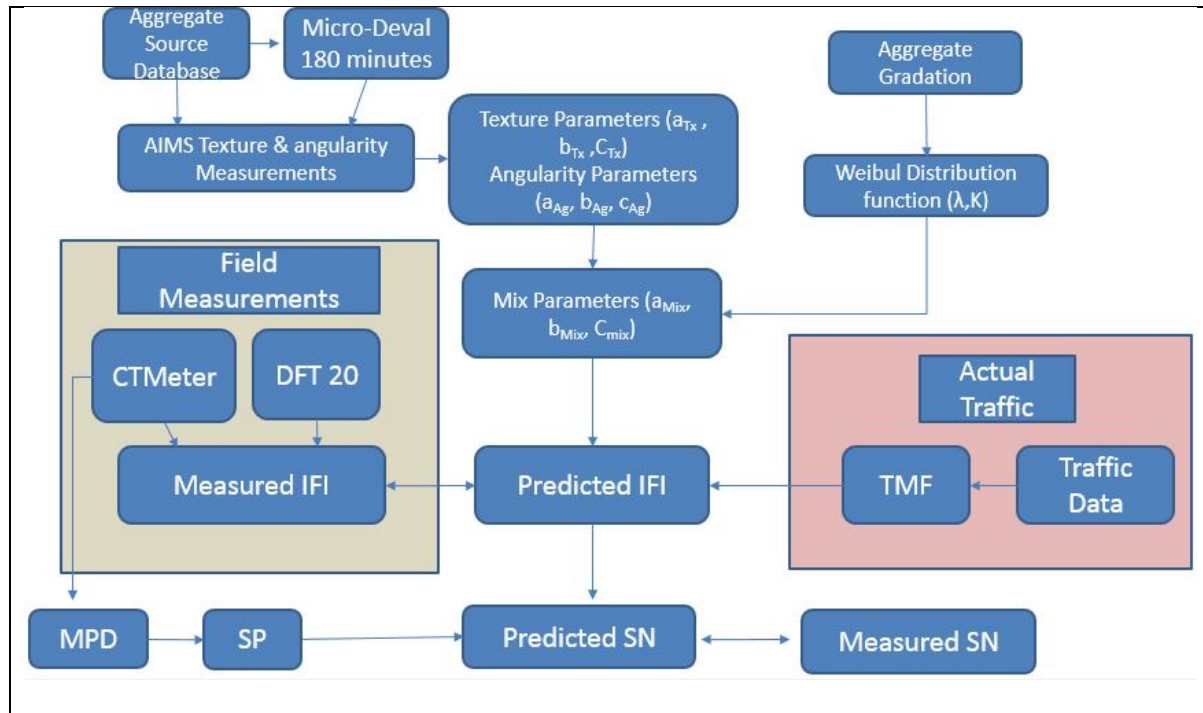


Figure 37. Flow Chart of the Research Methodology.

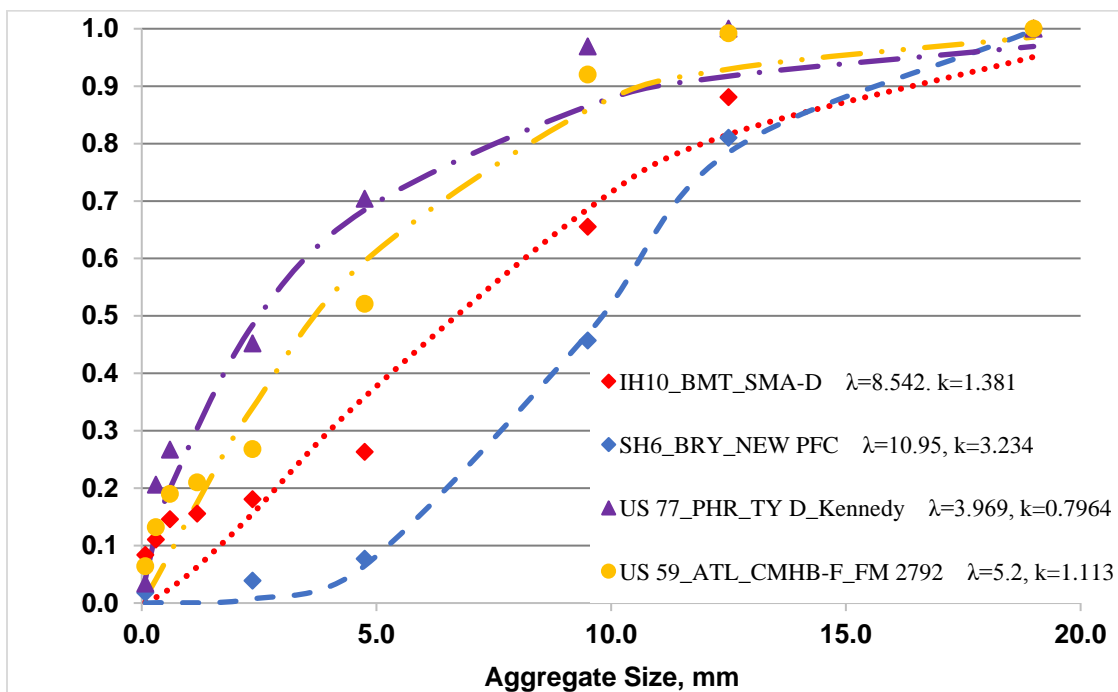


Figure 38. Weibull Distribution Function for Different Aggregate Sizes.



## **ANALYSIS OF AGGREGATE TEXTURE AND ANGULARITY**

A total number of 56 different aggregate type/sources were examined in this study. The aggregate shape characteristics were measured using the AIMS device for three different levels of polishing by the Micro-Deval device: (a) before Micro-Deval (BMD), or without any polishing; (b) after 105 min of polishing (AMD105); and (c) after 180 min of polishing (AMD180). However, the common practice at TxDOT is to measure the aggregate shape/texture characteristics before and after the Micro-Deval abrasion test (0 and 105 min). When developing the analytical models, the researchers considered both procedures to describe the change in angularity and texture of aggregates due to abrasion and polishing. Figure 39 and Figure 40 show examples of change in texture and angularity.

One can see that the loss of texture and angularity is significant after 105 min of polishing in the Micro-Deval. After that amount of time, polishing occurs at a much slower rate. Equations 3.3 and 3.4 were used to describe the change in aggregate texture and angularity, respectively. Figure 41 and Figure 42 show examples of the change in texture and angularity with the Micro-Deval polishing time. Figure 41 and Figure 42 report the regression constants of Equations 3.3 and 3.4 for the change in texture and angularity, respectively.

**Table 6. Scale and Shape Parameters of the Weibull Distribution.**

State	Section ID	Scale Parameter, $\lambda$	Shape Parameter, k	Coefficient of Correlation, $R^2$
Atlanta	IH 30_ATL_SMA_	5.47	1.03	0.94
	US 59_ATL_CMHB-F_FM 2792	5.20	1.11	0.96
	US 59_ATL_TY D_TRM 310	4.34	0.88	0.96
	US 59_ATL_TY D_SHELBY CO LINE	4.46	0.88	0.96
	US 271_ATL_CMHB-F_CAMP	5.20	1.21	0.95
Austin	IH 35 TOM Mix_AUS	4.96	1.44	0.97
	RM 3238_AUS_TOM	3.13	0.97	0.98
	US71_AUS_TOM	5.49	1.59	0.96
Beaumont	IH10_BMT_SMA-D	8.54	1.38	0.94
	SH 82_BMT_SMA-D	8.08	1.07	0.93
	SL 207_BMT_TY D	3.64	0.89	0.97
	US 69_BMT_PFC	10.26	2.45	0.99
	US 90_BMT_SMA-D	8.18	1.18	0.94
Bryan	IH 45_BRY_TY C	5.20	0.90	0.99
	IH 45_BRY_PFC	10.60	4.30	0.99
	SH 6_BRY_NEW PFC	10.95	3.23	0.99
	SH 6_BRY_OLD PFC	10.95	3.23	0.99
Laredo	IH 35_LRD_SMA_WEBB	7.96	1.57	0.96
	IH 35_LRD_SMA-C_LASALLE	9.82	1.56	0.95
Lufkin	US 59_LFK_PFC_Nacodoches	10.50	2.83	0.99
	SH 7_LFK_TY D_Houston	5.82	0.83	0.98
Odessa	IH 20_ODA_SP-C_Martin	5.10	1.03	0.98
	IH 20_ODA_SP-D_Midland_2012	4.76	0.99	0.98
	IH 20_ODA_SP-D_Midland_2013	4.79	0.97	0.97
	US 385_ODA_CMHB-F	5.39	1.65	0.98
	IH 20_ODA_PFC_2004	5.39	1.65	0.98
San Antonio	IH 10_SAT_SMA-D_BEXAR	9.37	1.41	0.92
	IH 10_SAT_TY C_BEXAR	5.10	0.73	0.97
	IH 37_SAT_PFC_BEXAR	10.51	2.99	0.99
YKM	IH 10_YKM_TY D_AUSTIN	3.96	0.85	0.96
	SH 36_YKM_TY D_AUSTIN	4.33	0.92	0.98
Pharr	US 77_PHR_TY D_Kennedy	3.96	0.79	0.98
	US 281_PHR_TY D_Hidalgo	3.81	0.77	0.97
Houston	SH 6 Bwp 2-1, Wp 2-1 Middle	4.85	0.93	0.98
	SH 6 Bwp 2-1 Bottom	2.89	0.69	0.96

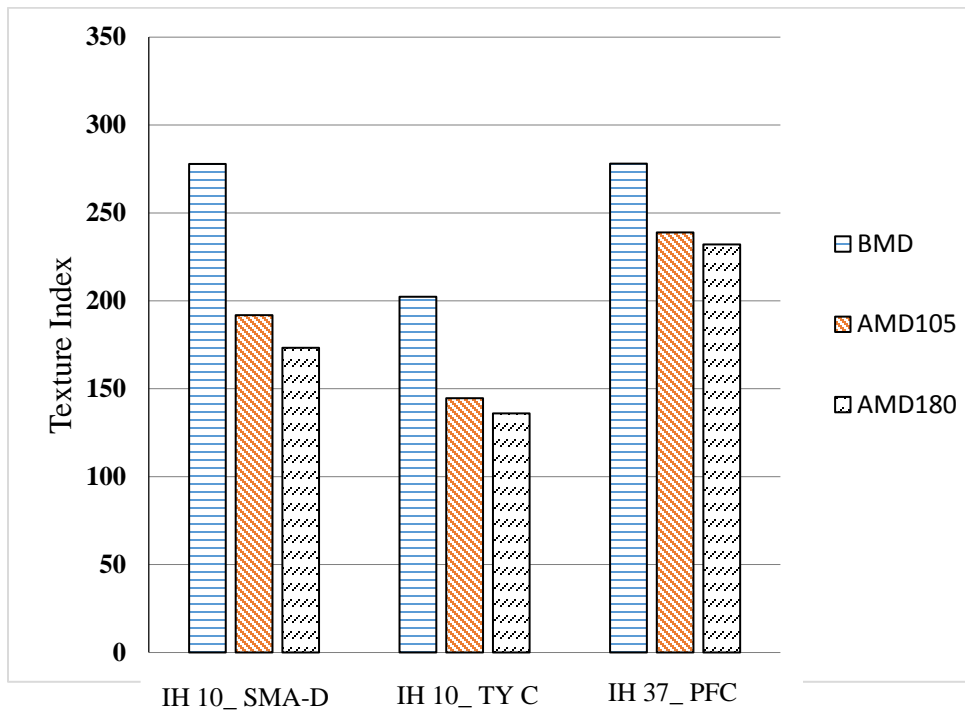


**Figure 39. Texture Indices of Sections in San Antonio.**

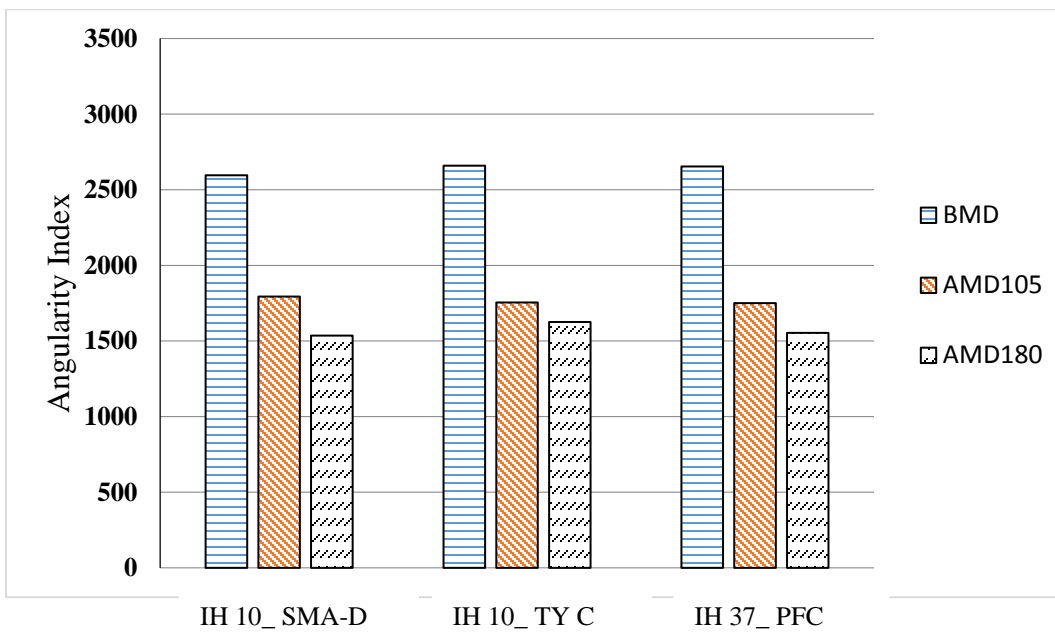


**Figure 40. Angularity Indices of Sections in San Antonio.**

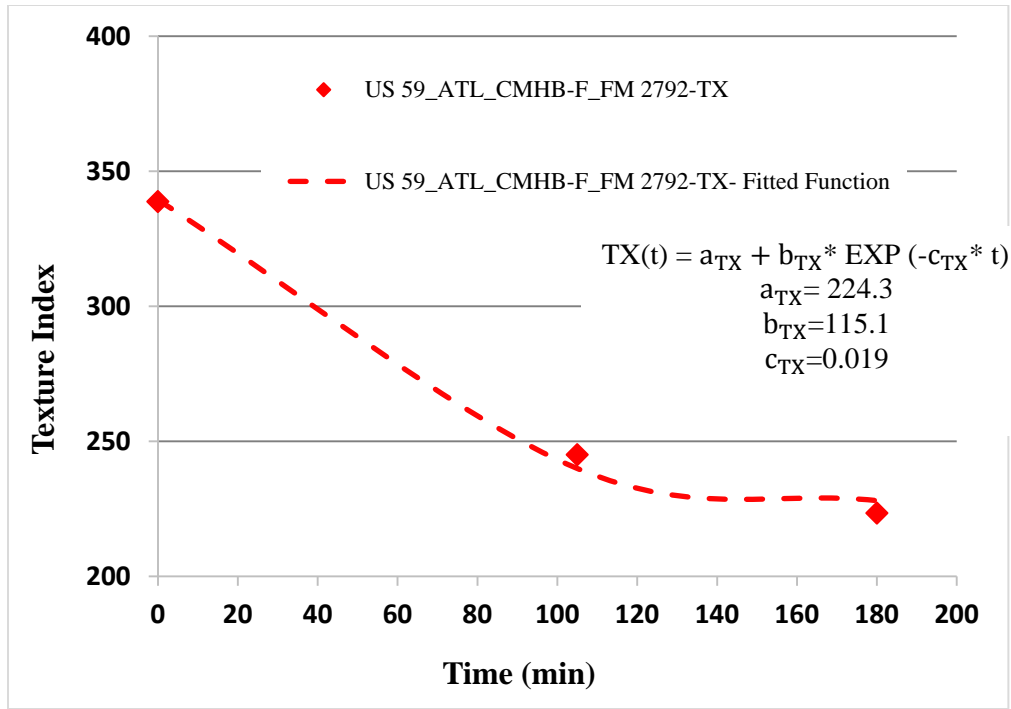


Figure 41. Regression Constants for Aggregate Texture.

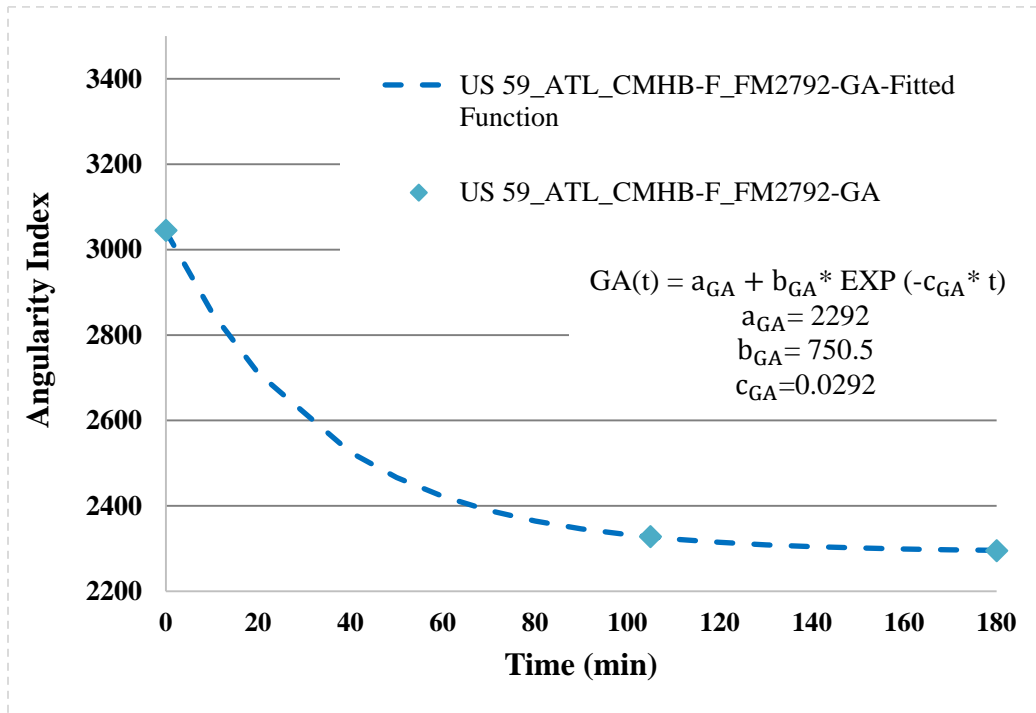


Figure 42. Regression Constants for Aggregate Angularity.

Determining the regression constants in Equations 3.3 and 3.4 requires three points of texture or angularity indices. The researchers used nonlinear regression analysis to predict the regression constants in Equations 3.3 and 3.4 using only two points of texture or angularity

indices (BMD and AMD105), which is the standard practice at TxDOT. Sixteen aggregate sources were used in the regression analysis to develop equations to predict initial measurements, terminal measurements, and rate of change of texture and angularity. SPSS software was used for the regression analysis. Equations 4.1 through 4.5 determine the regression parameters for texture loss using two measurements: BMD and BMD105.

- Texture coefficients:

$$a_{TX} + b_{TX} = 0.999BMD + 0.438 \quad (R^2 = 1) \quad (4.1)$$

$$a_{TX} = 0.864AMD + 14.985 \quad (R^2 = 0.949) \quad (4.2)$$

$$c_{TX} = \frac{0.492+TL}{59.506-(7.106 \times ARI)} \quad (R^2 = 0.60) \quad (4.3)$$

$$TL = \frac{BMD-AMD}{AMD} \quad (4.4)$$

$$ARI = \frac{AMD/BMD}{1-\left(\frac{AMD}{BMD}\right)^2} \quad (4.5)$$

where

$a_{TX} + b_{TX}$  = initial texture index.

$a_{TX}$  = terminal texture index.

$c_{TX}$  = rate of change in texture.

BMD, AMD = texture index before and after 105 min polishing in Micro-Deval.

TL, ARI = texture loss and aggregate roughness index, respectively.

Equations 4.6 through 4.10 determine the regression parameters for angularity change based on two measurements: BMD and BMD105.

- Angularity coefficients:

$$a_{GA} + b_{GA} = 0.999BMD + 2.646 \quad (R^2 = 1) \quad (4.6)$$

$$a_{GA} = 1.237AMD - 699.759 \quad (R^2 = 0.95) \quad (4.7)$$

$$c_{GA} = \frac{1.891+TL}{111.658+(1.081 \times ARI)} \quad (R^2 = 0.61) \quad (4.8)$$

$$TL = \frac{BMD - AMD}{AMD} \quad (4.9)$$

$$ARI = \frac{AMD/BMD}{1 - \left(\frac{AMD}{BMD}\right)^2} \quad (4.10)$$

where

$a_{GA} + b_{GA}$  = initial angularity index.

$a_{GA}$  = terminal angularity index.

$c_{GA}$  = rate of change in angularity.

BMD, AMD = angularity index before and after 105 min polishing in Micro-Deval.

TL, ARI = Angularity loss and aggregate roughness index, respectively.

Table 7 presents the regression coefficients of Equations 3.3 and 3.4 that describe the change in aggregate texture and angularity for all test aggregates evaluated in HMA test sections.

**Table 7. Regression Parameters of Aggregate Texture and Angularity.**

State	Section ID	Texture Parameters			Angularity Parameters		
		$a_{TX}$	$b_{TX}$	$c_{TX}$	$a_{GA}$	$b_{GA}$	$c_{GA}$
Atlanta	IH 30_ATL_SMA_	137.71	75.16	0.0200	2008	702.81	0.0190
	US 59_ATL_CMHB-F_FM 2792	224.32	115.12	0.0190	2292	750.52	0.0292
	US 59_ATL_TY D_TRM 310	218.13	122	0.0220	2267	786	0.0159
	US 59_ATL_TY D_SHELBY CO LINE	219.21	120.91	0.0190	2265	786.41	0.0159
	US 271_ATL_CMHB-F_CAMP	181.81	174.12	0.0175	1902	583.22	0.0273
Austin	IH 35 TOM Mix_AUS	226.45	103.27	0.0176	1565.35	1063.03	0.0206
	RM 3238_AUS_TOM	231.39	100.01	0.0173	1545.21	1104.08	0.0208
	US71_AUS_TOM	226.28	103.38	0.0176	1566.02	1061.67	0.0206
Beaumont	IH10_BMT_SMA-D	272.21	43.37	0.0180	2587.22	429.82	0.0175
	SH 82_BMT_SMA-D	241.11	136.72	0.0187	2586.64	503.47	0.0178
	SL 207_BMT_TY D	191.83	62.16	0.0230	1919	734	0.0296
	US 69_BMT_PFC	201.37	58.70	0.0172	2110.16	536.56	0.0179
	US 90_BMT_SMA-D	188.64	84.95	0.0177	1607.38	1029.71	0.0204
Bryan	IH 45_BRY_TY C	190.07	93.70	0.0181	1825.43	885.69	0.0195
	IH 45_BRY_PFC	129.29	64.01	0.0181	1307.11	1404.99	0.0227
	SH 6_BRY_NEW PFC	230.85	100.36	0.0168	1547.44	1099.53	0.0208
	SH 6_BRY_OLD PFC	230.85	100.36	0.0168	1547.44	1099.53	0.0208
Laredo	IH 35_LRD_SMA_WEBB	176.86	64.22	0.0175	1466.88	1254.77	0.0217
	IH 35_LRD_SMA-C_LASALLE	227.46	216.73	0.0171	1753.70	1118.91	0.0207
Lufkin	US 59_LFK_PFC_Nacodoches	231.84	115.82	0.0230	2300	786.20	0.0163
	SH 7_LFK_TY D_Houston	223.05	77.28	0.0170	2010.51	852.90	0.0193
Odessa	IH 20_ODA_SP-C_Martin	238.21	128.42	0.0190	1769	974.71	0.0179
	IH 20_ODA_SP-D_Midland_2012	219.52	122.51	0.0172	1706	1028	0.0167
	IH 20_ODA_SP-D_Midland_2013	226.11	116.22	0.0230	1706	1028	0.0167
	US 385_ODA_CMHB-F	282.19	145.36	0.0179	1774.20	993.70	0.0201
	IH 20_ODA_PFC_2004	282.19	145.36	0.0179	1774.20	993.70	0.0201
San Antonio	IH 10_SAT_SMA-D_BEXAR	172.96	105.33	0.0185	1252	1344	0.0207
	IH 10_SAT_TY C_BEXAR	133.52	68.87	0.0177	1576;	1083	0.0172
	IH 37_SAT_PFC_BEXAR	231.51	46.65	0.0178	1431	1223	0.0213
YKM	IH 10_YKM_TY D_AUSTIN	137.43	128.24	0.0180	1279	1374	0.0226
	SH 36_YKM_TY D_AUSTIN	66.84	51.81	0.0177	1558	1215	0.0277
PHARR	US 77_PHR_TY D_Kennedy	199.01	110.46	0.0188	2622.42	279.72	0.0166
	US 281_PHR_TY D_Hidalgo	177.10	121.52	0.0160	2615	189.83	0.0197
Houston	SH 6 Bwp 2-1, Wp 2-1 Middle	239.40	74.46	0.0172	2612.31	590.57	0.0182
	SH 6 Bwp 2-1 Bottom	239.41	74.46	0.0172	2612.31	590.57	0.0182

## DEVELOPMENT OF PREDICTIVE MODEL FOR IFI

Masad et al. (2010) and Kassem et al. (2013) developed IFI prediction models. The parameters for the IFI model developed by Masad et al. (2010) ( $a_{mix}$ ,  $a_{mix} + b_{mix}$ , and  $C_{mix}$ ), presented in Equations 2.7 through 2.9, relied on factors that describe aggregate texture and its resistance to abrasion and polishing, aggregate gradation, and number of polishing cycles in the laboratory. The parameters for the IFI model ( $a_{mix}$ ,  $a_{mix} + b_{mix}$ , and  $C_{mix}$ ) developed by Kassem et al. (2013), presented in Equations 2.11 through 2.13, used the same factors in addition to factors that describe the aggregate angularity. Kassem et al. (2013) demonstrated the measured IFI (Equation 2.2) and predicted IFI (Equation 2.6) using the parameters presented in Equations 2.11 through 2.13; Kassem et al.'s IFI model had better correlation because aggregate angularity is considered in addition to aggregate texture.

In this study, the models proposed by Kassem et al. (2013) were used and calibrated to fit the wide range of aggregates examined in this study. The model developed by Kassem et al. (2013) was based on a limited number of aggregate types (soft limestone, intermediate limestone, and sandstone). The study herein evaluated about 56 different aggregate types. The researchers used SPSS software in the IFI model development. Similar to Kassem et al.'s model (2013), the IFI model in this study included three analytical models for its parameters ( $a_{mix}$ ,  $a_{mix} + b_{mix}$ , and  $C_{mix}$ ). The  $a_{mix}$  presents the terminal IFI, the  $a_{mix} + b_{mix}$  presents the initial IFI, while  $C_{mix}$  presents the rate of change of the IFI. Equations 4.11 through 4.13 show the modified models.

$$a_{mix} = \frac{49.3144 + \lambda}{351.289 - 0.00193(AMD)^2} \quad (4.11)$$

$$a_{mix} + b_{mix} = 0.33 * \ln \left( \frac{1.43757 * (a_{TX} + b_{TX}) + 46.8933 * \lambda + 333.491 * k}{2.42031 * (a_{GA} + b_{GA})} \right) + 1.00801 \quad (4.12)$$

$$C_{mix} = 0.018 + 1.654C_{TX} + 1.346C_{GA} \quad (4.13)$$

where

$a_{mix}$  = terminal IFI.

$a_{mix} + b_{mix}$  = initial IFI.

$C_{mix}$  = rate of change in IFI.

$\lambda$ ,  $k$  = scale and shape parameters of Weibull distribution, respectively.



AMD = the texture after 150 min in Micro-Deval.

$a_{TX}, b_{TX}$  = regression constants for texture.

$a_{GA}, b_{GA}$  = regression constants for angularity.

$C_{TX}$  = rate of change in texture.

$C_{GA}$  = rate of change in angularity.

Equation 2.6 is a function of the number of polishing cycles in laboratory (N). Since the IFI models (Equations 4.11 to 4.13) were revised based on the traffic levels, a relationship developed by Masad et al. (2010) was used to convert the traffic level to a corresponding number of polishing cycles (N). This relationship is presented in Equation 4.14.

$$N = \text{TMF} \times 10^{\frac{1}{A+B \times c_{\text{mix}} + \frac{C}{c_{\text{mix}}}}} \quad (4.14)$$

where

N = number of polishing cycles in thousands.

A, B and C = regression coefficients (-0.452, -58.95,  $5.843 \times 10^{-6}$ ), respectively.

$c_{\text{mix}}$  = rate change in IFI.

TMF = traffic multiplication factor.

The TMF is calculated using Equation 4.15:

$$\text{TMF} = \frac{\text{Days between construction and field testing} \times \text{adjusted traffic}}{1000} \quad (4.15)$$

The adjusted traffic is calculated using Equation 4.16.

$$\text{Adjusted traffic} = \frac{\text{AADT} \times (100 - \text{PTT}) \times \text{DL}_{\text{AADT}}}{100} + \frac{\text{AADT} \times \text{PTT} \times \text{DL}_{\text{truck}} \times 20}{100} \quad (4.16)$$

where

AADT = average annual daily traffic for each section.

$\text{DL}_{\text{AADT}}$  = design lane factor of AADT (depends on number of lanes and urban/rural condition).

$\text{DL}_{\text{truck}}$  = design lane factor of trucks (depends on number of lanes and urban/rural condition).

PTT = percent truck traffic.

Figure 43 shows the correlation between the predicted and measured IFI. The data points in Figure 43 include the IFI measurements at the wheel path and at the shoulder or between the wheel path. Higher r-squared values indicate higher correlations between the predicted and measured IFI.

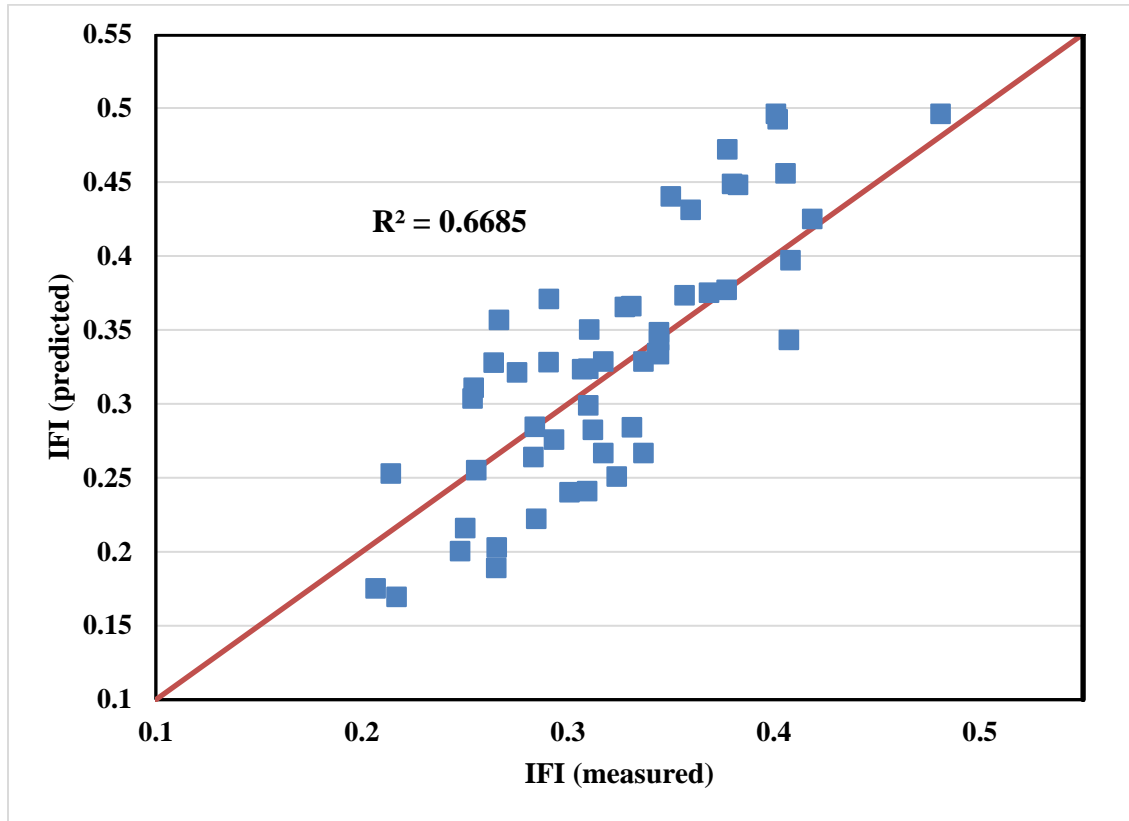


**Figure 43. Relationship between Predicted and Measured IFI.**

#### **ANALYSIS OF MEAN PROFILE DEPTH**

The researchers also developed a predictive model for MPD as a function of aggregate gradation and polishing cycles (or traffic level). The purpose of this model was to predict MPD if such information is not available for a given mixture. Nonlinear regression was conducted using the SPSS software, and the model is presented in Equation 4.17. Figure 44 shows the correlation between the measured MPD and the predicted MPD (r-squared = 0.74). Equation 4.17 indicates that the MPD decreases with traffic, and coarser mixtures have higher MPD.

$$\text{MPD} = (\lambda/34.180) - (0.398/k) + (k^{0.416}) - 0.003N \quad (4.17)$$

where

$\lambda, k$  = Weibull distribution parameters for aggregate gradation.

$N$  = number of polishing cycles in thousands.

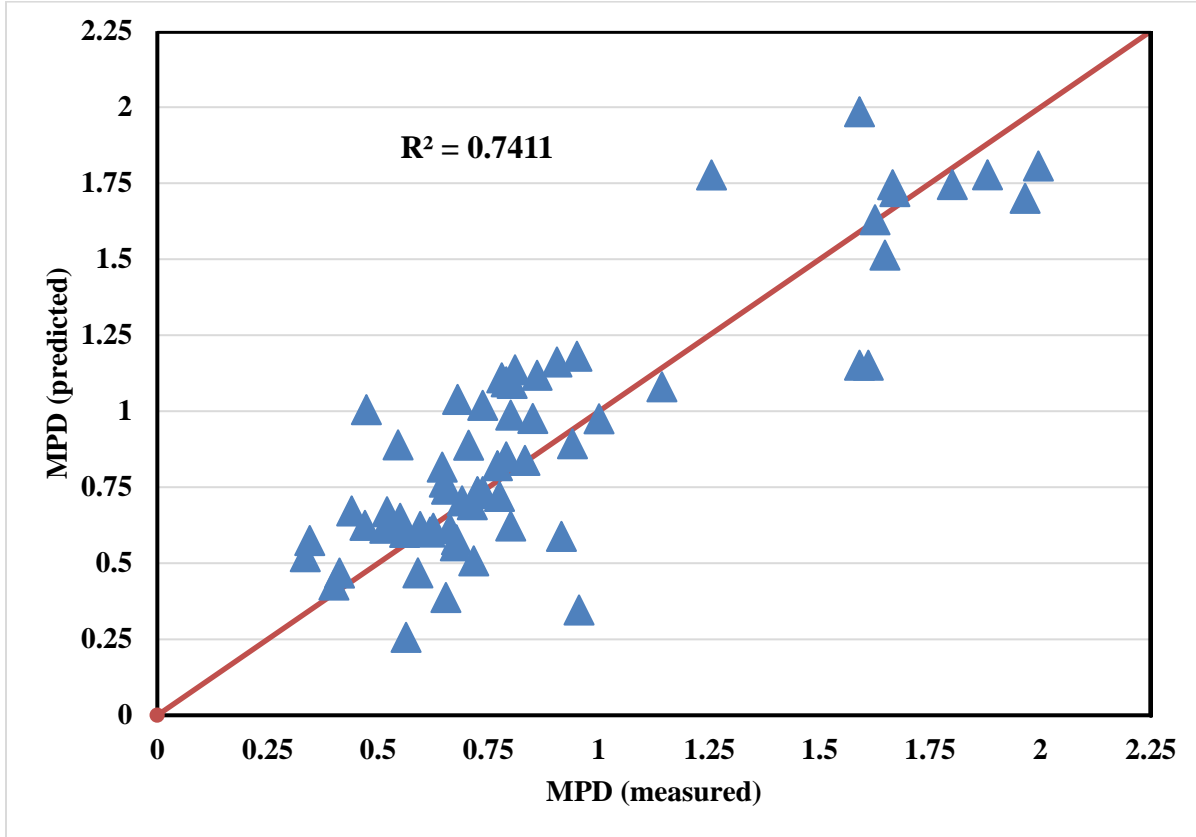


**Figure 44. Relationship between Measured and Calculated MPD Values.**

### SKID NUMBER ANALYSIS

The researchers used the developed IFI models (Equation 2.6 and Equations 4.11 through 4.13) to predict SN(50) using Equation 3.6. Equation 4.18 presents a modified form of Equation 3.6 to account for the difference between calculated and measured skid numbers in this study.

$$SN(50) = 4.81 + 140.32 (IFI - 0.045) e^{\frac{-20}{S_p}} \quad (4.18)$$

where

IFI: predicted international friction index.

$S_p$ : speed constant parameter.

The predicted SN(50) values calculated using Equation 4.18 were compared to the SN measured in the field using a skid trailer at 50 mph. Figure 45 shows the correlation between the measured and predicted SN. Overall, a good correlation was found between the calculated and measured skid resistance. Although the r-squared value is 0.63, such correlation is considered good given the influence of other factors affecting skid resistance (e.g., geometry of roadway, climatic condition, construction quality). Construction quality can affect the surface characteristics in many ways, such as segregation, bleeding of asphalt, and rough surface due to uneven paving. Asphalt bleeding can significantly reduce the skid number; however, it is associated with poor construction practice.

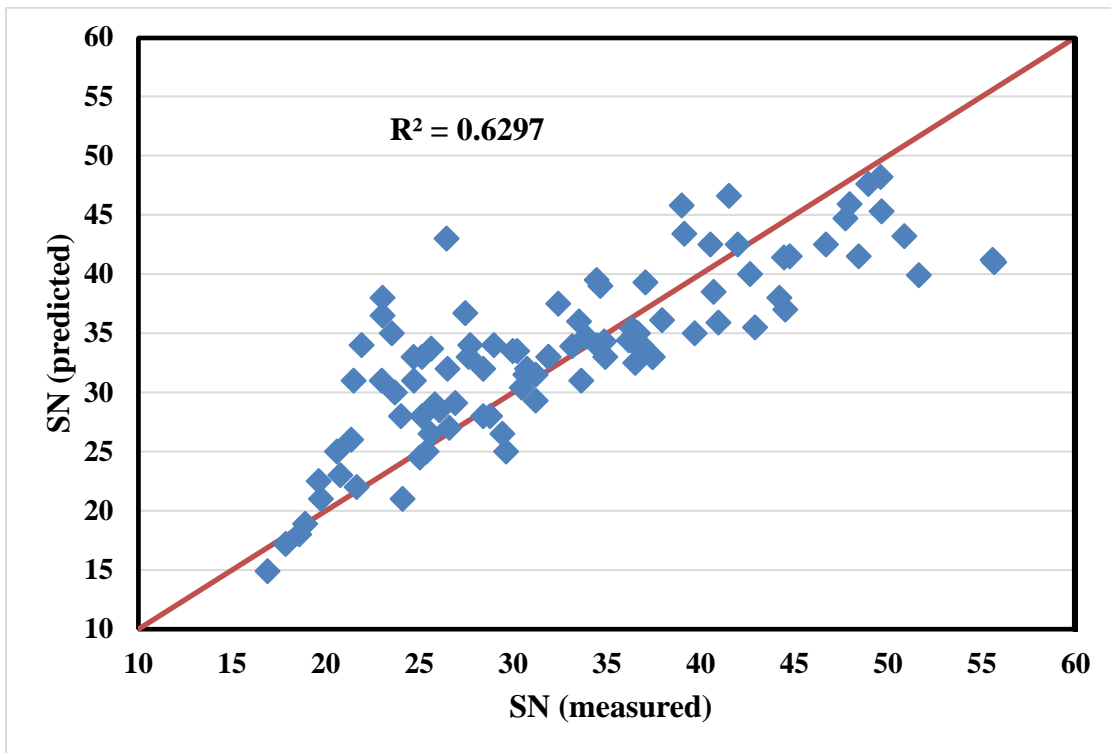


**Figure 45. Relationship between the Measured and Predicted SN.**

The researchers further investigated the effect of the traffic level on skid resistance. Traffic level is categorized in four groups, as presented in Table 8. The traffic level is expressed as TMF, depicted in Equation 4.15. Figure 46 shows the range of skid number values at different traffic levels. In general, the SN decreases with the increase in the traffic level. A higher traffic level causes more polishing to the surface of asphalt pavements and thus reduces SN.

**Table 8. Traffic Groups Based on TMF.**

Level	Traffic Multiplication Factor
Low	0–15,000
Medium	15,000–40,000
High	40,000–90,000
Very High	> 90,000

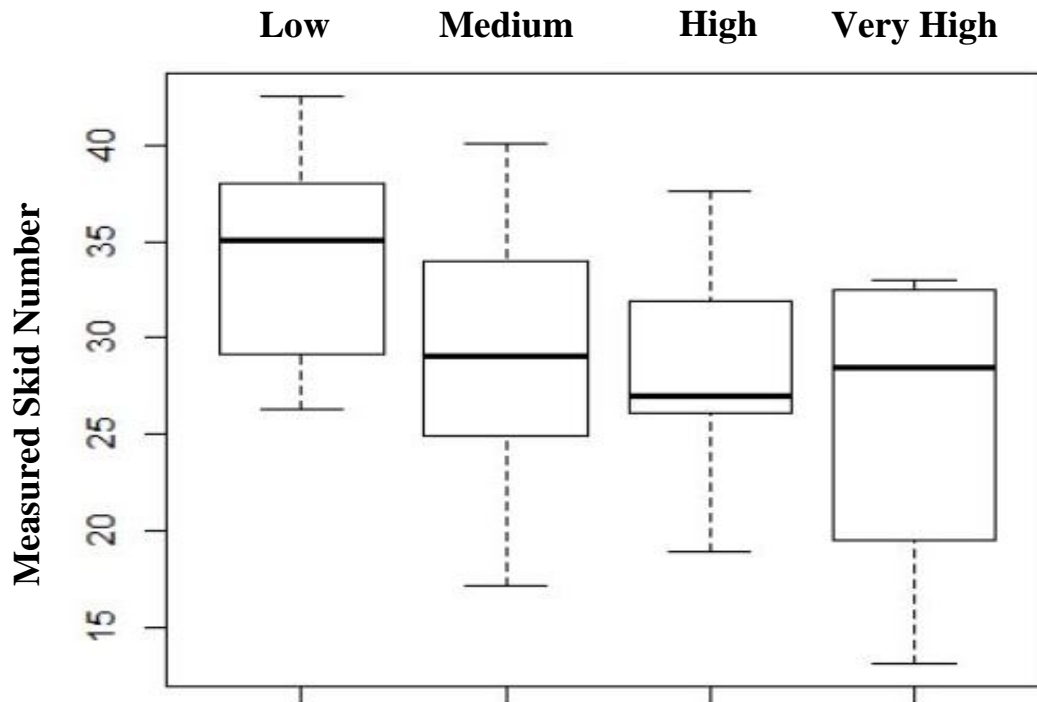


**Figure 46. Measured Skid Numbers in Terms of Traffic Level.**

### **HMA SKID RESISTANCE MODEL SENSITIVITY ANALYSIS**

This section discusses the researchers’ examination of the sensitivity of the HMA skid resistance model to various factors (e.g., aggregate gradation, type, and traffic level) that affect SN.

#### **Effect of Mixture Gradation**

Four mixtures with different aggregate gradations were evaluated: Type C dense-graded mixture, Type D dense-graded mixture (finer than Type C), PFC, and SMA-C. The performance of these mixtures in terms of skid number was assessed using the developed model. All variables (e.g., traffic level, aggregate characteristics) were held constant and only the aggregate gradation

was varied. Figure 47 shows that the mixtures with coarse aggregate gradations (such as PFC and SMA-C) had higher skid numbers. The coarse aggregate gradation provides higher macrotexture and thus yields higher SN.

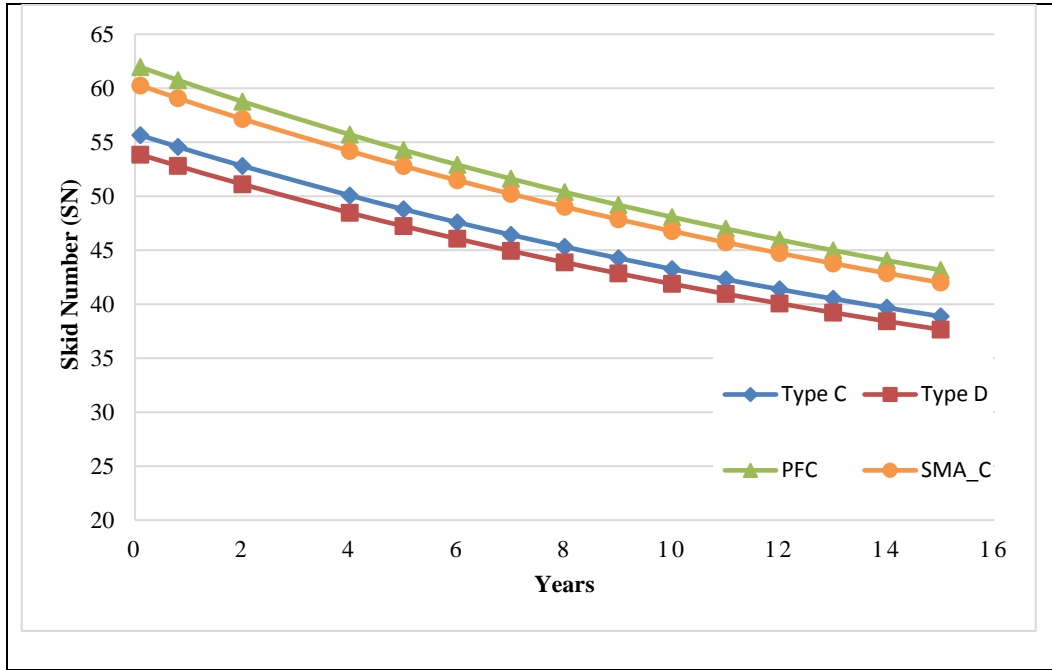


**Figure 47. Effect of Mixture Gradation on the Skid Number.**

**Effect of Traffic Level**

Figure 48 shows the effect of different traffic levels of AADT on skid resistance. The results showed that the skid number decreases with traffic level, as expected; however, the SN had a steep slope or reduction at higher traffic levels. Pavement surface experiences most polishing at higher traffic levels, which adversely affects skid resistance.

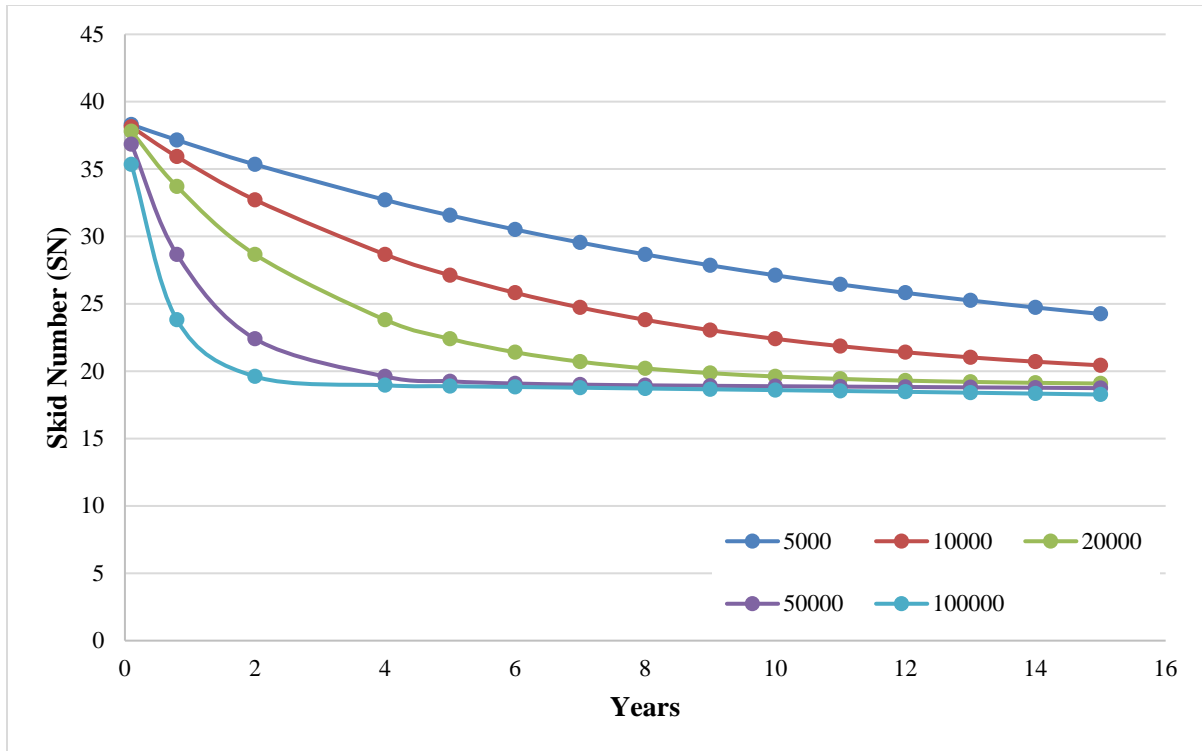


**Figure 48. Effect of AADT on the Skid Number.**

### **Effect of Aggregate Type**

Four different aggregate types (e.g., limestone, sandstone, dolomite, and different combinations) were examined. The traffic level and aggregate gradation were fixed. Figure 49 demonstrates that HMA mixtures prepared with aggregates with rough texture such as sandstone provide a higher skid number and lower rate of skid reduction than HMA mixtures with soft rock such as limestone. Thus, the recommendation is to use rough aggregates in asphalt pavements subjected to high traffic levels. Blending of aggregates that have a higher polishing resistance with local aggregates is recommended when transporting of good, quality aggregate is prohibited by cost concern.

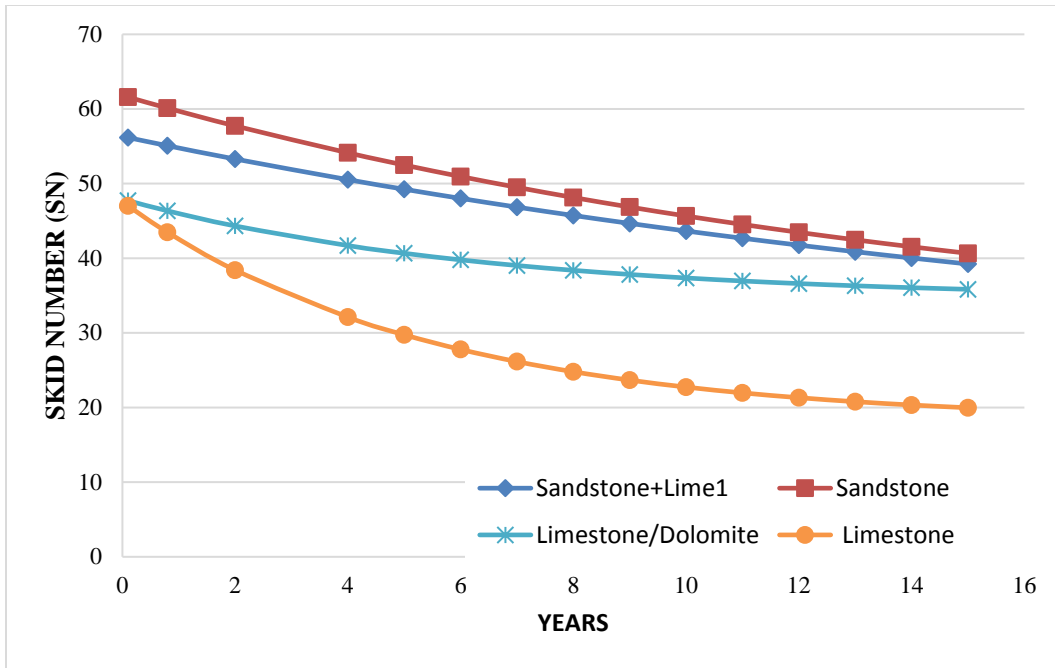


**Figure 49. Effect of Aggregate Texture on the Skid Number.**

**SUMMARY**

This chapter discussed the steps followed by the researchers in analyzing the field and laboratory data and developing the IFI and SN models. The developed prediction model describes the skid resistance of asphalt pavements as a function of aggregate shape characteristics (texture and angularity), aggregate gradation, and aggregate resistance to polishing and abrasion, and traffic level. The major difference with this model to the one developed by Masad et al. (2010) is the inclusion of aggregate angularity parameters. A good correlation was observed between predicted and measured SN. In addition, different factors affecting skid resistance were investigated. Coarse aggregate gradation with rough texture provided higher skid resistance compared to aggregates with fine gradation and smooth texture. Also, a steep reduction in the skid number was observed at higher traffic levels. Higher truck traffic accelerated the polishing of pavement at even faster rates. The model is capable of predicting skid resistance over the course of a roadway’s service life.



## **CHAPTER 5: DATA ANALYSIS AND RESULTS FOR SEAL COAT TEST SECTIONS**

In this chapter, the researchers performed similar steps described in Chapter 4 to analyze the test results and develop a skid prediction model for the seal coat surface. Figure 37 shows a flowchart of key parameters examined and used in developing the predictive models of the skid resistance of seal coat surfaces. The researchers developed mathematical indices to evaluate the aggregate resistance to abrasion and polishing and to describe the aggregate gradation. In addition, the researchers analyzed the field measurements and developed models to describe the IFI and SN.

### **ANALYSIS OF AGGREGATE GRADATION**

The cumulative two-parameter ( $\lambda$ ,  $\kappa$ ) Weibull distribution (Equation 3.5) was used to describe the aggregate gradation used in seal coat test sections. There are three aggregate grades of seal coat (Grade 3, Grade 4, and Grade 5). Each grade stands for a different aggregate size, with Grade 3 being the coarsest. Similar to its use with HMA, the MATLAB program was used to fit the Weibull function to the gradation of seal coat aggregate sizes. The scale ( $\lambda$ ) and shape parameters ( $\kappa$ ) were calculated by fitting the aggregate gradation to the cumulative two-parameter Weibull distribution. Table 9 presents the scale ( $\lambda$ ) and shape ( $\kappa$ ) and parameters for the aggregate gradations examined for developing the seal coat skid prediction model. Figure 50 shows an example of aggregate gradation of three seal coat sizes. The x-axis represents the aggregate size in millimeters, and the y-axis represents the cumulative percent passing of the aggregate. As one can see from Table 9 and Figure 50, the Weibull distribution function fits very well with the aggregate gradation (r-squared = 0.99).

**Table 9. Scale and Shape Parameters of the Weibull Distribution.**

<b>Aggregate Grade</b>	<b>No. of Sections</b>	$\lambda$	$\kappa$	$R^2$
Grade 3	11	12.24	8.80	0.99
Grade 4	19	9.17	5.14	0.99
Grade 5	2	5.55	5.37	0.99

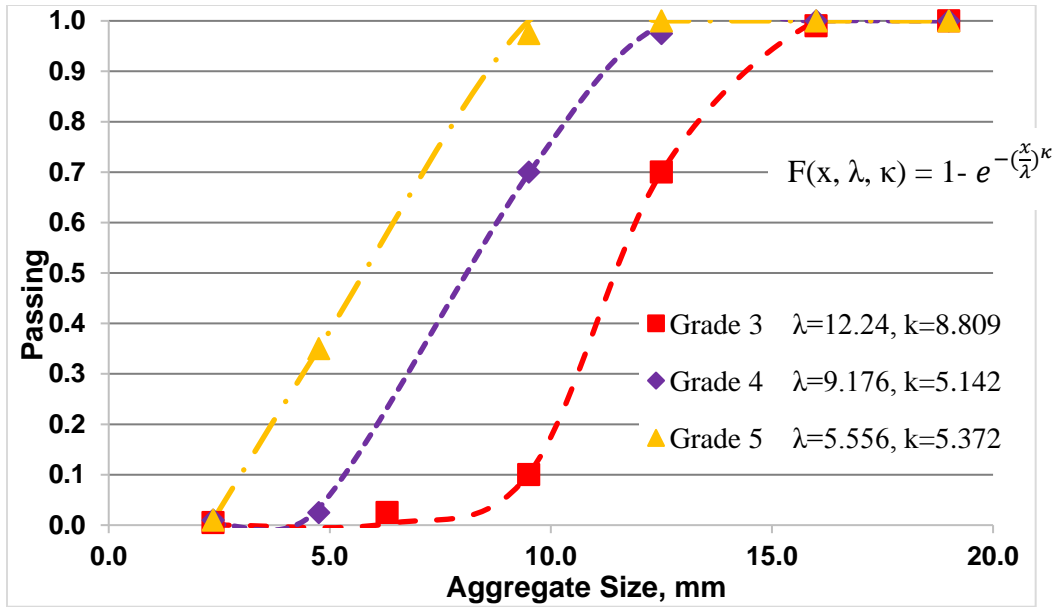


**Figure 50. Weibull Distribution Function for Different Aggregate Sizes.**

### **ANALYSIS OF AGGREGATE TEXTURE AND ANGULARITY**

A procedure similar to the procedure described in Section 4.2 was used in quantifying the aggregate shape characteristics. The AIMS was used to measure the texture and angularity before and after the Micro-Deval abrasion test. Figure 51 and Figure 52 show examples of the change in texture and angularity of seal coat aggregates due to abrasion and polishing at three stages: BMD, AMD105, and 180 min after polishing in the Micro-Deval. Both texture and angularity decreased due to abrasion and polishing. As mentioned earlier, the current practice at TxDOT is to measure the aggregate shape characteristics before and after the Micro-Deval abrasion test (0 and 105 min). The researchers considered both procedures when developing analytical models to describe the change in angularity and texture of aggregates used in seal coat. Figure 53 and Figure 54 show examples of the regression constants of the texture and angularity, respectively.

The researchers developed models to predict the regression constants in Equations 3.3 and 3.4 for the aggregates tested before and after 105 min of polishing in the Micro-Deval (BMD and AMD105). A total number of 19 aggregates were used in the regression analysis to develop equations to predict initial measurements, terminal measurements, and rate of change of texture and angularity. Also, SPSS software was used to conduct the regression analysis. Equations 5.1 through 5.10 determine the regression parameters for texture and angularity loss using two

measurements: BMD and AMD105. Equations 5.1 through 5.10 were developed based on the aggregates used in seal coat test sections evaluated in this study, while Equations 4.1 through 4.10 were developed based on the aggregates used in HMA test sections evaluated in this study. In the meantime, the researchers recommend measuring the texture and angularity at three different time points during Micro-Deval polishing for an accurate characterization.

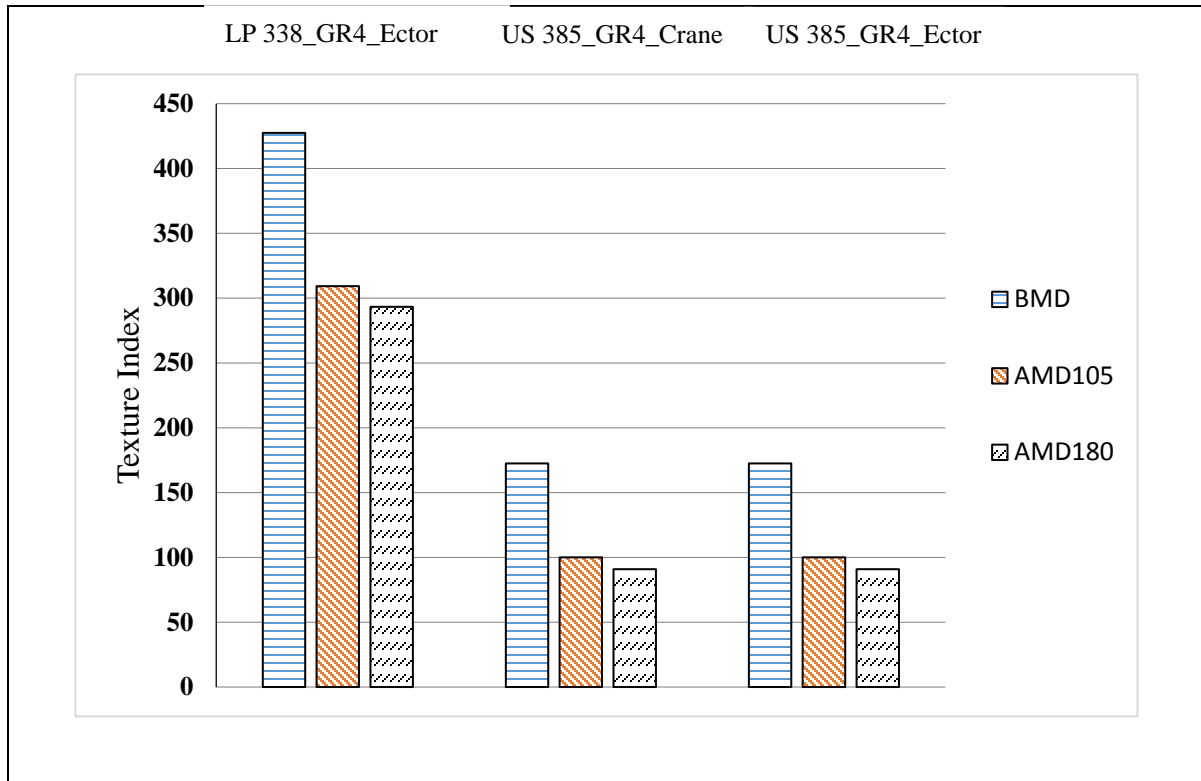


**Figure 51. Texture Indices of Sections in Odessa.**

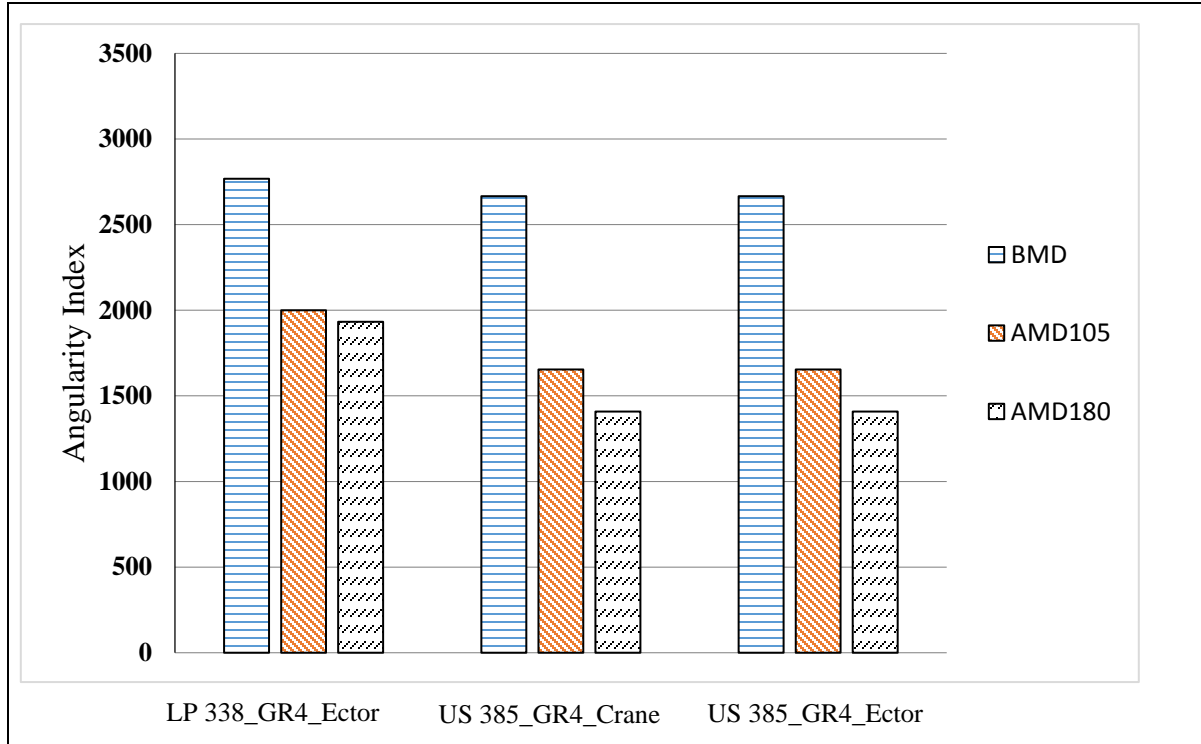


**Figure 52. Angularity Indices of Sections in Odessa.**

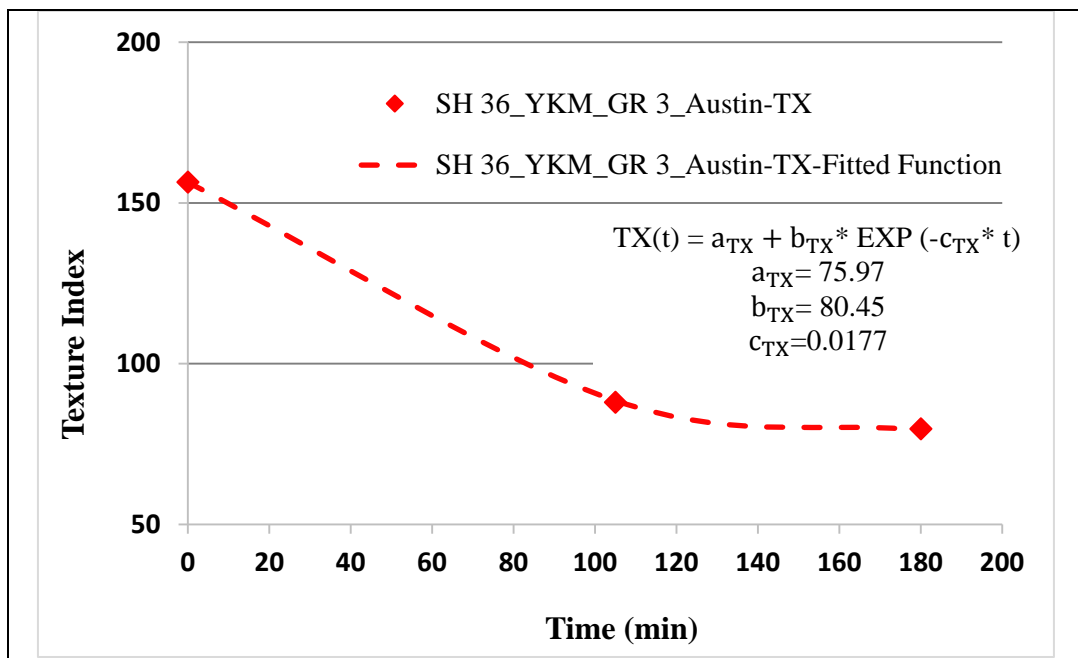


**Figure 53. Regression Constants for Aggregate Texture.**

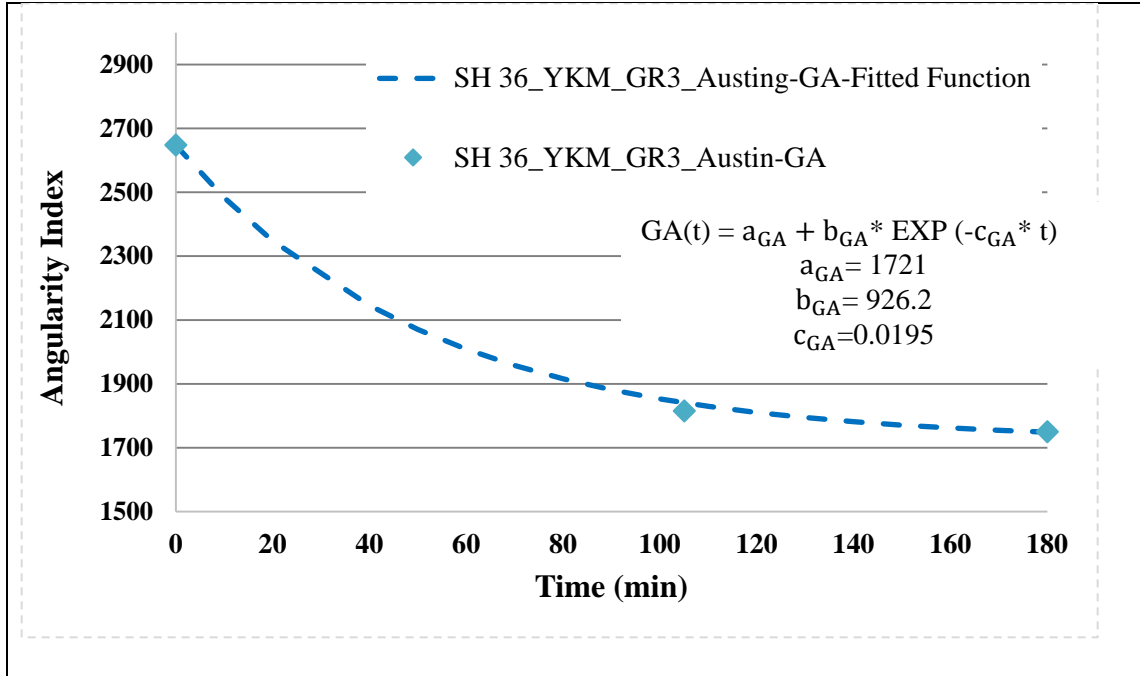


Figure 54. Regression Constants for Aggregate Angularity.

- Texture model coefficients:

$$a_{TX} + b_{TX} = BMD + 0.134 \quad (R^2 = 1) \quad (5.1)$$

$$a_{TX} = 1.011AMD - 17.918 \quad (R^2 = 0.95) \quad (5.2)$$

$$c_{TX} = \frac{1.555 + TL}{126.995 - (18.174 \times ARI)} \quad (R^2 = 0.58) \quad (5.3)$$

$$TL = \frac{BMD - AMD}{AMD} \quad (5.4)$$

$$ARI = \frac{AMD/BMD}{\sqrt{1 - \left(\frac{AMD}{BMD}\right)^2}} \quad (5.5)$$

where

$a_{TX} + b_{TX}$  = initial texture index.

$a_{TX}$  = terminal texture index.

$c_{TX}$  = rate of change in texture.

BMD, AMD = texture index before and after 105 min of polishing in Micro-Deval.

TL, ARI = texture loss and aggregate roughness index, respectively.

- Angularity model coefficients:

$$a_{GA} + b_{GA} = 0.994BMD + 21.084 \quad (R^2 = 1) \quad (5.6)$$

$$a_{GA} = 1.232AMD - 648.34 \quad (R^2 = 0.94) \quad (5.7)$$

$$c_{GA} = \frac{1.292+TL}{-9.77+(58.155 \times ARI)} \quad (R^2 = 0.61) \quad (5.8)$$

$$TL = \frac{BMD-AMD}{AMD} \quad (5.9)$$

$$ARI = \frac{AMD/BMD}{1 - \left(\frac{AMD}{BMD}\right)^2} \quad (5.10)$$

where

$a_{GA} + b_{GA}$  = initial angularity index.

$a_{GA}$  = terminal angularity index.

$c_{GA}$  = rate of change in angularity.

BMD, AMD = angularity index before and after 105 min of polishing in Micro-Deval.

TL, ARI = angularity loss and aggregate roughness index, respectively.

Table 10 summarizes the regression coefficients of aggregate texture and angularity evaluated in seal coat test sections.

**Table 10. Regression Parameters of Aggregate Texture and Angularity.**

State	Section ID	Texture Parameters			Angularity Parameters		
		$a_{TX}$	$b_{TX}$	$c_{TX}$	$a_{GA}$	$b_{GA}$	$c_{GA}$
Pharr	US 77_PHR_GR3_Cameron	211.61	287.86	0.0278	1707	1223	0.0160
	US 281_PHR_GR3_Hidalgo	312.17	269.61	0.0204	1285.62	1309.54	0.0422
	US 281_PHR_GR3_Brooke_TRM 752	211.63	287.84	0.0278	1707	1223	0.0160
	US 281_PHR_GR3_Brooke_TRM 722	312.17	269.61	0.0204	1285.62	1309.54	0.0422
Dallas-FW	US 377_FTW_GR3_Hood	99.72	120.31	0.0195	1426	1253	0.0220
	US 377_FTW_GR3_Tarrant	99.72	120.31	0.0195	1426	1253	0.0220
	SH 199_FTW_GR3_Parker	99.35	95.90	0.0197	1379.59	1275.29	0.0388
Brownwood	US 67_BWD_GR4_Coleman	99.72	120.31	0.0195	1426	1253	0.0220
	US 67_BWD_GR4_Brown	99.72	120.31	0.0195	1426	1253	0.0220
	US 183_BWD_GR4_Eastland	113.72	135.62	0.0178	1484	1257	0.0204
	US 377_BWD_GR4_Brown	99.72	120.32	0.0195	1426	1253	0.0220
San Antonio	US 90_SAT_GR4_Bexar	81.15	66.65	0.0210	1883	780.87	0.0159
	FM 1518_GR3_Bexar	232	34.76	0.0296	1477	1188	0.0161
	SH 16_SAT_GR4_Atascosa_TRM 626	419.22	43.43	0.0168	1931	1213	0.1650
	SH 16_SAT_GR 4_Atascosa_TRM 642	312.17	269.61	0.0204	1285.62	1309.54	0.0422
YKM	SH 36_YKM_GR 3_Austin	75.97	80.45	0.0177	1721	926.22	0.0195
Lufkin	US 59_LFK_GR3_Angelina	433.34	125.42	0.0176	1955.98	1005.25	0.0225
	US 69_LFK_GR4_Angelina	221.09	62.57	0.0176	1011.73	972.41	0.0273
	US 287_LFK_GR4_Trinity	221.09	62.57	0.0176	1011.73	972.41	0.0273
	FM 2213_LFK_GR5_San Augustine	221.09	62.57	0.0176	1011.73	972.41	0.0273
	US 59_LFK_GR4_Shelby	232	34.76	0.0168	1477	1188	0.0167
Odessa	LP 338_ODA_GR4_Ector	287.64	139.91	0.0169	1916	851.62	0.0201
	US 385_ODA_GR4_Crane	86.28	86.17	0.0181	1348	1323	0.0215
	US 385_ODA_GR4_Ector	86.28	86.17	0.0181	1348	1323	0.0215
Beaumont	SH 82_BMT_GR4_Jefferson	221.09	62.57	0.0176	1011.73	972.41	0.0273
	FM 365_BMT_GR4_Jefferson	221.09	62.57	0.0176	1011.73	972.41	0.0273
	FM 105_BMT_GR4_Orange	221.09	62.57	0.0176	1011.73	972.41	0.0273
Atlanta	US 80_ATL-GR4_Harrison	221.09	62.57	0.0176	1011.73	972.41	0.0273
	US 59_ATL_GR3_Cass_RG_TRM238	156.93	34.44	0.0182	2208	483	0.0181
	SH 77_ATL_GR4_Cass_TRM 745_SS	150.62	93.79	0.0179	1726	855.24	0.0195
	SH 77_ATL_GR4_Cass_TRM 720_RG	115	51.46	0.0169	2313	589.66	0.0176

**DEVELOPMENT PREDICTIVE MODEL FOR IFI FOR SEAL COAT**

Similar to the IFI models developed for HMA in Section 4.3, IFI models were also developed for seal coat. These models were used to describe parameters of IFI ( $a_{mix}$ ,  $a_{mix} +$

$b_{mix}$ , and  $C_{mix}$ ) of Equation 2.6. There are three models: one for initial IFI ( $a_{mix} + b_{mix}$ ), one for terminal IFI ( $a_{mix}$ ), and one for the rate of change in IFI ( $C_{mix}$ ). These models incorporate parameters that describe aggregate gradation, aggregate shape characteristics (texture and angularity) and its resistance to abrasion and polishing. These models provide good correlation between predicted IFI (Equation 2.6) and measured IFI (Equation 2.2). These models are presented in Equations 5.11 through 5.13. Equation 4.14 was used to convert the traffic level to a corresponding number of polishing cycles (N) since Equation 2.6 is a function of the number of polishing cycles in the laboratory (N).

$$a_{mix} = \frac{40.493 + \lambda}{330 - 0.0011(AMD)^2} \quad (5.11)$$

$$a_{mix} + b_{mix} = 0.4 * \ln \left( \frac{1.43757 * (a_{TX} + b_{TX}) + 46.8933 * \lambda + 3343.491 * k}{2.02031 * (a_{GA} + b_{GA})} \right) \quad (5.12)$$

$$C_{mix} = 2.654C_{TX} + 1.5C_{GA} \quad (5.13)$$

where

$a_{mix}$  = terminal IFI.

$a_{mix} + b_{mix}$  = initial IFI.

$C_{mix}$  = rate of change in IFI.

$\lambda, k$  = scale and shape parameters of Weibull distribution.

AMD = the texture after 150 min in Micro-Deval.

$a_{TX}, b_{TX}$  = regression constants for texture.

$a_{GA}, b_{GA}$  = regression constants for angularity.

$C_{TX}$  = rate of change in texture.

$C_{GA}$  = rate of change in angularity.

Figure 55 shows the correlation between the predicted and measured IFI. The data points in Figure 55 include the IFI measurements at the wheel path and at the shoulder or between the wheel path. Good correlation was found between the predicted IFI and measured IFI (r-squared of 0.68). Such correlation is considered fair since other factors may contribute to the change in skid resistance of seal coat over time. Such factors may include bleeding, raveling, and the like.



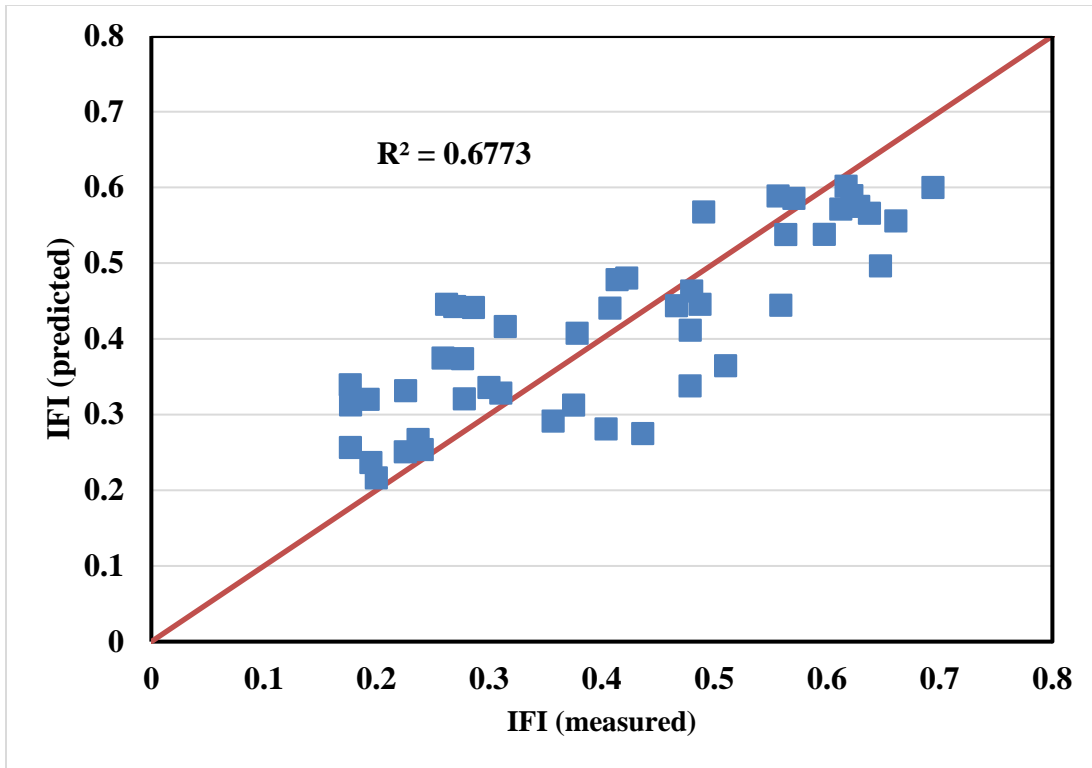


Figure 55. Relationship between Predicted and Measured IFI.

#### ANALYSIS OF MEAN PROFILE DEPTH

The researchers also developed a predictive model for MPD as a function of seal coat size and polishing cycles. The purpose of this model was to predict MPD of seal coat surfaces if such information is not available. Nonlinear regression was conducted using SPSS software, and the model is presented in Equation 5.14. Figure 56 shows the correlation between the measured MPD and the predicted MPD ( $r$ -squared = 0.53). Such correlation is considered fair given the wide range of seal coat sizes used in the field. Equation 5.14 demonstrated that MPD decreases with traffic, and coarser seal coat has a higher MPD.

$$\text{MPD} = (\lambda/5.403) + (3.491/k) + (k^{0.104}) + N^{-0.47} - 2.594 \quad (5.14)$$

where

$\lambda$ ,  $k$  = Weibull distribution parameters for aggregate gradation.

$N$  = number of polishing cycles in thousands.

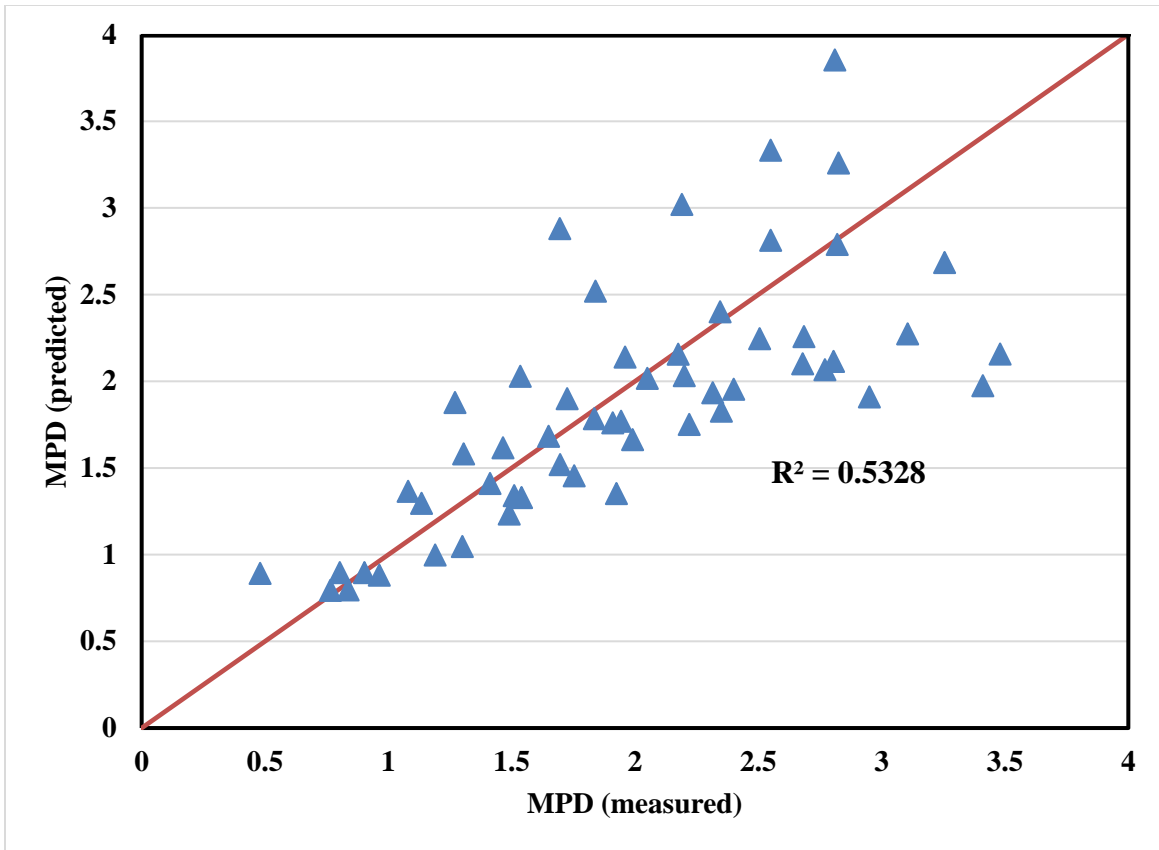


**Figure 56. Relationship between Measured and Calculated MPD Values.**

### SKID NUMBER ANALYSIS

The researchers used the developed IFI models (Equation 2.6 and Equations. 5.11 through 5.13) to predict SN (50) using Equation 3.6. Equation 5.15 presents a modified form of Equation 3.6 to account for the difference between calculated and measured skid numbers of seal coat test sections evaluated in this study.

$$SN(50) = 4.81 + 140.32 (IFI - 0.045) e^{\frac{-20}{S_p}} \quad (5.15)$$

where

IFI = predicted international friction index.

$S_p$  = speed constant parameter.

The predicted SN(50) values calculated using Equation 5.15 were compared to the SN measured in the field using a skid trailer at 50 mph. Figure 57 shows the relationship between the measured SN values in the field and the predicted SN using Equation 5.15. A fair relationship

was found ( $r$ -squared = 0.58). Such correlation is considered good for the seal coat surfaces since the skid performance of seal coat is highly affected by the quality of construction. For example, the researchers noticed that a number of test sections had bleeding.

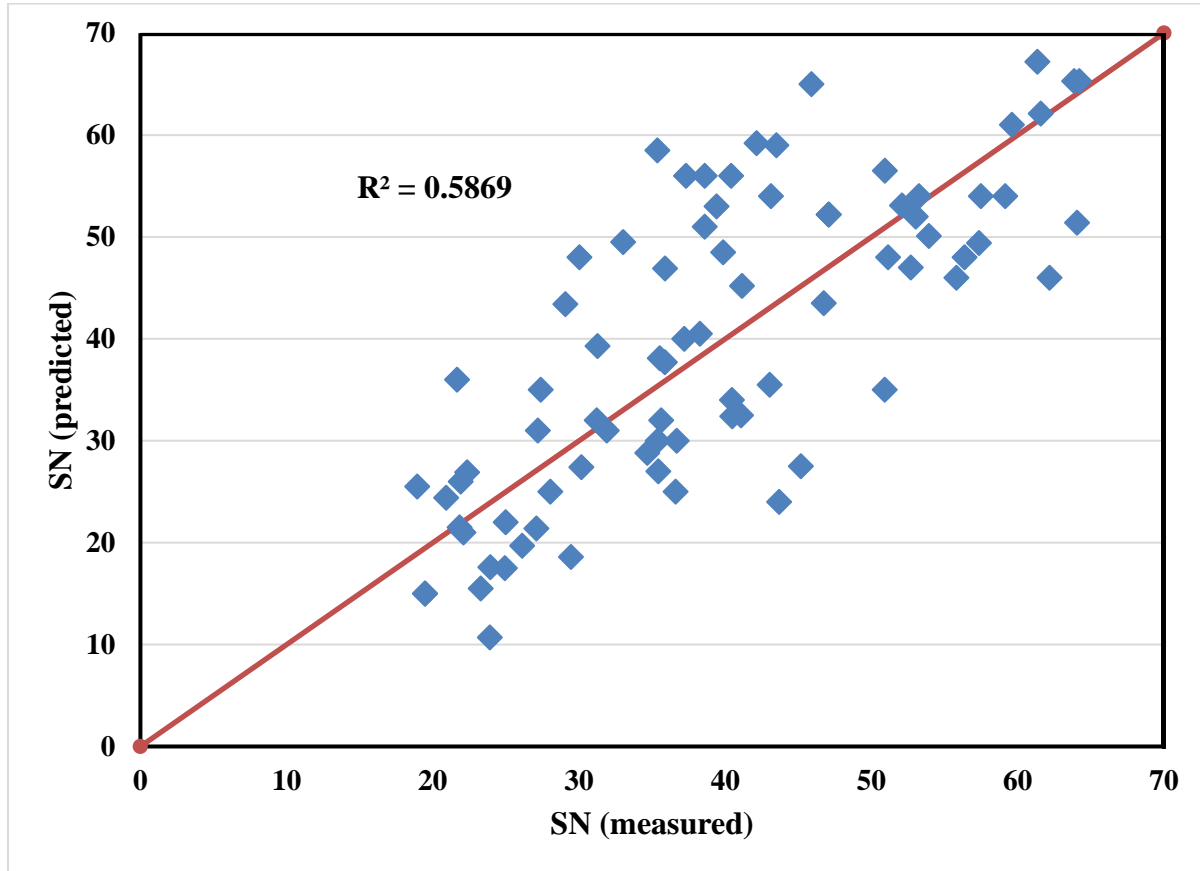


**Figure 57. Relationship between Measured and Predicted SN.**

The researchers investigated the effect of the traffic level on the skid resistance of seal coat test sections. The traffic level is categorized in four groups, as presented in Table 11. The traffic level is expressed as TMF, which is presented in Equation 4.15.

Figure 58 shows the range of skid number values for seal coat test sections at different traffic levels. Seal coat test sections that experience low traffic level had a higher SN, and in general, the SN decreases with increase in traffic levels. Higher traffic levels cause more polishing and steep skid reduction.

**Table 11. Traffic Groups Based on TMF.**

<b>Level</b>	<b>Traffic Multiplication Factor</b>
Low	0–5,000
Medium	5,000–20,000
High	20,000–40,000
Very High	> 40,000

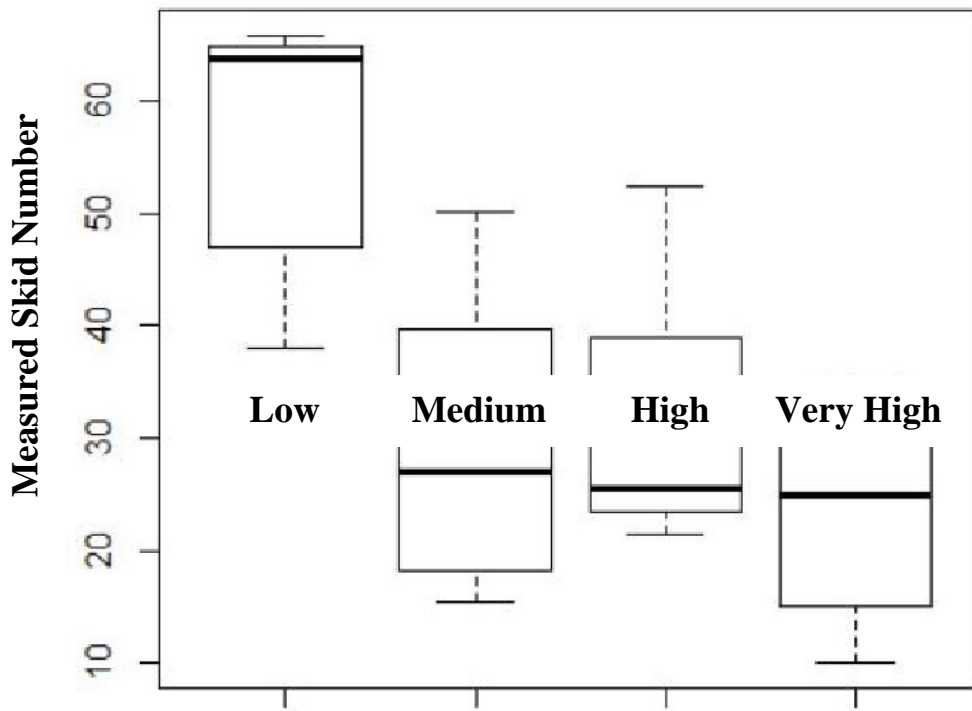


**Figure 58. Measured Skid Numbers at Different Traffic Level.**

### **SEAL COAT SKID RESISTANCE MODEL SENSITIVITY ANALYSIS**

The researchers examined the sensitivity of the seal coat skid resistance model to various factors (e.g., seal coat size, aggregate type, and traffic level) that affect SN.

#### **Effect of Seal Coat Size**

Three different sizes of seal coat were examined (Grade 3, Grade 4, and Grade 5). All variables (e.g., traffic level, aggregate characteristics) were held constant, and only the seal coat aggregate size was varied. Figure 59 shows the SN with times for the three different seal coat

grades. As expected, Grade 3 had a higher SN compared to Grade 4 and Grade 5. Grade 3 provides higher macrotexture and thus yields a higher SN than the other grades.

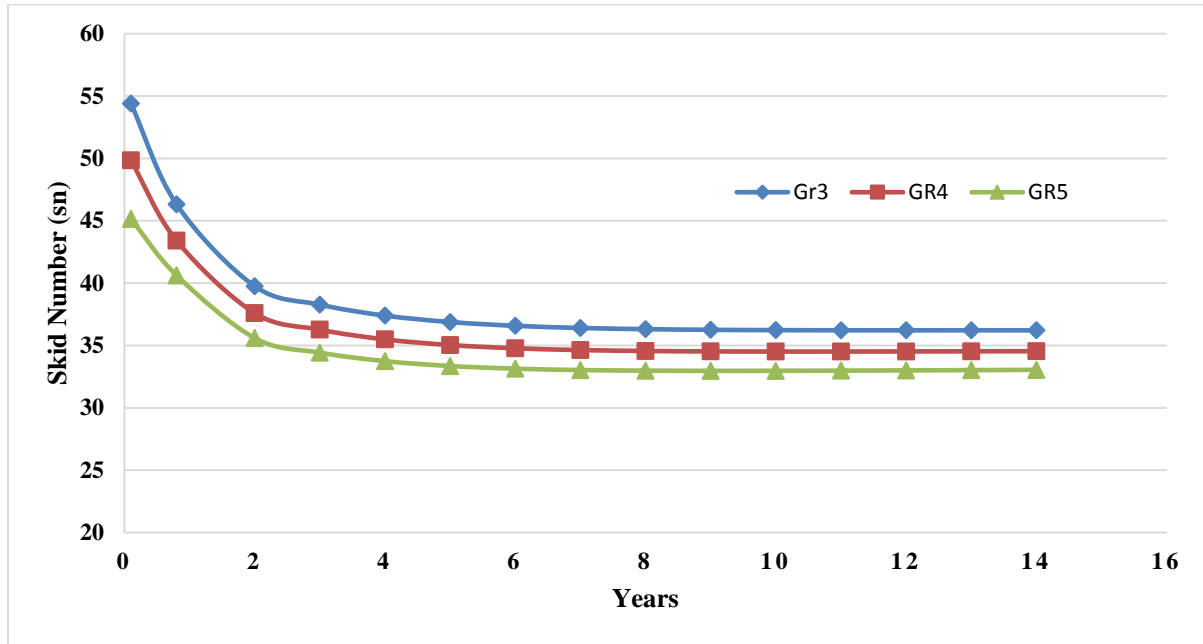


**Figure 59. Effect of Seal Coat Aggregate Size on the Skid Number.**

### Effect of Traffic Level

Figure 60 shows the effect of different traffic levels on the skid resistance of seal coat. The results demonstrated that the SN decreases as the traffic increases. Higher traffic level is associated with a steep reduction in the SN since it causes significant polishing in a relatively short time.

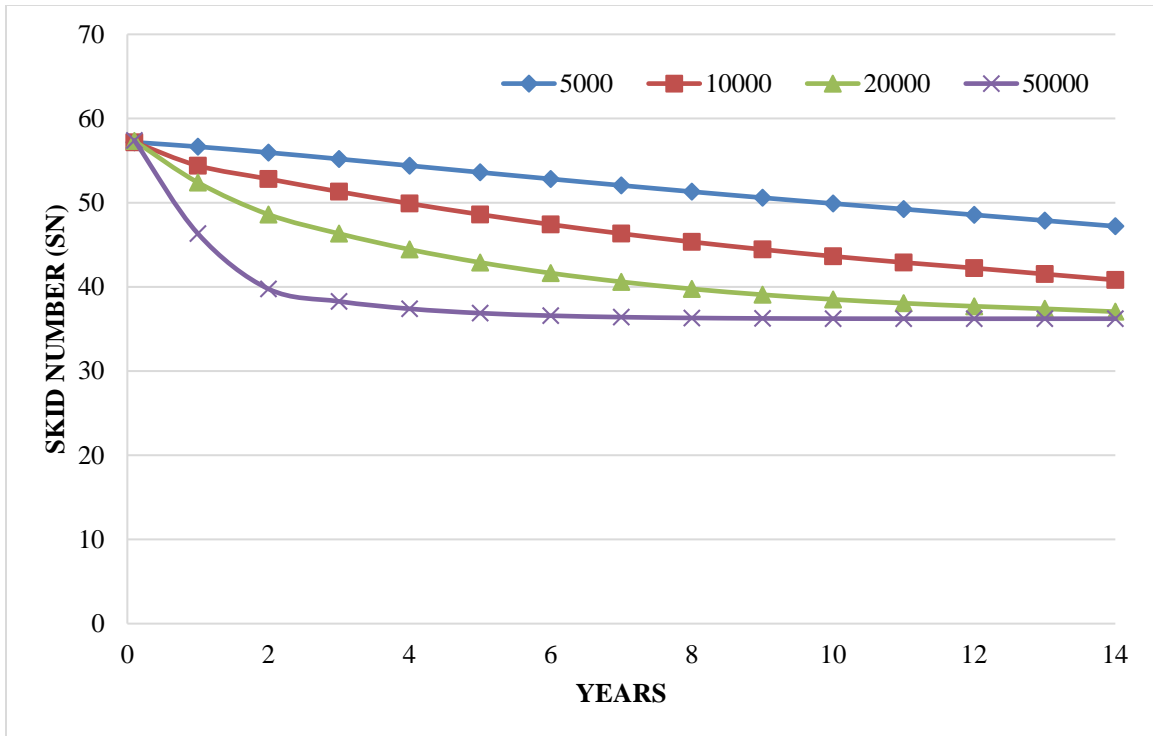


**Figure 60. Effect of AADT on the Skid Number.**

### Effect of Aggregate Type

Four different aggregate types/sources (Limestone 1, Limestone 2, sandstone, and igneous rock) were examined. Other variables, including the traffic level and aggregate gradation, were held constant. Figure 61 demonstrates that seal coat constructed with rough aggregates such as sandstone, which had better resistance to abrasion and polishing, provides a higher skid number and lower rate of skid reduction than seal coat surfaces constructed with relatively softer rocks (e.g., Limestone 1).

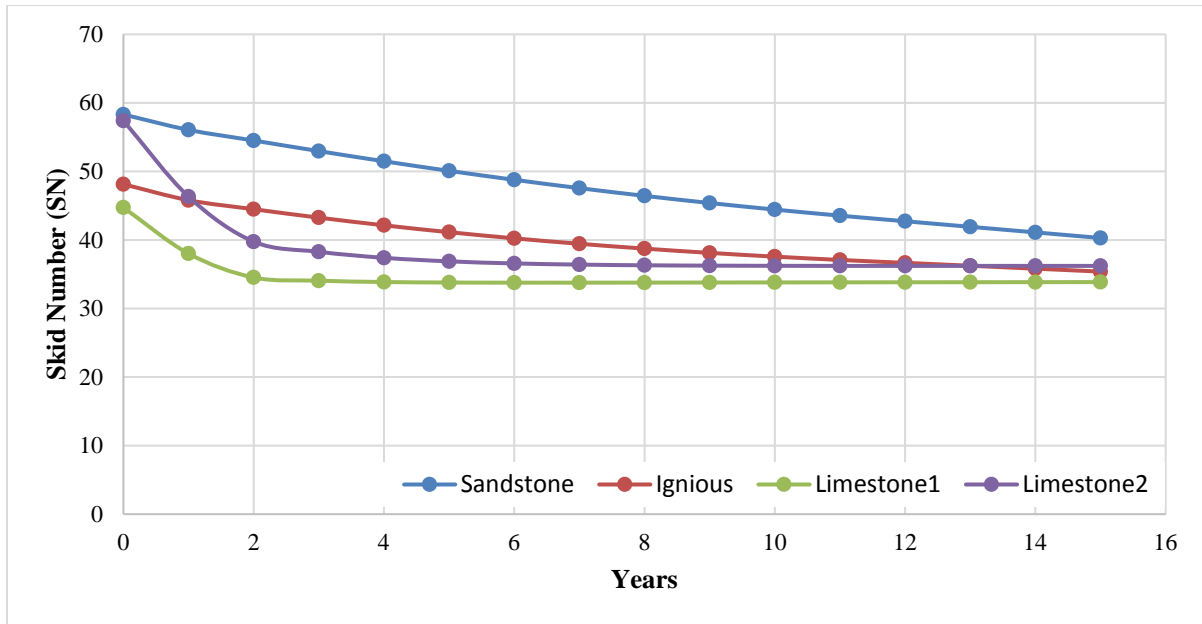


**Figure 61. Effect of Aggregate Texture on the Skid Number.**

## SUMMARY

This chapter discussed the development of the IFI and SN models for seal coat. The developed prediction model describes the skid resistance of seal coat as a function of seal coat aggregate size (gradation), aggregate shape characteristics (texture and angularity) and its resistance to polishing and abrasion, and traffic level. A fair correlation was found between predicted and measured SN. In addition, different factors affecting the skid resistance of seal coat were investigated. Grade 3 was found to yield higher MPD and SN than other grades. Seal coat constructed with rough aggregates had higher SN than seal coat with smooth aggregates. Also, higher traffic levels caused a steep reduction in the skid resistance of seal coat. The model is capable of predicting the skid resistance of seal coat over the course of its service life.





## **CHAPTER 6: A SYSTEM FOR PREDICTING SKID NUMBER USING DESKTOP APPLICATION**

Chapter 4 and 5 document the skid prediction models for asphalt mixture and seal coat surface, respectively. Both of these models feature similar inputs and equations with only minor variations. In order to simplify the calculation of predicted skid numbers, a desktop computer application was developed based on the macro tool developed earlier under Research Project 0-5627.

A computer application was developed using Access-based VBA language to execute the steps needed to calculate the skid resistance of asphalt pavement as a function of traffic. This section describes the program and the steps needed to calculate the pavement skid resistance for both asphalt mixture surface and seal coat surface.

In one folder named Application, the application has two Microsoft Access files: application file and data file. Once the user opens the application file by double clicking, he/she will notice the first page (Figure 62). This “About” page describes the function of the SAAP application. On the next page (Figure 63), the user needs to input a new project name or select one of the existing projects in order to proceed to the next window. Next, the user selects the type of pavement surface (Figure 64)—asphalt mixture or surface treatment. Depending on the surface-type selection, the application uses the appropriate prediction model. The inputs for both asphalt mixture and seal coat surface are very similar. In the next step, (Figure 65), the mixture gradation is inputted to the application. The user can either enter the gradation or select one of the standard mixture gradations used in the state of Texas. Similarly, if surface treatment is selected as the pavement surface, the user can either enter the gradation or select the standard aggregate grade. If the user selects to enter the gradation manually by selecting an <input gradation> radio button, a separate window pops up (Figure 66) where the amount of percent passing for selected sieves are entered. The user can select any number of sieves (minimum four) and enter the percent passing values for each selected sieve. This information is used to calculate the scale and shape factors ( $\lambda$  and  $\kappa$ ) of the combined gradation.

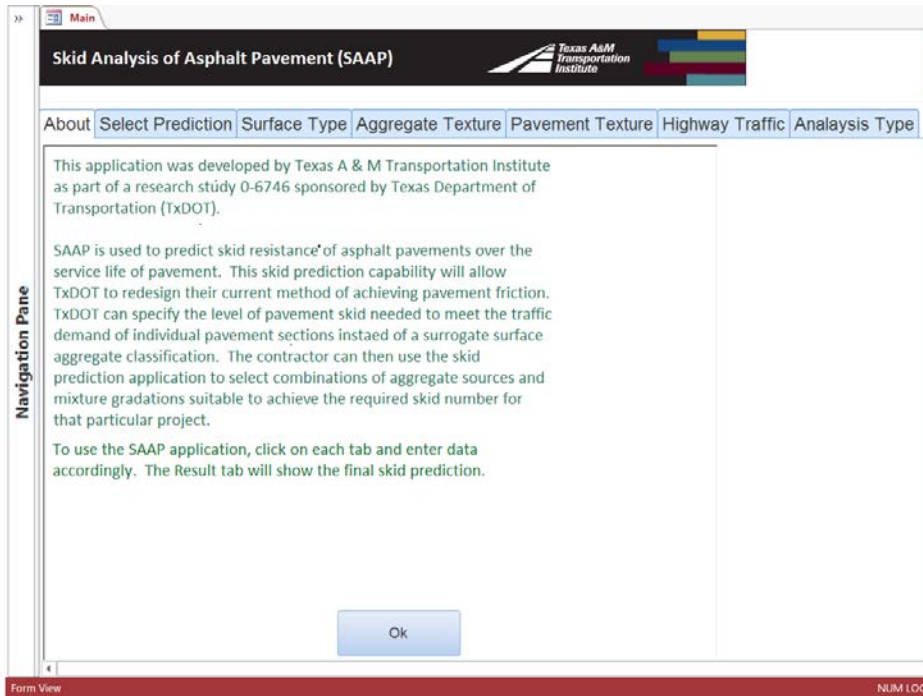


**Figure 62. Initial Window of the Program.**

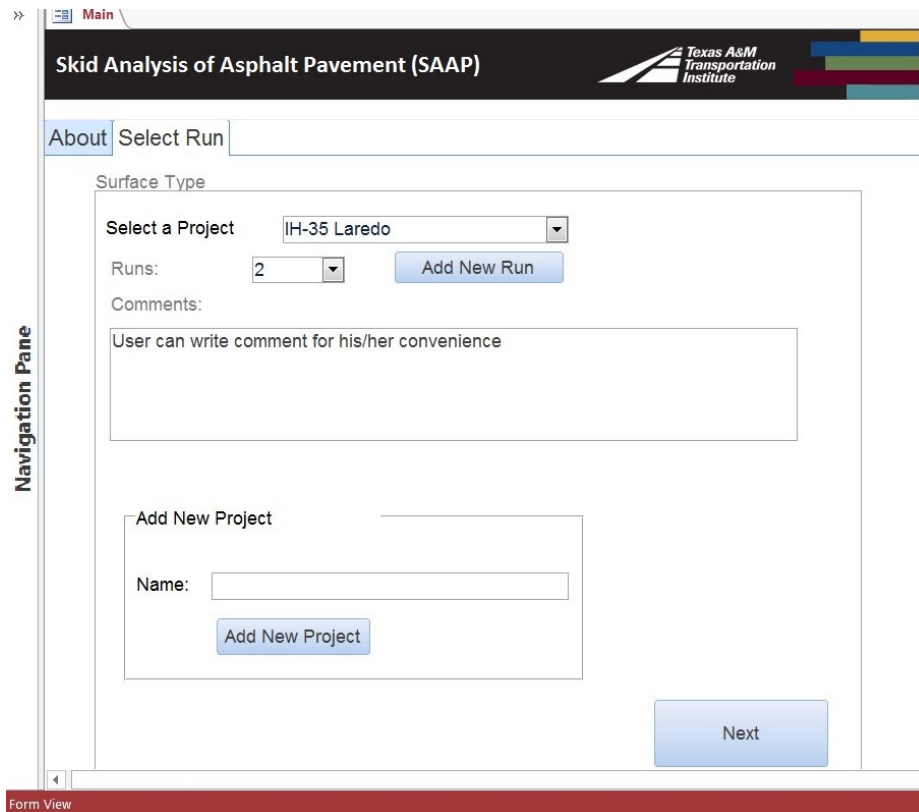


**Figure 63. Project Name Input.**

Skid Analysis of Asphalt Pavement (SAAP) Texas A&M  
Transportation  
Institute

About | Select Run | Surface Type

Project Name: IH-35 Laredo  
Run number: 2

**Choose Type of Surface**

Asphalt Mixture  
 Surface Treatment (Seal Coat)

Next

Navigation Pane

Form View

**Figure 64. Pavement Surface Type Input.**

Asphalt Mixture

Project Name: IH-35 Laredo  
Run number: 2

**Choose an option for Mixture Gradation Data**

Mixture Gradation  Input Gradation

Type C

Next

**Figure 65. Choice of Mixture Type.**

Asphalt Mixture

Project Name: IH-35 Laredo  
Run number: 2

Choose an option for Mixture Gradation Data

Mixture Gradation       Input Gradation

Sieve Size		Percent Passing
in	mm	
<input checked="" type="checkbox"/> 1	25	100.0
<input type="checkbox"/> 7/8	22.4	
<input checked="" type="checkbox"/> 3/4	19	100.0
<input type="checkbox"/> 5/8	16	
<input type="checkbox"/> 1/2	12.5	
<input checked="" type="checkbox"/> 3/8	9.5	83.4
<input checked="" type="checkbox"/> #4	4.75	59.1
<input checked="" type="checkbox"/> #8	2.36	39.2
<input type="checkbox"/> #16	1.18	
<input checked="" type="checkbox"/> #30	0.6	23.9
<input type="checkbox"/> #40	0.425	
<input checked="" type="checkbox"/> #50	0.3	16.7
<input type="checkbox"/> #80	0.18	
<input checked="" type="checkbox"/> #200	0.075	4.5

Next

**Figure 66. Manual Aggregate Gradation Input.**

In the next few steps, the aggregate texture and angularity values measured using AIMS are entered. The window shown in Figure 67 provides the options to input either the texture (and angularity) measured at two points (before polishing and after polishing for 105 minutes in the Micro-Deval) or the texture (and angularity) measured at three points (before polishing, after polishing for 105 min, and 180 min in the Micro-Deval). The use of three data points provides a more accurate estimation of aggregate resistance to polishing. This step will be followed by the appearance of windows to enter the texture data of aggregates from one or more sources. The user can select up to three aggregate sources used in the mixture. As shown in Figure 68, users can input the texture value of the component aggregate source(s). In the same window, the user needs to input the percentage ratio of each aggregate source relative to the combined gradation and the percent retained on the No. 4 sieve for each of the sources. This information is required to calculate the weighted average of texture and angularity of combined gradation when two or more aggregate sources are used.

Figure 69 shows the window that pops up if the user opts for three data points (Figure 67). Similar to Figure 68, the user inputs the ratio of aggregate in combined gradation and amount of percent retained on the No. 4 sieve for each source as well as their texture data measured by AIMS at three different polishing levels.

For the next step, the user inputs aggregate angularity data similar to aggregate texture data. Figure 70 or Figure 71 pops up depending on whether the user selected two data points or three data points for the texture/angularity measurement (Figure 67).

**Figure 67. Selection of AIMS Test Data Points.**

Source	Proportion of Aggregate in the Mix (%)	Percent Retained on Sieve #4	Texture Before Micro-Deval (BMD)	Texture After 105 Mins Micro-Deval (AMD)
Source 1	60	30	200	140
Source 2	30	80	300	210
Source 3	10	0	250	135

**Figure 68. Aggregate Texture Input for Two Data Points.**

AM Three Data Point Texture

**Texture Data Points** Note: BMD > AMD105 > AMD180 > 0

Enter Number of Aggregate Sources

Enter Name of Aggregate Source 1

Enter Name of Aggregate Source 2

Enter Name of Aggregate Source 3

Source 1	Source 2	Source 3
Proportion of Aggregate in the Mix (%)	30	10
Percent Retained on Sieve #4	80	0
Texture Before Micro-Deval (BMD)	300	250
Texture After 105 Mins Micro-Deval (AMD)	210	135
Texture After 180 Mins Micro-Deval (AMD)	195	125

**Figure 69. Aggregate Texture Input for Three Data Points.**

Angularity Data Points

**Angularity Data Points** Note: BMD > AMD105 > AMD180 > 0

Enter Number of Aggregate Sources

Enter Name of Aggregate Source 1

Enter Name of Aggregate Source 2

Enter Name of Aggregate Source 3

Source 1	Source 2	Source 3
Proportion of Aggregate in the Mix (%)	30	10
Percent Retained on Sieve #4	80	0
Angularity Before Micro-Deval (BMD)	1996	3045
Angularity After 105 mins Micro-Deval (AMD)	1450	2130

**Figure 70. Aggregate Angularity Input for Two Data Points.**

AM Three Data Point Texture

**Angularity Data Points**

Note: BMD > AMD105 > AMD180 > 0

Enter Number of Aggregate Sources: 3

Enter Name of Aggregate Source 1: S1

Enter Name of Aggregate Source 2: S2

Enter Name of Aggregate Source 3: S3

Source 1	Source 2	Source 3
Proportion of Aggregate in the Mix (%)	30	10
Percent Retained on Sieve #4	80	0
Angularity Before Micro-Deval (BMD)	1996	3045
Angularity After 105 mins Micro-Deval (AMD)	1450	2130
Angularity After 180 mins Micro-Deval (AMD)	1420	2075

Next

**Figure 71. Aggregate Angularity Input for Three Data Points.**

Once the user enters the aggregate angularity data and clicks the Next button, a new window (Figure 72) appears. At this stage, the user enters the mean profile depth of the pavement. There are two options: the user can enter the MPD value or let SAAP estimate the MPD values. The user can input the measure of mean profile depth for that particular mixture or grade (seal coat). It is preferred to have the measurement done at the initial stage of the pavement's service life. The SAAP projects the reduction of the MPD throughout its service life based on the traffic count. Alternately, the user can select the SAAP estimation option. That way, SAAP estimates the MPD values based on the shape and scale factors calculated from combined aggregate gradation and traffic count.

**Figure 72. Mean Profile Depth Input.**

After entering the MPD information, the user inputs the highway configuration and traffic data (Figure 73). In this step, users enter the information about the highway type (rural/urban or divided/undivided), the total number of through traffic lanes in each direction, the total AADT for both directions (for undivided highway, K roadbed) or the AADT for each direction (for divided highway, R or L roadbed), and the percent truck traffic (Figure 73). Using this information, the application calculates the adjusted AADT for the design lane. Again, the adjusted AADT is used to calculate the TMF. Please note that the current application does not consider the traffic growth factor.

When the user clicks the Next button on Figure 73, the software generates the skid number for 15 years at 1-year intervals starting from year one.



Project Name: IH-35 Laredo  
Run number: 2

**Enter Traffic Data**

Highway Type

Divided       Urban  
 Undivided       Rural

Total Number of Through Traffic Lanes in Each Direction

1 Lane     2 Lanes     3 Lanes     4 Lanes

Average Annual Daily Traffic (AADT) for Each Road Bed: 18530

Percent Truck Traffic: 6.3

Next

Navigation Pane

Form View

**Figure 73. Highway Type and Traffic Data Input.**

The next step (Figure 74) in the software provides options on how the user wants to see the output. In this window, there are three options for the display of results. The first option is to obtain a prediction of skid resistance as a function of years in service (up to 15 years). This chart also contains the project and prediction (iteration) number in the top left corner. The user can also print the chart by clicking the Print tab (Figure 75).

>> Main

## Skid Analysis of Asphalt Pavement (SAAP)

Texas A&M  
Transportation  
Institute

Project Name: IH-35 Laredo  
Run number: 2

Choose an Analysis for Skid Prediction

Predict Skid Resistance as a Function of Years of service

Classify an Asphalt Pavement section based on its Skid Resistance

Export Input \_Output Data to Excel file

Navigation Pane

FilePath

Form View

**Figure 74. Output Data Display Options.**

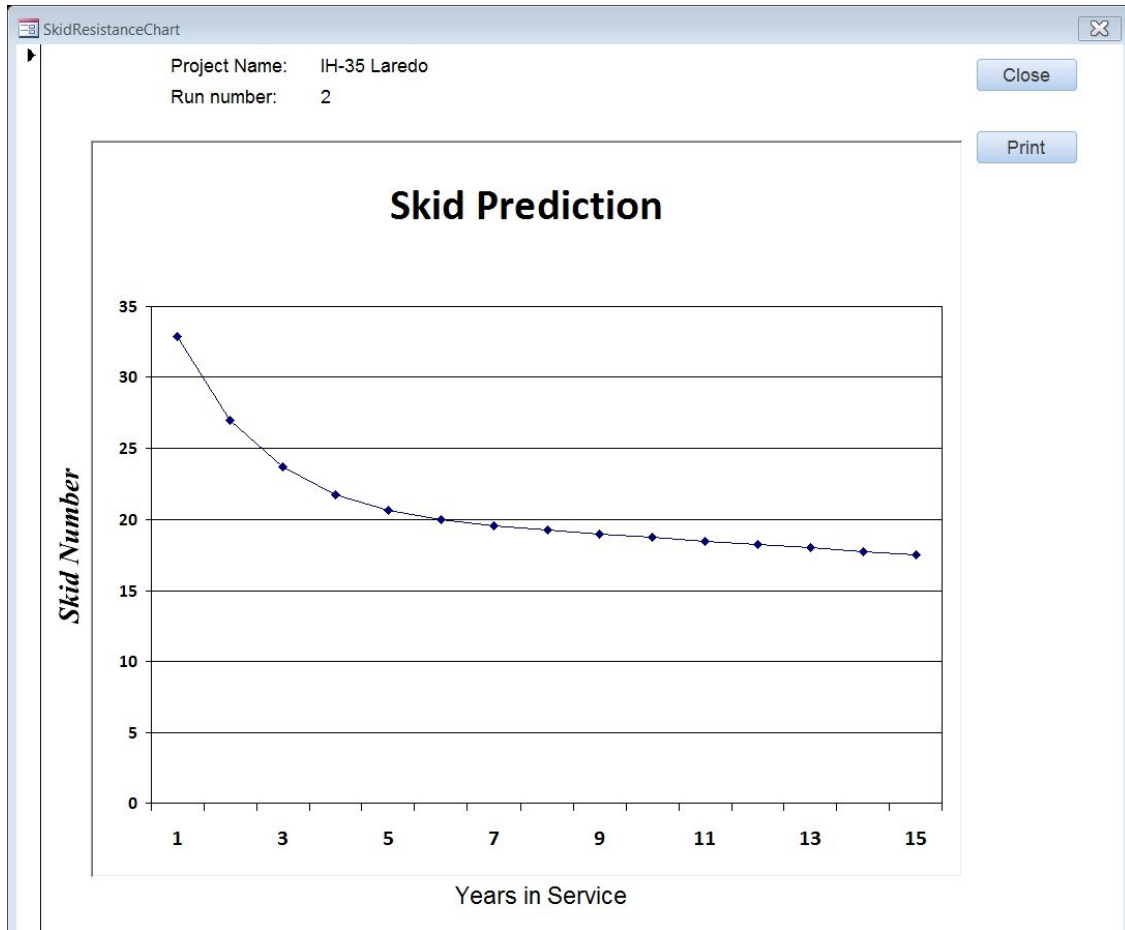


**Figure 75. Skid Prediction Chart for 15 Years.**

The second option is to get a classification of the pavement section based on its skid resistance after a specified number of years and corresponding threshold values. If the user selects “Classify an Asphalt Pavement Section Based on Its Skid Resistance,” a window (Figure 76) pops up in which the user needs to input some additional information required for pavement classification. These input parameters are:

- The length of service life in years for which a pavement section will be classified.
- The skid resistance threshold values based on which a pavement section will be classified (Figure 75). The first threshold value is the acceptable skid number above which the designer is not concerned. The second threshold value is the skid number above which (but below the acceptable value) one should monitor the surface condition more frequently and below which one should take corrective measure to restore surface friction.

After clicking on the Set button, a window with the pavement classification will be presented (Figure 77). Depending on the predicted skid number at the end of service life and designer selected threshold values, the pavement is classified as high, medium, or low. For display purposes, the high, medium, and low is shown as a green, yellow, and red bar chart, respectively.

The screenshot shows a software window titled "ClassificationParameter" with a close button in the top right corner. The main heading is "Set Classification Parameters" in orange text. Below the heading are four input fields with associated labels and operators:

- "Service Life (years)" with a dropdown menu showing the value "5".
- "Accepted (SN50) >=" with a dropdown menu showing the value "24".
- "21" with a dropdown menu, followed by "<= Monitor Pavement Frequently (SN50) <" and a text input field containing "24".
- "Takes Measures to Correct (SN50) <" with a text input field containing "21".

At the bottom center of the window is a blue button labeled "Set".

**Figure 76. Selection of Thresholds or Aggregate Classification.**

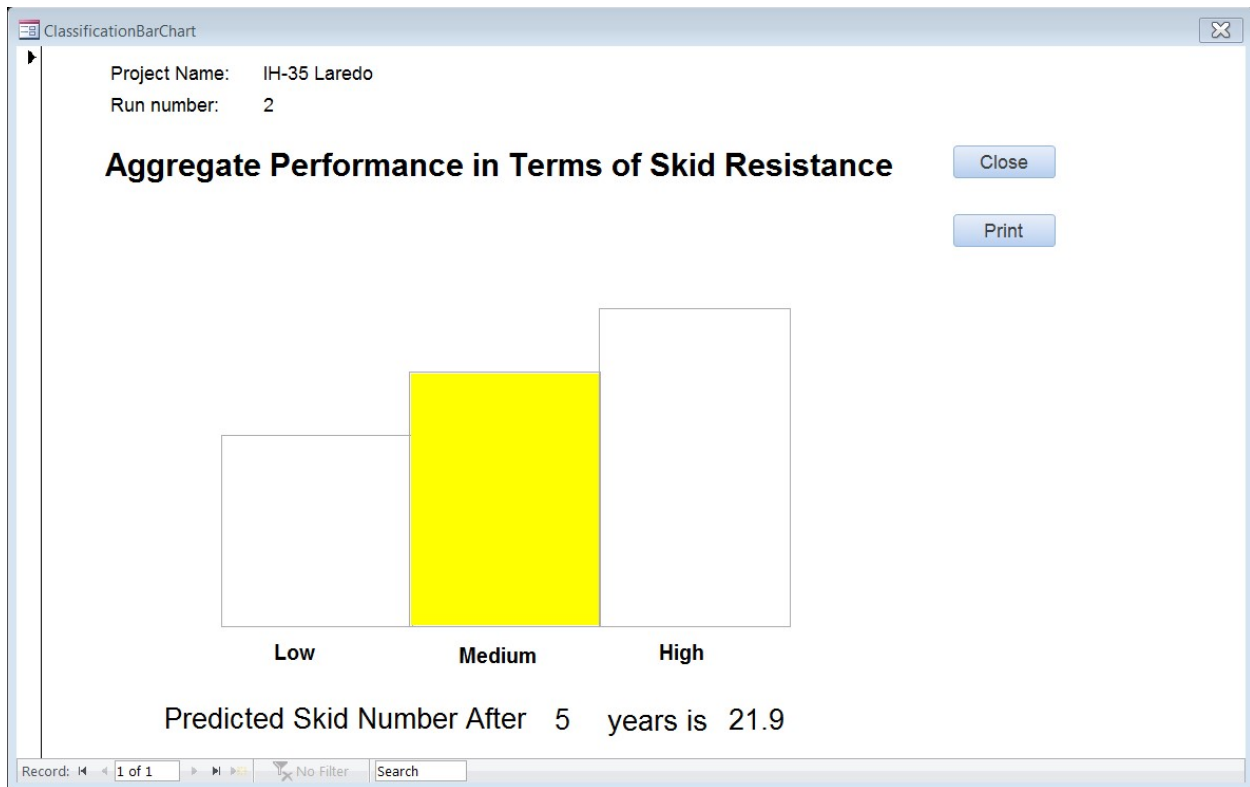


**Figure 77. Sample Aggregate Classification Based on Skid Performance.**

The third option for displaying the data is to export the input and output data into a Microsoft Excel spreadsheet. By clicking this button, the user can export the input and output file in a separate folder. Once the user selects this option a new window (Figure 78) pops up. The user has the option to change the input file name and the location folder. Once input file is saved, the same window provides the option to save output file where the user can save the output file with different name and location folder. Figure 79 and Figure 80 show sample input and output data in a spreadsheet. Input file records all the data or preferences selected by the user. The output file shows the projected skid number, IFI, MPD, and adjusted traffic count for each year starting from Year 1 to 15.

The application can be terminated by clicking the Exit Application button. The application saves all the input data entered previously. The user can also navigate through the application by clicking the tabs located on top of the windows.

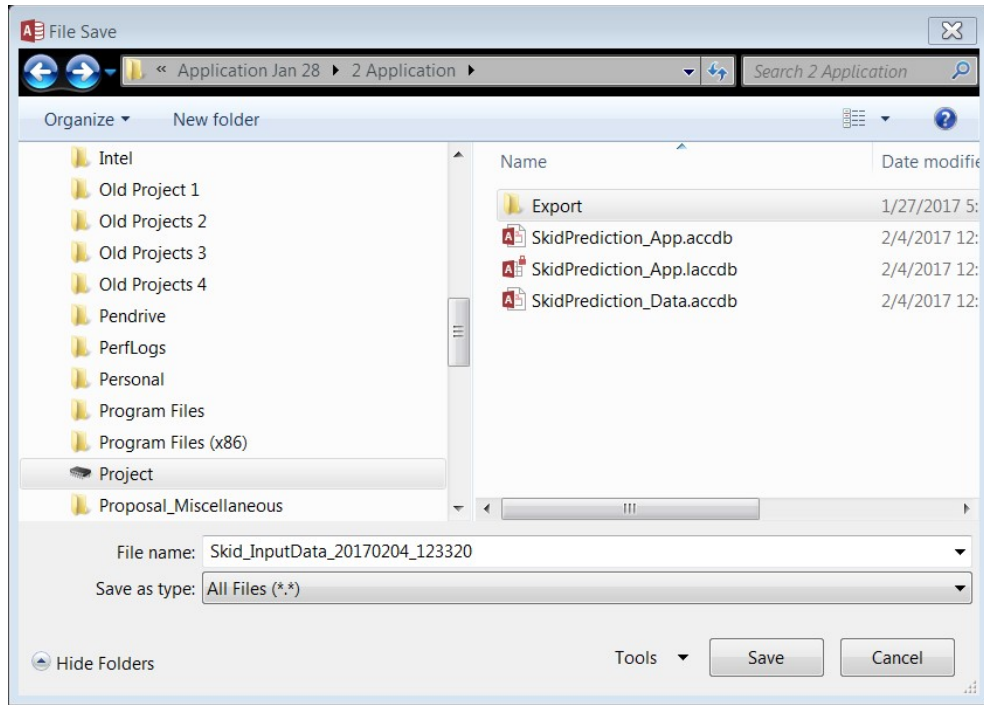


**Figure 78. Saving Input and Output Spreadsheet Files.**

The screenshot shows an Excel spreadsheet with the following data:

	A	B	C	D	E	F	G	H	I	J	K	L	M	N
1	INPUT NAME	INPUT VALUE												
2	Project Name	IH-35 Laredo												
3	Run Number	2												
4	Comments	User can write comment for his/her convenience												
5														
6	Surface Type	Asphalt Mixture												
7	Gradation Type	Mixture Gradation												
8	Gradation Name	Type C												
9	Data Points	3												
10	Number of Data Sources	3												
11														
12	TEXTURE DATASOURCES													
13	Name of Texture Data Source 1	S1												
14	Portion in the Mix	60												
15	Percent Retained on Sieve #4	30												
16	Texture Before Micro-Deval (BMD)	200												
17	Texture After 105 Mins Micro-Deval (AMD)	140												
18	Texture After 180 Mins Micro-Deval (AMD)	130												
19														
20	Name of Texture Data Source 2	S2												
21	Portion in the Mix	30												
22	Percent Retained on Sieve #4	80												
23	Texture Before Micro-Deval (BMD)	300												
24	Texture After 105 Mins Micro-Deval (AMD)	210												
25	Texture After 180 Mins Micro-Deval (AMD)	195												
26														
27	Name of Texture Data Source 3	S3												
28	Portion in the Mix	10												
29	Percent Retained on Sieve #4	0												
30	Texture Before Micro-Deval (BMD)	250												
31	Texture After 105 Mins Micro-Deval (AMD)	135												

**Figure 79. Sample Input Spreadsheet.**

Yr_In_Srvc_Nbr	Skid_Nbr	IFI	MPD	Adj_Trffc
1	34.78441	9414.722	0.650931	25793.76
2	29.18408	18829.44	0.633036	25793.76
3	25.64631	28244.17	0.615141	25793.76
4	23.39583	37658.89	0.597246	25793.76
5	21.94789	47073.61	0.579351	25793.76
6	20.99938	56488.33	0.561456	25793.76
7	20.36078	65903.06	0.543562	25793.76
8	19.91352	75317.78	0.525667	25793.76
9	19.58345	84732.5	0.507772	25793.76
10	19.32406	94147.22	0.489877	25793.76
11	19.10617	103561.9	0.471982	25793.76
12	18.91138	112976.7	0.454087	25793.76
13	18.72799	122391.4	0.436192	25793.76
14	18.5485	131806.1	0.418297	25793.76
15	18.36795	141220.8	0.400403	25793.76

**Figure 80. Sample Output Spreadsheet.**

## **AGGREGATE CLASSIFICATION SYSTEM BASED ON PROPOSED MODEL**

In this section, the model is used to illustrate the influence of aggregate characteristics and aggregate gradation on skid resistance. In addition, the results presented herein demonstrate how this model can be used to select the optimum aggregate characteristics and gradation such that the required skid resistance level is achieved given a certain traffic level. Table 12 presents an example of classification through threshold values set by the user.

The analysis involved the use of four AADT/lane levels with five percent truck traffic in all cases representing interstate, U.S. highway, state highway, and farm-to-market sections from the state of Texas. Five different mix types commonly used in the state of Texas were selected, and scale and shape parameters of the corresponding Weibull function were determined. In order to facilitate the comparison between the various sections, the SN(50) values in Table 12 were used to classify the pavement sections after 5 years of service. All the highways were considered

as divided, two-lane each way, and located in urban area. Results were obtained the SAAP application.

**Table 12. Skid Number Threshold Values after Five Years of Service.**

<b>Aggregate Class</b>	<b>SN Threshold Value</b>
High	$SN(50) \geq 30$
Medium	$20 \leq SN(50) < 30$
Low	$SN(50) < 20$

Table 13 shows the classification of the various pavement sections. Both Aggregate J, and K are combination of aggregates from three different sources. Aggregate P entirely consists of aggregates from one source. PFC, SMA-C, and SMA-D all three mixtures demonstrate high skid performance (Level H after 5 years) at all traffic levels when designed with Aggregate K. At same scenario, Type C mixture showed medium skid performance (Level M after 5 years) at high traffic levels and Type D mixture showed medium performance at both medium and high traffic level. Similarly, Aggregate J, and P showed different degrees of performance based on the traffic levels and mixtures types. Aggregate P even exhibited low skid performance (Level L after 5 years) for most traffic levels when used in Type D mixture and low performance for medium to high traffic when used in Type C mixture.

These results clearly demonstrate how the proposed models provides flexibility for engineers to select an aggregate source and a mixture design that achieve the required skid number after a certain traffic level. It also show that an aggregate (or combination of aggregates) may show different performance based on the type of mixtures and the traffic level they are subjected to.



**Table 13. Aggregate Classification for Different Roads.**

AADT/Lane	Mix Type				
	Type C	Type D	PFC	SMA-C	SMA-D
Aggregate J					
500	H	H	H	H	H
5000	H	M	H	H	H
15000	M	L	H	H	M
34000	M	L	H	M	M
Aggregate K					
500	H	H	H	H	H
5000	H	H	H	H	H
15000	H	M	H	H	H
34000	M	M	H	H	H
Aggregate P					
500	M	M	H	H	H
5000	M	L	H	H	M
15000	L	L	M	M	M
34000	L	L	M	M	L



## **CHAPTER 7: CONCLUSIONS AND RECOMMENDATIONS**

### **CONCLUSIONS**

Skid resistance is a key component in road safety. In this study, the researchers developed prediction models for the IFI and SN for flexible pavements with an asphalt mixture and seal coat as the surface course. These models were developed based on a comprehensive testing program in the field and laboratory. Field testing included measurements of the coefficient of friction using DFT, the MPD using CTMeter, and the skid number using a skid trailer. In the laboratory, the researchers used test methods to quantify the aggregate resistance to abrasion and polishing in addition to determining the measurements of aggregate texture and angularity using the AIMS apparatus. Statistical methods were used to develop the prediction models for friction and SN for HMA and seal coat. The main findings of this study are summarized below:

- The results showed good correlations between the developed models and experimental measurements.
- The developed skid prediction model for HMA incorporates parameters that describe aggregate shape characteristics (texture and angularity), aggregate gradation, aggregate resistance to polishing and abrasion, and traffic level.
- The skid prediction model for seal coat incorporates parameters that describe seal coat aggregate gradation, aggregate shape characteristics (texture and angularity), aggregate resistance to polishing and abrasion, and traffic level.
- The model results demonstrated that aggregate and surface characteristics as well as traffic level have a significant effect on skid resistance and the rate of skid reduction. Higher traffic levels caused a steep reduction in the skid number due to significant surface polishing in a short time.
- Asphalt mixtures prepared with coarse aggregate gradations had higher macrotexture and higher skid resistance than asphalt mixtures with fine aggregate gradations.
- Aggregate texture and the rate of texture change is the most influential factor affecting the skid resistance of both asphalt mixtures and surface-treatment surfaces.
- Seal coat Grade 3 was found to yield higher MPD and skid number than other grades.

- The AIMS and Micro-Deval tests were found to be proper tools to evaluate aggregate shape characteristics and their resistance to abrasion and polishing.
- The models are capable of predicting the skid resistance of HMA and seal coat over the course of their service life.

## **RECOMMENDATIONS**

Based on the findings of this study, the following recommendations are made for implementation and future research.

- These models can be used during mix design (or gradation of seal coat) procedure to optimize the aggregate selection and aggregate gradation to produce mixtures with adequate friction. Maintenance personnel can also utilize this tool to predict the future skid number for in-service roads in order to figure out the timing of corrective treatment related to its frictional resistance.
- The skid value of seal coat sections depends highly on the quality of construction. Asphalt bleeding or flushing can drastically reduce the skid resistance on seal coat surfaces regardless of the quality of aggregate. More test sections of seal coat should be included in future studies.
- Skid prediction models for both HMA and seal coat need to be validated with more field measurements, especially on roads whose conditions differ from that of Texas roads. Such measurements should cover more asphalt mixture types, aggregate type, and sources, aggregate combinations, traffic levels, and different climatic conditions.
- These prediction models were developed with data obtained from skid testing with smooth tires at 50 mph. In order to apply these models at different conditions, models should be calibrated for local test conditions (e.g., ribbed tires, different test speeds).
- State DOTs or agencies can build their aggregate texture and angularity database under their aggregate quality monitoring program. Mixture designers can use such databases in conjunction with skid prediction models to determine the future skid resistance of the intended mixture under traffic.

- Aggregate imaging measurement systems need modification in order to characterize aggregates with different shades of color.
- Design lane factors for AADT and trucks used to determine the traffic on design lane should be revisited based on more robust data.



## REFERENCES

- AASHTO (2002). AASHTO Designation TP 58-00: Standard Test Method for Resistance of Coarse Aggregate to Degradation by Abrasion in the Micro-Deval Apparatus. AASHTO Provisional Standards, American Association of State Highway and Transportation Officials, Washington, D.C.
- Ahammed, A. M., and S. L. Tighe (2007). Evaluation of Concrete Pavements Surface Friction Using LTPP Data: Preliminary Analysis and Texture Performance Models. In Transportation Research Board 86th Annual Meeting (No. 07-0727).
- Al Rousan, T. M. (2005). Characterization of Aggregate Shape Properties Using a Computer Automated System (Doctoral dissertation, Texas A&M University).
- ASTM (2009). Annual Book of ASTM Standards, Vol. 04.03, American Society for Testing and Materials, West Conshohocken, PA.
- Burchett J. L., and R. L. Rizenbergs (1980). Seasonal Variations in the Skid Resistance of Pavements in Kentucky. Transportation Research Record, No. 788.
- Cairney, P. (1997). Skid Resistance and Crashes: A Review of the Literature (No. ARR 311).
- Crouch, L., J. Gothard, G. Head, and W. Goodwin (1995). Evaluation of Textural Retention of Pavement Surface Aggregates. Transportation Research Record, No. 1486, Transportation Research Board, Washington, D.C.
- Dahir, S. H., and J. J. Henry (1978). Alternatives for the Optimization of Aggregate and Pavement Properties Related to Friction and Wear Resistance (No. FHWA-RD-78-209 Final Rpt.).
- Descornet, G. (1989). A Criterion for Optimizing Surface Characteristics. Transportation Research Record, No. 1215.
- Dunford, A. (2013). Friction and the Texture of Aggregate Particles Used in the Road Surface Course (Doctoral dissertation, University of Nottingham).

- FHWA (1990). Nationwide Personal Transportation Survey, NPTS Databook. Report FHWA-PL-94-010, Federal Highway Administration, U.S. Department of Transportation, Washington, DC.
- Flintsch, G. W., K. K. McGhee, and E. de Leon (2005). Field Validation of Macrotexture-Based Hot Mix Asphalt Segregation Detection Methods. *Journal of the Association of Asphalt Paving Technologists*.
- Forster, S. W. (1989). Pavement Microtexture and Its Relation to Skid Resistance. *Transportation Research Record*, No. 1215.
- Fuentes, L. G. (2009). Investigation of the Factors Influencing Skid Resistance and the International Friction Index (Doctoral dissertation, University of South Florida).
- Fülöp, I. A., I. Bogardi, A. Gulyas, and M. Csicsely-Tarpay (2000). Use of Friction and Texture in Pavement Performance Modeling. *Journal of Transportation Engineering*, Vol. 126, No. 3.
- Fwa, T. F., Y. S. Choo, and Y. Liu (2004). Effect of Surface Macrotexture on Skid Resistance Measurements by the British Pendulum Test. *Journal of Testing and Evaluation*, Vol. 32, No. 4.
- Galambos, V., B. Hegmon, and K. Rice (1997) Pavement Texture and Available Skid Resistance. Federal Highway Administration, U.S. Department of Transportation, Washington, D.C.
- Gargett, T. (1990). The Introduction of a Skidding-Resistance Policy in Great Britain.
- Hall, J. W., K. L. Smith, L. Titus-Glover, J. C. Wambold, T. J. Yager, and Z. Rado (2009). Guide for Pavement Friction. NCHRP Project.
- Henry, J. J. (1986). Tire Wet-Pavement Traction Measurement: A State-of-the-Art Review. ASTM Special Technical Publication 929: The Tire Pavement Interface. ASTM, Philadelphia.



- Henry, J. J. (2000). NCHRP Synthesis of Highway Practice 291: Evaluation of Pavement Friction Characteristics. Transportation Research Board, National Research Council, Washington, D.C.
- Henry, J. J., and S. H. Dahir (1979). Effects of Textures and the Aggregates That Produce Them on the Performance of Bituminous Surfaces. Transportation Research Record.
- Henry, J. J., and J. C. Wambold (1992). Use of Smooth-Treaded Test Tire in Evaluating Skid Resistance. Transportation Research Record, No. 1348, Transportation Research Board, National Research Council, Washington, D.C.
- Hogervorst, D. (1974). Some Properties of Crushed Stone for Road Surfaces. Bulletin of the International Association of Engineering Geology-Bulletin de l'Association Internationallement de Géologie de l'Ingénieur, Vol. 10, No. 1.
- Ivey, D. L., D. L. Bullard, J. R. Lock, and L. I. Griffin III (1992). Texas Skid Initiated Accident Reduction Program: Final Report. Report 910-1F, TTI: 2-18-89/910, TX-92/910-1F, Texas Department of Transportation.
- Kane, M., K. Scharnigg, M. Conter, P. Roe, and G. Schwalbe (2009). Report on Different Parameters Influencing Skid Resistance, Rolling Resistance and Noise Emissions. TYROSAFE Deliverable D.
- Kassem, E., E. Masad, A. Awed, and D. Little (2012). Laboratory Evaluation of Friction Loss and Compactability of Asphalt Mixtures (No. SWUTC/12/476660-00025-1).
- Kassem, E., A. Awed, E. Masad, and D. Little (2013). Development of Predictive Model for Skid Loss of Asphalt Pavements. Transportation Research Record: Journal of the Transportation Research Board, No. 2372.
- Kennedy, C. K., A. E. Young, and I. C. Butler (1990). Measurement of Skidding Resistance and Surface Texture and the Use of Results in the United Kingdom.
- Kowalski, K. J. (2007). Influence of Mixture Composition on the Noise and Frictional Characteristics of Flexible Pavements. ProQuest.

- Krugler, P. E., T. J. Freeman, J. E. Wirth, J. P. Wikander, C. K. Estakhri, and A. J. Wimsatt (2012). Performance Comparison of Various Seal Coat Grades Used in Texas (No. FHWA/TX-12/0-6496-1).
- Luis, M. G., and D. Hess (2010). Evaluation of the Effect of Pavement Roughness on Skid Resistance. *Journal of Transportation Engineering*, Vol. 136, No. 7.
- Mahmoud, E., and E. Masad (2007). Experimental Methods for the Evaluation of Aggregate Resistance to Polishing, Abrasion, and Breakage. *Journal of Materials in Civil Engineering*, Vol. 19, No. 11.
- Mahone, D. C. (1975). An Evaluation of the Effects of Tread Depth, Pavement Texture, and Water Film Thickness on Skid Number-Speed Gradients. Virginia Highway and Transportation Research Council, Charlottesville, VA.
- Masad, E., A. Luce, E. Mahmoud, and A. Chowdhury (2007). Relationship of Aggregate Texture to Asphalt Pavement Skid Resistance Using Image Analysis of Aggregate Shape. Final Report for Highway IDEA Project.
- Masad, E., A. Rezaei, A. Chowdhury, and T. J. Freeman (2010). Field Evaluation of Asphalt Mixture Skid Resistance and Its Relationship to Aggregate Characteristics (No. 0-5627-3). Texas Transportation Institute.
- McQuaid, G., P. Millar, and D. Woodward (2014). A Comparison of Techniques to Determine Surface Texture Data. In *Civil Engineering Research in Ireland Conference*, Belfast, Ireland.
- Mustaffar, M., O. bin Che Puan, and L. T. Chai (2004, August). Application of Digital Photogrammetry to Quantification of Road Surface Distresses. In the 6th Malaysian Road Conference, Kuala Lumpur, Malaysia.
- National Highway Traffic Safety Administration (NHTSA) (2014). Traffic Safety Facts 2014—A Compilation of Motor Vehicle Crash Data from the Fatality Analysis Reporting System and the General Estimates System.

- Noyce, D. A., H. U. Bahia, J. M. Yambo, and G. Kim (2005). Incorporating Road Safety into Pavement Management: Maximizing Asphalt Pavement Surface Friction for Road Safety Improvements. Draft Literature Review and State Surveys, Midwest Regional University Transportation Center (UMTRI), Madison, Wisconsin.
- Pashindu, H. R., T. F. Fwa, and G. P. Ong (2010). Evaluation of Aircraft Landing Overrun Risk. 7th International Conference on Road and Airfield Pavement Technology, Bangkok, Thailand.
- Prowell, B. D., J. Zhang, and E. R. Brown (2005). Aggregate Properties and the Performance of Superpave-Designed Hot Mix Asphalt. Transportation Research Board, No. 539.
- Putov, V. V., A. V. Putov, A. D. Stotckaia, V. N. Sheludko, and K. V. Ignatiev (2016). The Measurement Method of Runway Frictional Properties Correlated with the Braking Performance of Aircraft. In Soft Computing and Measurements (SCM), 2016 XIX IEEE International Conference, IEEE.
- Rezaei, A., E. Masad, and A. Chowdhury (2011). Development of a Model for Asphalt Pavement Skid Resistance Based on Aggregate Characteristics and Gradation. Journal of Transportation Engineering, Vol. 137, No. 12.
- Rizenbergs, R. L., J. L. Burchett, and C. T. Napier (1972). Skid Resistance of Pavements. Report No. KYHPR-64-24, Part II. Lexington, KY: Kentucky Department of Highways.
- Roque, R., D. Anderson, and M. Thompson (1991). Effect of Material, Design, and Construction Variables on Seal-Coat Performance. Transportation Research Record, No. 1300.
- Rose, J. G., B. M. Gallaway, and K. D. Hankins (1970). Macrotexture Measurement and Related Skid Resistance at Speeds from 20 to 60 Miles per Hour. Highway Research Record.
- Saito, K., T. Horiguchi, A. Kasahara, H. Abe, and J. J. Henry (1996). Development of Portable Tester for Measuring Skid Resistance and Its Speed Dependency on Pavement Surfaces. Transportation Research Record, No. 1536, Transportation Research Board, National Research Council, Washington, D.C.

- Sarsam, S. I., and H. N. Al Shareef (2015). Assessment of Texture and Skid Variables at Pavement Surface.
- Shafii, M. A. (2009). Skid Resistance and the Effect of Temperature (Doctoral dissertation, Universiti Teknologi Malaysia).
- Smith, H. A. (1977). Pavement Contributions to Wet-Weather Skidding Accident Reduction. Transportation Research Record, No. 622.
- Sullivan, B. W. (2005, May). Development of a Fundamental Skid Resistance Asphalt Mix Design Procedure. In Proceedings, International Conference on Surface Friction, Christchurch, New Zealand.
- Tang, T.C., K. Anupam, C. Kasbergen, and A. Scarpas (2016). Study of Influence of Operating Parameters on Braking Distance. Paper presented at TRB 96<sup>th</sup> Annual Meeting, Washington DC.
- Wagner, C., J. Studdard, and M. S. Gardiner (2004). Evaluation of Hot Mix Asphalt Macro- and Microtexture. Journal of Testing and Evaluation, Vol. 32, No. 1.
- Wambold, J. C., C. E. Antle, J. J. Henry, and Z. Rado (1995). International PIARC Experiment to Compare and Harmonize Texture and Skid Resistance Measurements: Final Report.
- West, T., J. Choi, D. Bruner, H. Park, and K. Cho (2001). Evaluation of Dolomite and Related Aggregates Used in Bituminous Overlays for Indiana Pavements. Transportation Research Record: Journal of the Transportation Research Board, No. 1757.
- Wu, Z., B. King, C. Abadie, and Z. Zhang (2012). Development of Design Procedure to Predict Asphalt Pavement Skid Resistance. Transportation Research Record: Journal of the Transportation Research Board, No. 2306.

**APPENDIX A:  
ASPHALT MIXTURE TEST SECTION RESULTS**

**Table 14. Combined Mixture Gradation.**

Section ID	Sieve Size, Cumulative Passing %								
	No. 200	No. 50	No. 30	No. 16	No. 8	No. 4	3/8"	1/2"	3/4"
IH 30_ATL_SMA_	8.1	15.9	18	21.1	27.8	49.5	86.3	100	—
US 59_ATL_CMHB-F_FM 2792	6.4	13.2	19	21	26.8	52.1	92	99.2	100
US 59_ATL_TY D_TRM 310	5.6	18.7	22	—	36.8	58.6	93.4	99.1	100
US 59_ATL_TY D_SHELBY CO LINE	5.9	18.3	21.4	—	37.6	56.5	91.8	99	100
US 271_ATL_CMHB-F_CAMP	5.4	15.2	17.6	21.1	25.3	40.3	97.2	100	100
IH 35 TOM Mix_AUS	6.6	10.2	13	17.3	24.1	56.3	100	100	100
RM 3238_AUS_TOM	8.7	14.2	21.1	30.2	47.5	79.4	99.6	100	—
US71_AUS_TOM	6.5	10.7	12.9	16	21	47.3	99.3	100	—
IH10_BMT_SMA-D	8.4	11.1	14.6	15.6	18.1	26.3	65.5	88.1	100
SH 82_BMT_SMA-D	8.8	13.1	15.9	18.5	24.2	30.2	66.5	85.9	100
SL 207_BMT_TY D	4	14.5	26.5	—	40.5	67.9	98.6	100	100
US 69_BMT_PFC	1.6	—	—	—	5.4	14.9	54.3	83	100
US 90_BMT_SMA-D	8.1	11.1	13.8	18	23	28.7	65.1	89	100
IH 45_BRY_TY C	2.8	10.4	15.5	—	35.4	61.3	80.4	—	100
IH 45_BRY_PFC	2	—	—	—	3.1	4.7	45.4	88.9	100
SH 6_BRY_NEW PFC	1.8	—	—	—	3.9	7.7	45.7	81	100
SH 6_BRY_OLD PFC	1.8	—	—	—	3.9	7.7	45.7	81	100
IH 35_LRD_SMA_WEBB	10.1	—	—	—	22.5	30.3	70.1	93.1	100
IH 35_LRD_SMA-C_LASALLE	8	10.7	12.7	15.5	19.8	21.3	47.8	87.8	100
US 59_LFK_PFC_Nacodoches	1.9	—	—	—	3.7	9.5	52.7	80.5	100
SH 7_LFK_TY D_Houston	4.9	14.8	20.8	—	32.6	51.9	78.4	—	100
IH 20_ODA_SP-C_Martin	7.6	12.4	16.1	21.9	30.7	55.7	87	98.5	100
IH 20_ODA_SP-D_Midland_2012	7.8	12.9	17	23.4	34.7	56.5	90.6	99.2	100
IH 20_ODA_SP-D_Midland_2013	7.7	13.7	17.9	24.4	34.1	55.5	90.5	99.2	100
IH 10_SAT_SMA-D_BEXAR	8.1	11.9	13.1	15.5	19	24.1	54.9	86.2	100
IH 10_SAT_TY C_BEXAR	5.2	17.4	24.5	—	39.6	53.9	80.6	—	100
IH 37_SAT_PFC_BEXAR	2	—	—	—	2.8	8.7	52	83	100
IH 10_YKM_TY D_AUSTIN	3.6	17.4	27	—	38.7	61.3	96.2	100	100
SH 36_YKM_TY D_AUSTIN	3.3	13.5	22	—	38.3	60.5	91.1	99.9	100
US 77_PHR_TY D_Kennedy	4.6	16.9	24.4	—	44.6	61.4	89.1	98.8	100
US 281_PHR_TY D_Hidalgo	4.9	20	26.3	—	42.1	64.4	90.4	98.5	100

**Table 15. Combined Mixture Gradation (Former Sieve Sizes)**

Section ID	Sieve Size, Cumulative Passing %						
	No. 200	No. 80	No. 40	No. 10	No. 4	3/8"	1/2"
SH 6 Bwp 2-1, Wp 2-1 Middle	3.3	8.1	13.5	34.9	58.3	82	99.7
SH 6 Bwp 2-1 Bottom	4.4	19.0	30.1	45.9	69.4	98.4	100
US 385_ODA_CMHB-F	5.6	8	11.3	21.7	49.4	98.9	100
IH 20_ODA_PFC_2004	5.6	8	11.3	21.7	49.4	98.9	100

**Table 16. Aggregate Texture and Angularity Data.**

Section ID	Texture			Angularity		
	BMD	AMD105	AMD180	BMD	AMD105	AMD180
IH 30_ATL_SMA_	212.865	146.956	139.730	2711.048	2103.727	2031.181
US 59_ATL_CMHB-F_FM 2792	338.796	245.080	223.442	3042.002	2326.436	2295.421
US 59_ATL_TY D_TRM 310	340.293	231.230	223.177	3053.064	2415.128	2312.008
US 59_ATL_TY D_SHELBY CO LINE	340.098	235.487	223.212	3051.622	2412.691	2309.846
US 271_ATL_CMHB-F_CAMP	355.781	211.213	187.858	2485.036	1935.100	1906.148
IH 35 TOM Mix_AUS	329.621	244.752		2628.379	1831.138	
RM 3238_AUS_TOM	331.297	250.479		2649.302	1814.856	
US71_AUS_TOM	329.565	244.562		2627.683	1831.680	
IH10_BMT_SMA-D	315.475	297.725		3017.425	2657.225	
SH 82_BMT_SMA-D	377.775	261.721		3090.563	2656.750	
SL 207_BMT_TY D	253.704	201.486	189.059	2652.508	1951.370	1922.113
US 69_BMT_PFC	259.897	215.728		2646.732	2271.563	
US 90_BMT_SMA-D	273.437	200.993		2637.083	1865.109	
IH 45_BRY_TY C	283.627	202.653		2711.190	2041.385	
IH 45_BRY_PFC	193.050	132.300		2712.175	1622.375	
SH 6_BRY_NEW PFC	331.112	249.844		2646.984	1816.660	
SH 6_BRY_OLD PFC	331.112	249.844		2646.984	1816.660	
IH 35_LRD_SMA_WEBB	240.897	187.361		2721.731	1751.527	
IH 35_LRD_SMA-C_LASALLE	444.207	245.921		2872.847	1983.396	
US 59_LFK_PFC_Nacodoches	347.048	249.150	227.080	3086.559	2442.439	2342.207
SH 7_LFK_TY D_Houston	300.203	240.824		2863.631	2191.003	
IH 20_ODA_SP-C_Martin	366.900	252.524	245.190	2743.733	1917.715	1807.820
IH 20_ODA_SP-D_Midland_2012	342.062	239.151	225.472	2733.780	1884.024	1756.817
IH 20_ODA_SP-D_Midland_2013	342.113	239.193	225.512	2733.800	1884.093	1756.922
US 385_ODA_CMHB-F	427.542	309.266		2768.035	1999.970	
IH 20_ODA_PFC_2004	427.542	309.266		2768.035	1999.970	
IH 10_SAT_SMA-D_BEXAR	277.855	191.877	173.304	2596.041	1794.027	1535.405
IH 10_SAT_TY C_BEXAR	202.321	144.655	135.983	2659.633	1754.349	1625.360
IH 37_SAT_PFC_BEXAR	278.050	238.885	232.119	2653.709	1750.563	1553.372
IH 10_YKM_TY D_AUSTIN	263.446	105.022	84.846	2652.319	1602.676	1394.093
SH 36_YKM_TY D_AUSTIN	118.595	75.3504	68.607	2772.539	1623.814	1565.969
US 77_PHR_TY D_Kennedy	309.350	213		2902.400	2685.675	
US 281_PHR_TY D_Hidalgo	298.826	197.464	185.798	2804.579	2638.757	2620.220
SH 6 Bwp 2-1, Wp 2-1 Middle	313.753	259.750		3203.438	2677.501	
SH 6 Bwp 2-1 Bottom	313.753	259.750		3203.438	2677.501	

**Table 17. Traffic Data.**

TxDOT District	Section ID	Design Lane Factor for AADT	Design Lane Factor for Truck	Average AADT	Avg. % Truck Traffic
Atlanta	IH 30_ATL_SMA_	0.7	0.8	13860	37
	US 59_ATL_CMHB-F_FM 2792	0.7	0.9	4478	16.2
	US 59_ATL_TY D_TRM 310	0.7	0.9	5202	15.2
	US 59_ATL_TY D_SHELBY CO LINE	0.7	0.9	6572	22.2
	US 271_ATL_CMHB-F_CAMP	0.4	0.45	13268	15.2
Austin	IH 35 TOM Mix_AUS	0.4	0.5	28317	27.1
	RM 3238_AUS_TOM	0.5	0.5	4540	4.4
	US71_AUS_TOM	0.7	0.9	20500	6.3
Beaumont	IH10_BMT_SMA-D	0.7	0.8	22700	22.5
	SH 82_BMT_SMA-D	0.4	0.45	7764	18.8
	SL 207_BMT_TY D	0.5	0.5	4860	11.9
	US 69_BMT_PFC	0.6	0.8	28164	8.8
	US 90_BMT_SMA-D	0.4	0.45	3928	10.7
Bryan	IH 45_BRY_TY C	0.7	0.8	13150	34
	IH 45_BRY_PFC	0.7	0.8	13150	34
	SH 6_BRY_NEW PFC	0.7	0.9	12860	14
	SH 6_BRY_OLD PFC	0.7	0.9	12120	15
Laredo	IH 35_LRD_SMA_WEBB	0.4	0.5	11400	24
	IH 35_LRD_SMA-C_LASALLE	0.8	0.9	6700	28
Lufkin	US 59_LFK_PFC_Nacodoches	0.8	0.9	13970	22.6
Odessa	IH 20_ODA_SP-C_Martin	0.8	0.9	7614	37.6
	IH 20_ODA_SP-D_Midland_2012	0.8	0.9	7480	37.4
	IH 20_ODA_SP-D_Midland_2013	0.7	0.8	16430	27.4
	US 385_ODA_CMHB-F	0.8	0.9	3642	12.8
San Antonio	IH 10_SAT_SMA-D_BEXAR	0.7	0.8	25330	18.8
	IH 10_SAT_TY C_BEXAR	0.7	0.9	25180	11.7
	IH 37_SAT_PFC_BEXAR	0.7	0.9	13380	21.4
Yoakum	IH 10_YKM_TY D_AUSTIN	0.7	0.8	20000	25
	SH 36_YKM_TY D_AUSTIN	0.5	0.5	5500	18
Pharr	US 77_PHR_TY D_Kennedy	0.8	0.9	4700	27
	US 281_PHR_TY D_Hidalgo	0.8	0.9	11313	28

**A-4 CTMETER DATA**

**Table 18. Beaumont CTMeter Data.**

CTM, (mm)	Beaumont				
	IH-10	LP-207	SH-82 SMA	US-69	US-90
WP1	0.77	0.67	0.50	1.63	1.02
WP2	0.97	0.69	0.59	1.70	0.98

**Table 19. Odessa CTMeter Data.**

CTM (mm)	Odessa			
	I- 20_Midland_SPD12	I- 20_Martin_PFC	I- 20_Martin_SPC	I- 20_Midland_2013
WP1	0.70	1.61	0.74	0.76
WP2	0.73	1.61	0.77	0.66
WP3	0.71	—	0.70	0.65
WP4	—	—	—	—
BWP1	—	—	0.65	0.82
BWP2	—	—	—	—
BWP3	—	—	—	—
BWP4	—	—	0.65	0.73
Shoulder1	0.8	1.61	—	—
Shoulder2	—	1.57	—	—
Shoulder3	—	—	—	—
Shoulder4	0.65	—	—	—

**Table 20. Atlanta CTMeter Data.**

CTM (mm)	Atlanta				
	IH-30-ATL	US-59- Panola- CMHBF	US-59- Panola- FM999	US-59- Panola- TRM311	US-271-ATL
WP1	0.61	0.68	0.38	0.52	0.81
WP2	0.68	0.6	0.35	0.53	0.73
WP3	0.71	0.7	0.34	0.6	0.77
WP4	0.71	0.64	0.31	0.59	—
BWP1	0.66	—	—	—	0.71
BWP2	—	—	—	—	—
BWP3	0.79	—	—	—	0.7
BWP4	—	—	—	—	—
Shoulder1	—	0.67	0.69	0.5	0.66
Shoulder2	—	—	—	—	—
Shoulder3	—	0.62	0.56	0.44	0.52
Shoulder4	—	—	—	—	—



**Table 21. Pharr and San Antonio CTMeter Data.**

CTM (mm)	Pharr		San Antonio				
	US-77-Ken	US-281-TyD	I-10-Bex-SMA	I-10-Bex-TyC	I-37-PFC	US-90-Uvalde	US-281-ATS
WP1	0.73	0.7	0.81	0.57	1.65	0.39	0.52
WP2	0.69	0.64	0.64	0.58	1.58	0.35	0.46
WP3	0.73	0.62	0.76	0.54	1.78	0.33	—
WP4	—	—	—	—	—	—	—
BWP1	—	—	0.93	0.63	1.74	—	2.43
BWP2	—	—	—	—	—	—	2.63
BWP3	—	—	0.63	0.5	1.86	—	—
BWP4	—	—	—	—	—	—	—
Shoulder1	0.33	0.6	—	0.4	—	0.36	—
Shoulder2	—	—	—	—	—	—	—
Shoulder3	0.34	0.58	—	—	—	0.4	—
Shoulder4	—	—	—	—	—	—	—

**Table 22. Laredo CTMeter Data.**

CTM (mm)	Laredo			
	IH-35-LRD-LAS-NB	IH-35-LRD-LAS-SB	IH-35-LRD-NP-COT-S	IH-35-LRD-LRD-Webb
WP1	0.42	0.48	0.27	1.2
WP2	0.44	0.47	0.24	1.1
WP3	—	0.47	—	1.25
WP4	—	—	—	1.02
BWP1	0.46	—	1.03	—
BWP2	0.51	—	1.07	—
BWP3	—	—	—	—
BWP4	—	—	—	—
Shoulder1	—	0.94	1.19	0.83
Shoulder2	—	—	1.1	—
Shoulder3	—	0.96	—	0.98
Shoulder4	—	—	—	—

**Table 23. Lufkin, Houston, and YKM CTMeter Data.**

CTM (mm)	Lufkin		Houston	YKM	
	SH7-LFK	US-59-Noco	SH-6	IH-10	SH-36-HMA
WP1	0.62	1.76	1.55	0.45	0.63
WP2	0.6	1.71	1.60	0.45	0.69
WP3	0.61	1.79	1.42	0.36	0.59
WP4	0.55	—	1.74	0.39	0.56
BWP1	0	1.86	—	—	—
BWP2	—	—	—	—	—
BWP3	—	1.81	—	—	—
BWP4	—	—	—	—	—
Shoulder1	0.66	—	1.96	0.71	0.56
Shoulder2	—	—	—	—	—
Shoulder3	0.8	—	2.13	0.64	0.54
Shoulder4	—	—	—	—	—

**Table 24. Austin CTMeter Data.**

CTM (mm)	Austin		
	FM3328	I35-Austin	SH-71
WP1	0.58	0.82	0.8
WP2	0.51	0.77	0.74
WP3	0.47	0.78	0.83
WP4	—	—	—
BWP1	—	0.84	—
BWP2	—	—	—
BWP3	—	—	—
BWP4	—	—	—
Shoulder1	0.45	—	0.97
Shoulder2	0.43	0.8	0.75
Shoulder3	—	—	—
Shoulder4	—	—	—

**Table 25. Bryan CTMeter Data.**

CTM (mm)	Bryan			
	IH45-PFC	IH45-TYC	SH6-PFC-new	SH6-PFC-old
WP1	1.30	1	1.80	1.54
WP2	1.21	0.91	1.53	1.71
WP3	—	—	—	—
WP4	—	—	—	—
BWP1	1.59	0.97	2.14	1.89
BWP2	1.59	0.86	1.85	1.87
BWP3	—	—	—	—
BWP4	—	—	—	—
Shoulder1	—	—	—	—
Shoulder2	—	—	—	—
Shoulder3	—	—	—	—
Shoulder4	—	—	—	—

**A-5 DFT DATA**

**Table 26. Beaumont DFT Data.**

DFT at 20 km/h	Beaumont				
	IH-10	LP-207	SH-82 SMA	US-69	US-90
WP1	0.42	0.50	0.52	0.61	0.53
WP2	0.40	0.54	0.52	0.40	0.54
WP3	0.42	0.55	—	0.38	—
WP4	0.42	0.56	—	0.36	—
BWP1	—	—	—	—	—
BWP2	—	—	—	—	—
BWP3	—	—	—	—	—
BWP4	—	—	—	—	—
Shoulder1	0.7	0.71	0.69	0.49	0.63
Shoulder2	—	—	0.69	—	—
Shoulder3	0.605	0.68	—	0.46	—
Shoulder4	—	—	—	—	—

**Table 27. Odessa DFT Data.**

DFT at 20 km/h	Odessa			
	I-20_Midland_SPD12	I-20_Martin_PFC	I-20_Martin_SPC	I-20_Midland_2013
WP1	0.53	0.55	0.39	0.49
WP2	0.52	0.57	0.40	0.48
WP3	0.53	—	0.37	0.48
WP4	—	—	—	—
BWP1	—	—	0.49	0.61
BWP2	—	—	—	—
BWP3	—	—	—	—
BWP4	—	—	0.50	0.6
Shoulder1	0.73	0.68	—	—
Shoulder2	—	0.72	—	—
Shoulder3	—	—	—	—
Shoulder4	0.75	—	—	—

**Table 28. Atlanta DFT Data.**

DFT at 20 km/h	Atlanta				
	IH-30-ATL	US-59-Panola-CMHB	US-59-Panola-FM999	US-59-Panola-TRM311	US-271-ATL
WP1	0.73	0.49	0.57	0.535	0.71
WP2	0.73	0.51	0.60	0.54	0.71
WP3	0.73	0.53	0.56	0.55	0.73
WP4	0.73	0.54	0.57	0.53	—
BWP1	0.78	—	—	—	0.76
BWP2	—	—	—	—	—
BWP3	0.78	—	—	—	0.73
BWP4	—	—	—	—	—
Shoulder1	—	0.66	0.785	0.72	0.77
Shoulder2	—	—	—	—	—
Shoulder3	—	0.71	0.79	0.74	0.85
Shoulder4	—	—	—	—	—

**Table 29. Pharr and San Antonio DFT Data.**

DFT at 20 km/h	Pharr		San Antonio				
	US-77-Ken	US-281-TyD	I-10-Bex-SMA	I-10-Bex-TyC	I-37-PFC	US-90-Uvalde	US-281-ATS
WP1	0.47	0.44	0.46	0.49	0.39	—	0.31
WP2	0.46	0.43	0.43	0.48	0.38	0.58	0.28
WP3	0.45	0.43	0.47	0.46	0.4	0.58	—
WP4	—	—	—	—	—	—	—
BWP1	—	—	0.45	0.45	0.31	—	0.60
BWP2	—	—	—	—	—	—	0.63
BWP3	—	—	0.42	0.44	0.33	—	—
BWP4	—	—	—	—	—	—	—
Shoulder1	0.62	0.57	—	0.69	—	0.73	—
Shoulder2	—	—	—	—	—	—	—
Shoulder3	0.61	0.54	—	—	—	0.75	—
Shoulder4	—	—	—	—	—	—	—

**Table 30. Laredo DFT Data.**

DFT at 20 km/h	Laredo			
	IH-35-LRD-LAS-NB	IH-35-LRD-LAS-SB	IH-35-LRD-NP-COT-S	IH-35-LRD-LRD-Webb
WP1	0.39	0.37	0.205	0.43
WP2	0.40	0.37	0.225	0.44
WP3	—	0.36	—	0.40
WP4	—	0.36	—	0.46
BWP1	0.43	—	—	—
BWP2	0.42	—	0.54	—
BWP3	—	—	—	—
BWP4	—	—	—	—
Shoulder1	—	0.57	0.61	0.62
Shoulder2	—	—	0.62	—
Shoulder3	—	0.54	—	0.63
Shoulder4	—	—	—	—

**Table 31. Lufkin, Houston, and YKM DFT Data.**

DFT at 20 km/h	Lufkin		Houston	YKM	
	SH7-LFK	US-59-Noco	SH-6	IH-10	SH-36-HMA
WP1	0.63	0.45	0.41	0.40	0.29
WP2	—	0.4	0.44	0.41	0.33
WP3	0.61	0.43	0.41	0.40	0.30
WP4	0.59	—	0.40	0.41	0.29
BWP1	—	0.53	—	—	—
BWP2	—	—	—	—	—
BWP3	—	0.46	—	—	—
BWP4	—	—	—	—	—
Shoulder1	0.74	—	0.40	0.59	0.61
Shoulder2	—	—	—	—	—
Shoulder3	0.76	—	0.45	0.64	0.63
Shoulder4	—	—	—	—	—

**Table 32. Austin DFT Data.**

DFT at 20 km/h	Austin		
	FM3328	I35-Austin	SH-71
WP1	0.64	0.49	0.49
WP2	0.65	0.44	0.50
WP3	0.65	0.49	0.51
WP4	—	—	—
BWP1	—	—	—
BWP2	—	0.56	—
BWP3	—	—	—
BWP4	—	—	—
Shoulder1	0.84	—	0.62
Shoulder2	0.86	0.57	0.63
Shoulder3	—	—	—
Shoulder4	—	—	—

**Table 33. Bryan DFT Data.**

DFT at 20 km/h	Bryan			
	IH45-PFC	IH45-TYC	SH6-PFC-new	SH6-PFC-old
WP1	0.35	0.34	0.31	0.36
WP2	0.33	0.34	0.29	0.35
WP3	—	—	—	—
WP4	—	—	—	—
BWP1	0.41	0.37	0.37	0.45
BWP2	0.39	0.33	0.33	0.44
BWP3	—	—	—	—
BWP4	—	—	—	—
Shoulder1	—	—	—	—
Shoulder2	—	—	—	—
Shoulder3	—	—	—	—
Shoulder4	—	—	—	—





**APPENDIX B:  
SEAL COAT TEST SECTION RESULTS**

**Table 34. Aggregate Gradation (Cumulative Percent Retained).**

Sieve Size	Cumulative Retained (%)		
	Grade 3	Grade 4	Grade 5
1"	—	—	—
7/8"	—	—	—
3/4"	0	—	—
5/8"	0-2	0	—
1/2"	20-40	0-5	0
3/8"	80-100	20-40	0-5
1/4"	95-100	—	—
No. 4	—	95-100	50-80
No. 8	99-100	98-100	98-100

**Table 35. Aggregate Texture and Angularity Data.**

Section ID	Texture			Angularity		
	BMD	AMD105	AMD180	BMD	AMD105	AMD180
US 77_PHR_GR3_Cameron	499.365	227.121	213.534	2926.364	1945.145	1735.848
US 281_PHR_GR3_Hidalgo	581.650	326.500		2589.625	1569.775	
US 281_PHR_GR3_Brooke_TRM 752	499.365	227.121	213.534	2926.364	1945.145	1735.848
US 281_PHR_GR3_Brooke_TRM 722	581.650	326.500		2589.625	1569.775	
US 377_FTW_GR3_Hood	219.709	125.641	105.146	2676.475	1702.489	1496.160
US 377_FTW_GR3_Tarrant	219.709	125.641	105.146	2676.475	1702.489	1496.160
SH 199_FTW_GR3_Parker	195.125	116		2649.700	1646.050	
US 67_BWD_GR4_Coleman	219.709	125.641	105.146	2676.475	1702.489	1496.160
US 67_BWD_GR4_Brown	219.709	125.641	105.146	2676.475	1702.489	1496.160
US 183_BWD_GR4_Eastland	249.449	125.035	116.680	2738.360	1693.279	1518.136
US 377_BWD_GR4_Brown	219.709	125.641	105.146	2676.475	1702.489	1496.160
US 90_SAT_GR4_Bexar	147.835	90.971	83.988	2646.301	2214.888	1922.761
FM 1518_GR3_Bexar	266.692	238.899	233.901	2664.419	1728.358	1552.914
SH 16_SAT_GR4_Atascosa_TRM 626	462.408	434.028	424.305	3144.438	1972.419	1940.779
SH 16_SAT_GR 4_Atascosa_TRM 642	581.650	326.500		2589.625	1569.775	
SH 36_YKM_GR 3_Austin	156.480	88.002	79.740	2648.315	1815.372	1749.992
US 59_LFK_GR3_Angelina	558.637	446.350		2957.900	2113.900	
US 69_LFK_GR4_Angelina	283.537	236.412		1974.913	1347.463	
US 287_LFK_GR4_Trinity	283.537	236.412		1974.913	1347.463	
FM 2213_LFK_GR5_San Augustine	283.537	236.412		1974.913	1347.463	
US 59_LFK_GR4_Shelby	266.692	238.899	233.901	2664.419	1728.358	1552.914
LP 338_ODA_GR4_Ector	427.542	309.266	293.333	2768.035	1999.971	1932.344
US 385_ODA_GR4_Crane	172.532	100.092	90.883	2665.842	1654.067	1408.696
US 385_ODA_GR4_Ector	172.532	100.092	90.883	2665.842	1654.067	1408.696
SH 82_BMT_GR4_Jefferson	283.537	236.412		1974.913	1347.463	
FM 365_BMT_GR4_Jefferson	283.537	236.412		1974.913	1347.463	
FM 105_BMT_GR4_Orange	283.537	236.412		1974.913	1347.463	
US 80_ATL-GR4_Harrison	283.537	236.412		1974.913	1347.463	
US 59_ATL_GR3_Cass_RG_TRM238	191.247	165.049	159.389	2691.062	2288.818	2230.886
SH 77_ATL_GR4_Cass_TRM 745_SS	244.489	156.482	152.577	2579.935	1931.762	1787.538
SH 77_ATL_GR4_Cass_TRM 720_RG	166.072	132.860	120.722	2905.053	2391.690	2358.177

**Table 36. Traffic Data.**

TxDOT District	Section ID	Design Lane Factor for AADT	Design Lane Factor for Truck	Average AADT	Avg % Truck Traffic
Pharr	US 77_PHR_GR3_Cameron	0.8	0.9	8500	22
	US 281_PHR_GR3_Hidalgo	0.8	0.9	8482	29
	US 281_PHR_GR3_Brooke_TRM 752	0.8	0.9	6000	34
	US 281_PHR_GR3_Brooke_TRM 722	0.8	0.9	7336	32
Dallas-FW	US 377_FTW_GR3_Hood	0.8	0.9	10923	9.2
	US 377_FTW_GR3_Tarrant	0.8	0.9	13055	7.5
	SH 199_FTW_GR3_Parker	0.5	0.5	5822	18.2
Brownwood	US 67_BWD_GR4_Coleman	0.4	0.45	5665	13.5
	US 67_BWD_GR4_Brown	0.4	0.45	5846	13.5
	US 183_BWD_GR4_Eastland	0.5	0.5	2395	15.8
	US 377_BWD_GR4_Brown	0.4	0.45	13186	7.8
San Antonio	US 90_SAT_GR4_Bexar	0.7	0.9	24357	3.6
	FM 1518_GR3_Bexar	0.5	0.5	2854	19.7
	SH 16_SAT_GR4_Atascosa_TRM 626	0.8	0.9	4532	13.8
	SH 16_SAT_GR 4_Atascosa_TRM 642	0.5	0.5	9000	21.3
YKM	SH 36_YKM_GR 3_Austin	0.5	0.5	5500	18
Lufkin	US 59_LFK_GR3_Angelina	0.7	0.8	11760	28.2
	US 69_LFK_GR4_Angelina	0.4	0.45	12888	13.3
	US 287_LFK_GR4_Trinity	0.5	0.5	1746	28.1
	FM 2213_LFK_GR5_San Augustine	0.5	0.5	500	13.5
	US 59_LFK_GR4_Shelby	0.4	0.45	10250	34.2
Odessa	LP 338_ODA_GR4_Ector	0.5	0.5	4171	27
	US 385_ODA_GR4_Crane	0.8	0.9	2484	15.5
	US 385_ODA_GR4_Ector	0.8	0.9	3929	12
Beaumont	SH 82_BMT_GR4_Jefferson	0.5	0.5	1877	11
	FM 365_BMT_GR4_Jefferson	0.5	0.5	3820	7
	FM 105_BMT_GR4_Orange	0.8	0.45	13264	5.6
Atlanta	US 80_ATL-GR4_Harrison	0.5	0.5	3464	7.7
	US 59_ATL_GR3_Cass_RG_TRM238	0.8	0.9	8826	21
	SH 77_ATL_GR4_Cass_TRM 745_SS	0.5	0.5	2935	12
	SH 77_ATL_GR4_Cass_TRM 720_RG	0.8	0.9	1193	19

## B-4 CTMETER DATA

**Table 37. Beaumont and Odessa CTMeter Data.**

CTM (mm)	Beaumont			Odessa			
	FM-105	FM-365	SH-82 Seal Coat	LP_338_Seal Coat	US_385_C MHBFB	US_385_Seal Coat_Ector	US_385_Seal Coat_Crane
WP1	2.38	2.62	1.18	0.81	0.89	0.72	1.55
WP2	2.42	2.54	1.20	0.94	0.78	0.96	1.53
WP3	—	2.61	—	0.96	0.74	0.83	—
WP4	—	2.42	—	—	—	—	—
BWP1	2.46	3.12	2.28	1.72	—	1.51	2.14
BWP2	2.42	—	2.1	—	—	—	2.26
BWP3	—	3	—	—	—	—	—
BWP4	—	—	—	1.96	—	1.56	—
Shoulder1	—	—	—	—	0.77	—	2.97
Shoulder2	—	—	—	—	—	—	—
Shoulder3	—	—	—	—	—	—	—
Shoulder4	—	—	—	—	0.85	—	—

**Table 38. Atlanta CTMeter Data.**

CTM (mm)	Atlanta			
	SH-77-Atlanta	SH-77-Cass-Gravel	US-59-Cass	US-80-Harrison
WP1	1.31	2.57	1.8	2.03
WP2	1.33	2.44	2.03	1.9
WP3	1.53	—	1.9	1.9
WP4	1.26	—	—	—
BWP1	—	2.79	—	—
BWP2	—	2.81	—	—
BWP3	—	—	—	—
BWP4	—	—	—	—
Shoulder1	3.26	—	3.13	2.49
Shoulder2	—	—	—	—
Shoulder3	2.39	—	3.38	2.61
Shoulder4	—	—	—	—

**Table 39. Pharr CTMeter Data.**

CTM (mm)	Pharr			
	US-77-Camer	US-281-Haidalgo-SealCoat	US-281-Brook-742	US-281-718
WP1	1.9	0.62	0.81	0.45
WP2	2.27	1.57	0.8	0.51
WP3	2	0.7	0.8	0.48
WP4	1.79	—	—	—
BWP1	2.42	2.33	1.84	—
BWP2	—	—	—	—
BWP3	2.27	2.37	1.61	1.27
BWP4	—	—	—	—
Shoulder1	—	—	—	—
Shoulder2	—	—	—	—
Shoulder3	—	—	—	—
Shoulder4	—	—	—	—

**Table 40. San Antonio CTMeter Data.**

CTM (mm)	San Antonio				
	FM-1518	US-90-Seal Coat	SH-16-McMullen	SH-16-ATS-TRM642	SH-16-ATS-TRM626
WP1	2.31	2.48	1.42	1.05	1.29
WP2	2.04	2.25	1.35	1.22	1.73
WP3	—	—	—	—	—
WP4	—	—	—	—	—
BWP1	2.81	3	—	2.49	2.72
BWP2	—	2.37	—	2.14	2.82
BWP3	—	—	—	—	—
BWP4	—	—	—	—	—
Shoulder1	—	—	2.93	—	—
Shoulder2	—	—	2.98	—	—
Shoulder3	—	—	—	—	—
Shoulder4	—	—	—	—	—

**Table 41. YKM and Brownwood CTMeter Data.**

CTM (mm)	YKM	Brownwood			
	SH-36-SealCoat	US67-Brown	US67-Coleman	US183-Eastland	US377-Brown
WP1	1.37	1.15	0.82	1.45	1.89
WP2	1.24	1.01	0.71	1.48	1.96
WP3	—	—	—	—	—
WP4	—	—	—	—	—
BWP1	—	1.96	—	1.71	—
BWP2	—	1.9	—	1.68	—
BWP3	—	—	—	—	—
BWP4	—	—	—	—	—
Shoulder1	3.48	2.38	2.05	—	2.68
Shoulder2	—	—	—	—	—
Shoulder3	—	—	—	—	—
Shoulder4	—	—	—	—	—

**Table 42. Dallas-FW CTMeter Data.**

CTM (mm)	Dallas-FW		
	SH 199-Parker	US 377-Hood	US 377-Tarrant
WP1	2.65	—	2.23
WP2	2.14	2.49	0.48
WP3	—	—	2.38
WP4	—	—	—
BWP1	2.92	—	—
BWP2	2.69	—	—
BWP3	—	—	—
BWP4	—	—	—
Shoulder1	—	2.9	3.21
Shoulder2	—	3	3.41
Shoulder3	—	—	—
Shoulder4	—	—	—

**Table 43. Lufkin CTMeter Data.**

Measurement Location	CTM (mm)				
	Lufkin-FM2213	US 59-Shelby	US-59-LFK-ANG	US-69-LFK-ANG	Grovton-287
WP1	1.53	1.62	1.97	1.15	2.78
WP2	1.65	1.42	2	1.12	2.82
WP3	—	1.43	1.96	1.64	2.86
WP4	—	—	1.93	1.74	—
BWP1	1.93	2.24	—	—	3.09
BWP2	2.02	2.20	—	—	—
BWP3	—	—	—	—	3.26
BWP4	—	—	—	—	—
Shoulder1	—	—	2.83	2.88	—
Shoulder2	—	—	—	—	—
Shoulder3	—	—	2.53	3.33	—
Shoulder4	—	—	—	—	—

**B-5 DFT DATA**

**Table 44. Beaumont and Odessa DFT Data.**

DFT at 20 km/h	Beaumont			Odessa			
	FM-105	FM-365	SH-82 Seal Coat	LP_338_S eal Coat	US_385_CMHB F	US_385_SealCoat_Ector	US_385_Seal Coat_Crane
WP1	0.93	0.88	0.98	0.44	0.54	0.2	0.35
WP2	0.84	—	0.98	0.50	0.54	0.26	0.35
WP3	—	0.83	—	0.50	0.54	0.25	—
WP4	—	0.87	—	—	—	—	—
BWP1	0.91	0.42	0.90	0.55	—	0.35	0.45
BWP2	0.84	—	0.93	—	—	—	0.43
BWP3	—	0.80	—	—	—	—	—
BWP4	—	—	—	0.56	—	0.34	—
Shoulder1	—	—	—	—	0.69	—	0.64
Shoulder2	—	—	—	—	—	—	—
Shoulder3	—	—	—	—	—	—	—
Shoulder4	—	—	—	—	0.69	—	—

**Table 45. Atlanta DFT Data.**

DFT at 20 km/h	Atlanta			
	SH-77-Atlanta	SH-77-Cass-Gravel	US-59-Cass	US-80-Harrison
WP1	0.72	0.63	0.56	0.98
WP2	0.71	0.61	0.60	0.965
WP3	—	—	0.57	0.99
WP4	0.78	—	—	—
BWP1	—	0.69	—	—
BWP2	—	0.64	—	—
BWP3	—	—	—	—
BWP4	—	—	—	—
Shoulder1	0.96	—	0.79	0.97
Shoulder2	—	—	—	—
Shoulder3	0.84	—	0.73	0.98
Shoulder4	—	—	—	—

**Table 46. Pharr DFT Data.**

DFT at 20 km/h	Pharr			
	US-77-Camer	US-281-Haidalgo-SealCoat	US-281-Brook-742	US-281-718
WP1	0.31	0.28	0.24	0.25
WP2	0.28	0.30	0.27	0.28
WP3	0.29	0.33	0.25	0.26
WP4	0.30	—	—	—
BWP1	0.31	0.58	0.27	0.55
BWP2	—	—	—	—
BWP3	0.36	0.58	0.26	0.51
BWP4	—	—	—	—
Shoulder1	—	—	—	—
Shoulder2	—	—	—	—
Shoulder3	—	—	—	—
Shoulder4	—	—	—	—



**Table 47. San Antonio DFT Data.**

DFT at 20 km/h	San Antonio				
	FM-1518	US-90-Seal Coat	SH-16-McMullen	SH-16-ATS-TRM642	SH-16-ATS-TRM626
WP1	0.69	0.39	0.47	0.56	0.53
WP2	0.66	0.34	0.49	0.57	0.53
WP3	—	—	—	—	—
WP4	—	—	—	—	—
BWP1	0.75	0.41	—	0.69	0.65
BWP2	—	0.43	—	0.71	0.61
BWP3	—	—	—	—	—
BWP4	—	—	—	—	—
Shoulder1	—	—	0.67	—	—
Shoulder2	—	—	0.63	—	—
Shoulder3	—	—	—	—	—
Shoulder4	—	—	—	—	—

**Table 48. YKM and Brownwood DFT Data.**

DFT at 20 km/h	YKM	Brownwood			
	SH-36-SealCoat	US67-Brown	US67-Coleman	US183-Eastland	US377-Brown
WP1	0.44	0.19	0.23	0.32	0.22
WP2	0.41	0.18	0.19	0.22	0.26
WP3	—	—	—	—	—
WP4	—	—	—	—	—
BWP1	—	0.24	—	0.31	—
BWP2	—	—	—	0.32	—
BWP3	—	—	—	—	—
BWP4	—	—	—	—	—
Shoulder1	0.74	0.41	0.31	—	—
Shoulder2	—	—	—	—	—
Shoulder3	—	—	—	—	—
Shoulder4	—	—	—	—	—

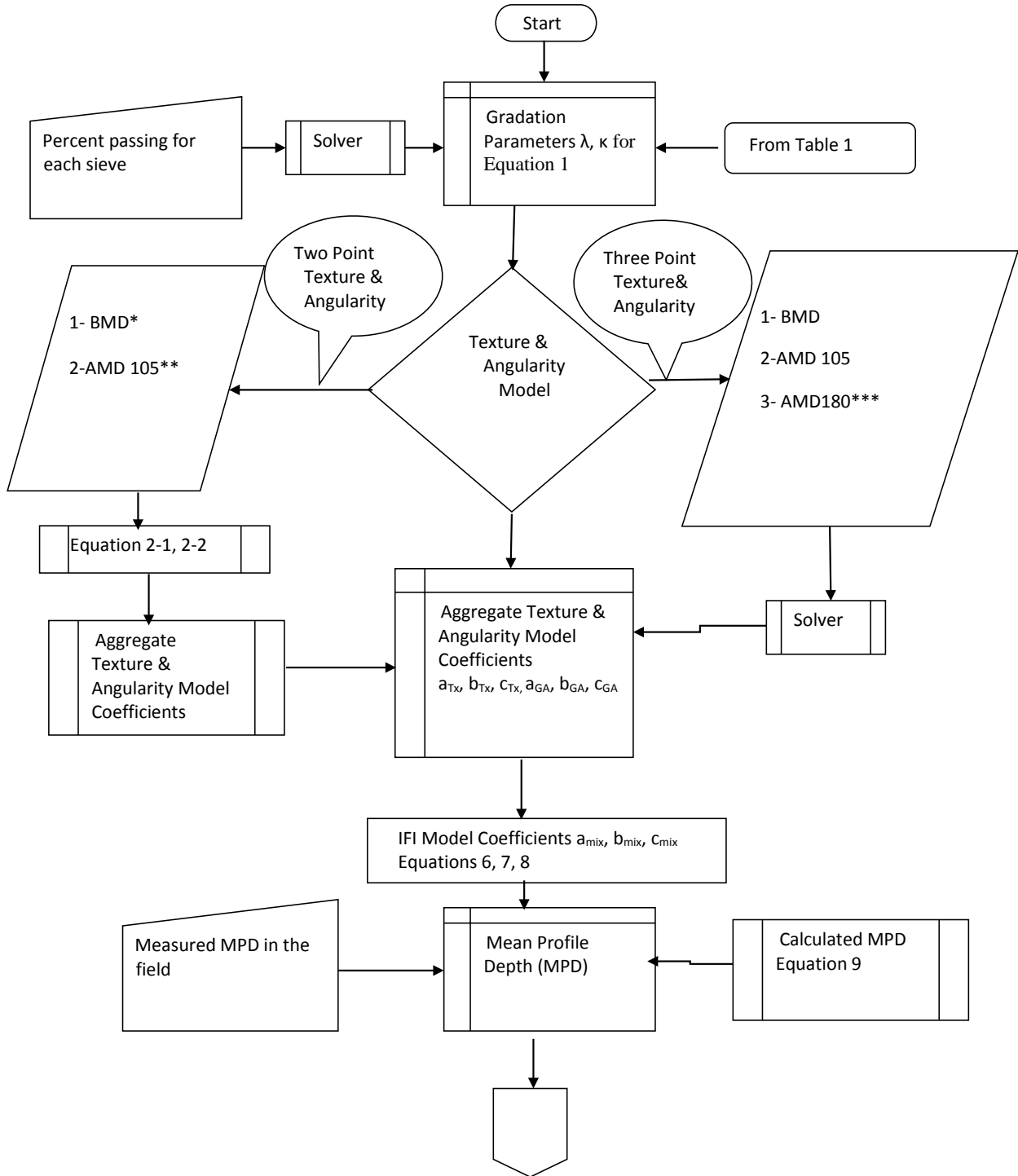
**Table 49. Fort Worth DFT Data.**

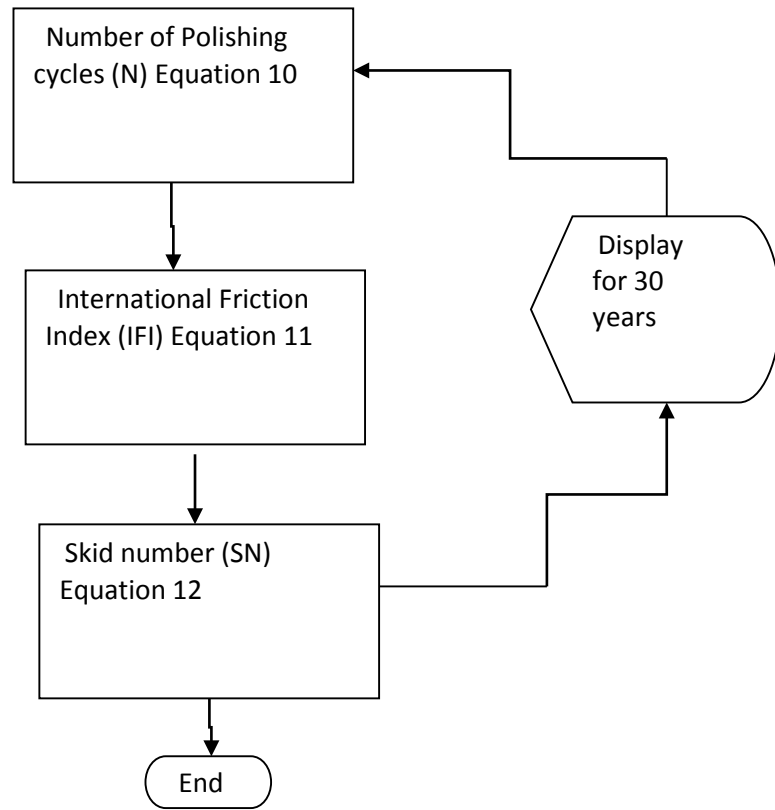
DFT at 20 km/h	Dallas-FW		
	SH 199-Parker	US 377-Hood	US 377-Tarrant
WP1	0.27	0.25	0.22
WP2	0.25	0.24	0.16
WP3	—	—	0.24
WP4	—	—	—
BWP1	0.39	—	—
BWP2	0.30	—	—
BWP3	—	—	—
BWP4	—	—	—
Shoulder1	—	0.59	—
Shoulder2	—	—	0.51
Shoulder3	—	—	—
Shoulder4	—	—	—

**Table 50. Lufkin DFT Data.**

DFT at 20 km/h	Lufkin				
	Lufkin-FM2213	US 59-Shelby	US-59-LFK-ANG	US-69-LFK-ANG	US-287
WP1	—	0.59	—	0.86	0.72
WP2	0.86	0.58	0.31	0.87	—
WP3	—	0.55	0.31	0.88	0.41
WP4	—	—	0.31	0.89	—
BWP1	—	0.65	—	—	0.71
BWP2	0.81	0.66	—	—	—
BWP3	—	—	—	—	0.79
BWP4	—	—	—	—	—
Shoulder1	—	—	0.45	0.83	—
Shoulder2	—	—	—	0	—
Shoulder3	—	—	0.56	0.83	—
Shoulder4	—	—	—	—	—

## APPENDIX C: SAAP FLOW CHART FOR ASPHALT MIXTURE





\* Texture or Angularity before Micro-Deval measured by AIMS.

\*\* Texture or Angularity after 105 minutes in Micro-Deval measured by AIMS.

\*\*\* Texture or Angularity after 180 minutes in Micro-Deval measured by AIMS.

**1. Determine the gradation parameters  $\lambda$  and  $\kappa$ .**

1a. Option 1—Input gradation (percent passing) for any combination of the following standard sieves:

**1", 7/8", 3/4", 5/8", 1/2", 3/8", #4, #8, #10, #16, #30, #80, #200.**

Use the solver to fit Equation 1 to the gradation curve. **The output is the parameters  $\lambda$  and  $\kappa$ .**

$$F(x; \lambda, \kappa) = 1 - e^{-\left(\frac{x}{\lambda}\right)^\kappa} \quad \text{Equation 1}$$

1b. Option 2: **Select a standard mix gradation from the table below.** The default values for  $\lambda$  and  $\kappa$  in Table 1 will be used.

**Table 1.** Scale and shape parameters

Mix Design	Scale Parameter $\lambda$	Shape Parameter $\kappa$
Type C	5.204	0.9018
Type D	3.648	0.894
PFC	10.26	2.45
SMA-D	8.542	1.381
Crack Attenuating Mixture (CAM)	3.168	1.000
SMA-C	9.82	1.568
CMHB-C	8.578	1.077
TOM	3.134	0.9747
SP-C	5.109	1.032
SP-D	4.764	0.9991
CMHB-F	5.205	1.218

**2. Input number of aggregate sources used in the mix and the percent retained sieve #4 for each source.**

**3. Input aggregate texture/angularity data for each aggregate source.**

**3a. Option 1—input:**

- Texture/angularity measured using AIMS at t = 0 polishing time.
- Texture/angularity measured using AIMS at t = 105 minutes of polishing.

Then use Equations 3 to 5 to output  $a_{Tx}$ ,  $a_{Tx}+b_{Tx}$ ,  $c_{Tx}$ ,  $a_{Gai}$ ,  $a_{Gai}+b_{Gai}$  and  $c_{Gai}$ :

$$a_{Tx} + b_{Tx} = 0.999BMD_{Tx} + 0.438 i \quad \text{Equation 3}_1$$

$$a_{GA} + b_{GA} = 0.999BMD_{GA} + 2.646 i \quad \text{Equation 3\_2}$$

$$a_{Tx} = 0.864AMD_{Tx} + 14.985 i \quad \text{Equation 4\_1}$$

$$a_{GA} = 1.237AMD_{GA} - 699.759 i \quad \text{Equation 4\_2}$$

$$c_{Tx} = \frac{A+TL}{B+C \times ARI} i \quad \text{Equation 5\_1}$$

Where: A = 0.492, B = 59.506, C = -7.106

$$c_{GA} = \frac{A+TL}{B+C \times ARI} i \quad \text{Equation 5\_2}$$

Where: A = 1.891, B = 111.658, C = 1.081

$$TL = \frac{BMD - AMD}{BMD} i \quad \text{Equation 5(a)}$$

$$ARI = \frac{AMD/BMD}{1-(AMD/BMD)^2} i \quad \text{Equation 5(b)}$$

Where:

i stands for an aggregate source. TL and ARI should be calculated separately for texture and angularity.

### 3b. Option 2—input:

- Texture measured using AIMS at t = 0 polishing time.
- Texture measured using AIMS at t = 105 minutes of polishing.
- Texture measured using AIMS at t = 180 minutes of polishing.

Use solver to fit Equation 2 to three data points and determine  $a_{Tx}$ ,  $b_{Tx}$ , and  $c_{Tx}$ :

$$\text{Texture } (t) = a_{Tx} + b_{Tx} \cdot \exp(-c_{Tx} \cdot t) i \quad \text{Equation 2\_1}$$

$$\text{Angularity } (t) = a_{GA} + b_{GA} \cdot \exp(-c_{GA} \cdot t) i \quad \text{Equation 2\_2}$$

### 4. Calculate the weighted average $a_{Tx}$ , $b_{Tx}$ , $c_{Tx}$ , $a_{GA}$ , $b_{GA}$ , and $c_{GA}$ for all aggregate sources as follows:

$$\overline{a_{Tx}} = \sum_{i=1}^n \alpha_i w_i a_{Tx}$$

$$\overline{b_{Tx}} = \sum_{i=1}^n \alpha_i w_i b_{Tx}$$

$$\overline{c_{Tx}} = \sum_{i=1}^n \alpha_i w_i c_{Tx}$$

$$\overline{a_{GA}} = \sum_{i=1}^n \alpha_i w_i a_{GA}$$

$$\overline{b_{GA}} = \sum_{i=1}^n \alpha_i w_i b_{GA}$$

$$\overline{c_{GA}} = \sum_{i=1}^n \alpha_i w_i c_{GA}$$

$$\alpha_i = \frac{\text{Percent retained on sieve \#4 in aggregate } i}{\text{Sum of the percent retained on sieve \#4 for all aggregates}}$$

$w_i$  = percent of aggregate  $i$  in the mix

- 5. Use the parameters obtained from the previous steps to calculate  $a_{mix}$ ,  $b_{mix}$ , and  $c_{mix}$  using Equation 6, 7, and 8.**

$$a_{mix} = \frac{49.3144 + \lambda}{351.289 - 0.00193 \times (AMD_{Tx})^2} \quad \text{Equation 6}$$

$$a_{mix} + b_{mix} = 0.33 \ln \frac{(1.43757(a_{Tx} + b_{Tx}) + 46.8933\lambda + (333.491k))}{(2.42031 \times (a_{GA} + b_{GA}))} + 1.0081 \quad \text{Equation 7}$$

$$c_{mix} = 0.018 + (1.654c_{Tx} + 1.346c_{GA}) \quad \text{Equation 8}$$

- 6. Obtain the mixture MPD.**

6a. Option 1: Enter the MPD values from experimental measurements.

6b. Estimate MPD from gradation parameters using Equation 9.

$$\text{MPD} = (\lambda/34.180) - (0.398/k) + (k^{0.416}) - 0.003N \quad \text{Equation 9}$$

- 7. Input highway and traffic information:**

Divided/undivided, number of lanes in each direction, total AADT in both directions (undivided) or total AADT in one direction for divided highway, percent of truck traffic.

**8. Calculate TMF using Equation 10a.**

The TMF is calculated using Equation 4.15

$$TMF = \frac{\text{Number of days between construction and field testing} \times \text{adjusted traffic}}{1000} \quad (4.15)$$

The adjusted traffic is calculated using Equation 4.16.

$$\text{Adjusted traffic} = \frac{AADT \times (100 - PTT) \times DL_{AADT}}{100} + \frac{AADT \times PTT \times DL_{truck} \times 20}{100} \quad (4.16)$$

Where:

AADT: average annual daily traffic for each roadbed (both direction for undivided and one direction for divided highway).

$DL_{AADT}$ : design lane factor of AADT (depends on number of lanes and urban/rural condition).

$DL_{truck}$ : design lane factor of trucks (depends on number of lanes and urban/rural condition).

PTT: percent truck traffic.

**Rural Highway**

Number of Lanes in each direction	Undivided		Divided	
	$DL_{AADT}$	$DL_{truck}$	$DL_{AADT}$	$DL_{truck}$
1	0.50	0.50	N/A	N/A
2	0.40	0.45	0.80	0.90
3	0.30	0.40	0.40	0.50

**Urban Highway**

Number of Lanes in each direction	Undivided		Divided	
	$DL_{AADT}$	$DL_{truck}$	$DL_{AADT}$	$DL_{truck}$
1	0.50	0.50	N/A	N/A
2	0.30	0.40	0.70	0.90
3	0.25	0.35	0.40	0.50
4	N/A	N/A	0.30	0.40

**9. Calculate equivalent number of polishing cycles N using Equation 10.**

$$N = TMF \times 10^{\frac{1}{A + B \times c_{mix} + \frac{C}{c_{mix}}}} \quad \text{Equation 10}$$



Where:

$$A = -0.452, B = -58.95, C = 5.834 \times 10^{-6}.$$

- 10. Calculate IFI as a function of equivalent number of polishing cycles using Equation 11.**

$$IFI(N) = a_{mix} + b_{mix} \times \exp(-c_{mix} \cdot N) \quad \text{Equation 11}$$

- 11. Calculate SN as a function of vehicles using Equation 12.**

$$SN_{50}(N) = 4.81 + 140.32[IFI(N) - 0.045] \times e^{\frac{-20}{SP}} \quad \text{Equation 12}$$

$$S_p = 14.2 + 89.7MPD \quad \text{Equation 12(a)}$$

- 12. Plot SN as a function N.**

- 13. Input parameters for ranking a road section.**

Skid resistance service life that the road should be resurfaced afterwards, Skid resistance threshold values.

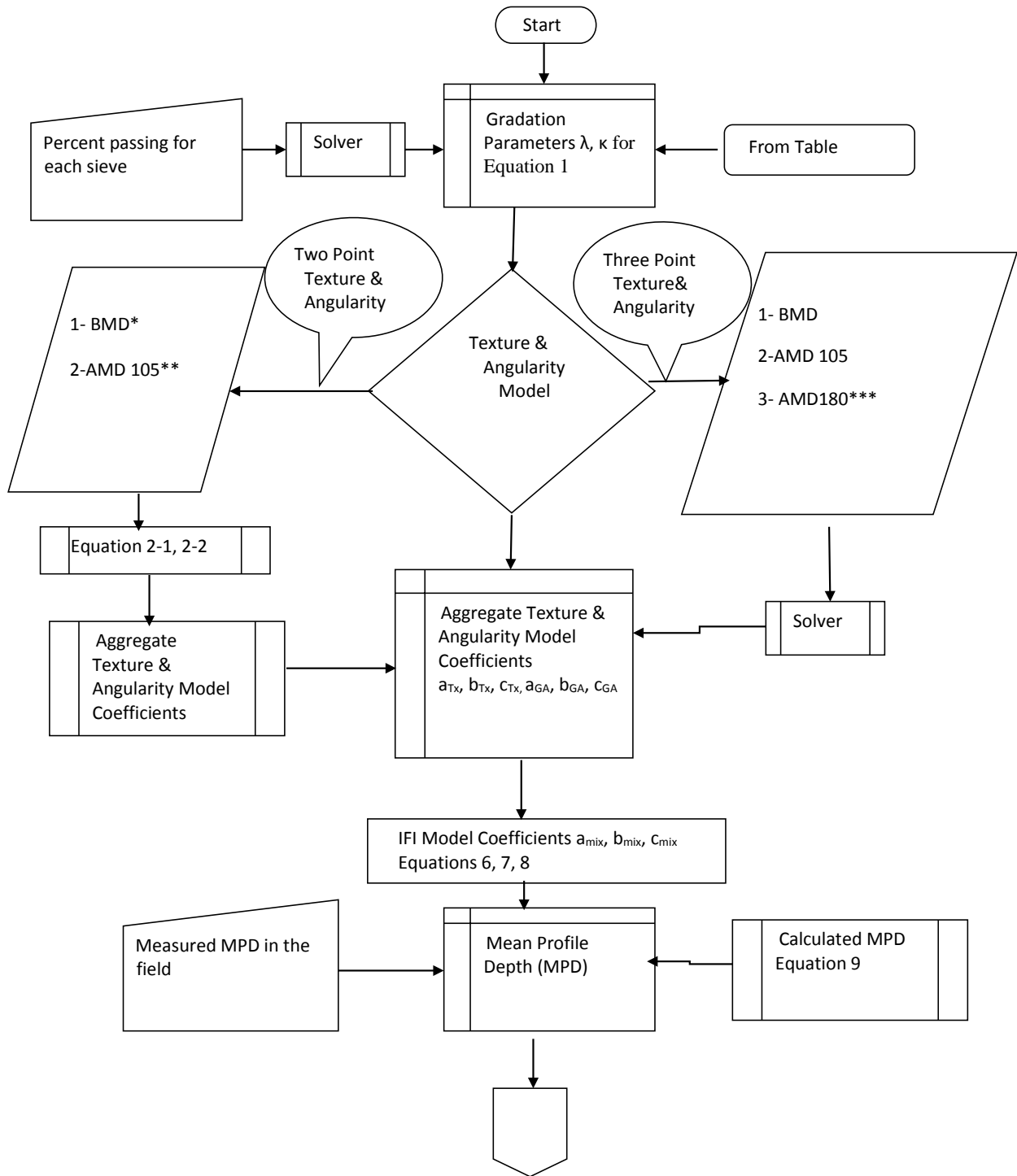
- 14. Rank a road section based on the following skid number values.**

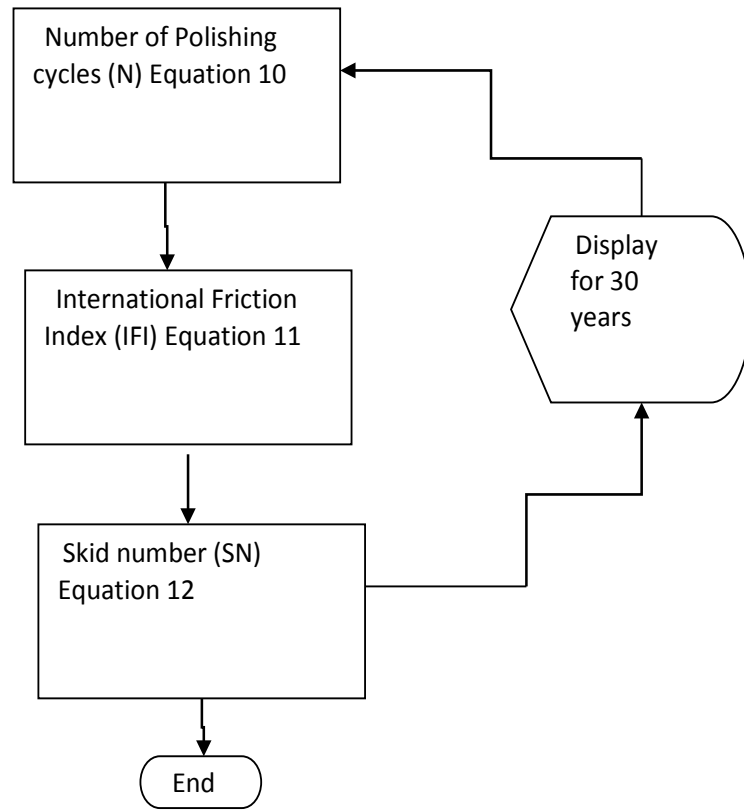
Example of a situation where user can define threshold values of skid number—what he/she thinks is acceptable (high), acceptable but requires frequent monitoring (medium), or not acceptable (low).

Aggregate Class	SN Threshold Value
High	$SN(50) \geq 30$
Medium	$21 \leq SN(50) < 30$
Low	$SN(50) < 21$



## APPENDIX D: SAAP FLOW CHART FOR SURFACE TREATMENT





- \* Texture or Angularity before Micro-Deval measured by AIMS.
- \*\* Texture or Angularity after 105 minutes in Micro-Deval measured by AIMS.
- \*\*\* Texture or Angularity after 180 minutes in Micro-Deval measured by AIMS.

**1. Determine the gradation parameters  $\lambda$  and  $\kappa$ .**

1a. Option 1—Input gradation (percent passing) for any combination of the following standard sieves:

**1", 7/8", 3/4", 5/8", 1/2", 3/8", #4, #8, #16, #30, #50, #80, #200.**

Use the solver to fit Equation 1 to the gradation curve. **The output is the parameters  $\lambda$  and  $\kappa$ .**

$$F(x; \lambda, \kappa) = 1 - e^{-(x/\lambda)^\kappa} \quad \text{Equation 1}$$

1b. Option 2: **Select a standard mix gradation from the table below.** The default values for  $\kappa$  and  $\lambda$  in this Table 1 will be used.

**Table 1.** Scale and shape parameters

Mix Design	Scale Parameter $\lambda$	Shape Parameter $\kappa$
Grade 3	12.24	8.809
Grade 4	9.176	5.142
Grade 5	5.556	5.372

**2. Input number of aggregate sources used in the mix and the percent passing sieve #4 for each source.**

**3. Input aggregate texture data for each aggregate source.**

3a. Option 1—input:

- Texture measured using AIMS at  $t = 0$  polishing time.
- Texture measured using AIMS at  $t = 105$  minutes of polishing.

Then use Equations 3 to 5 to output  $a_{Tx}$ ,  $a_{Tx}+b_{Tx}$ ,  $c_{Tx}$ ,  $a_{GA}$ ,  $a_{GA}+b_{GA}$  and  $c_{GA}$ :

$$a_{Tx} + b_{Tx} = BMD + 0.134 i \quad \text{Equation 3}_1$$

$$a_{GA} + b_{GA} = 0.994BMD + 21.084 i \quad \text{Equation 3}_2$$

$$a_{Tx} = 1.011AMD - 17.918 i \quad \text{Equation 4}_1$$

$$a_{GA} = 1.232AMD - 648.34 i \quad \text{Equation 4}_2$$

$$c_{Tx} = \frac{A+TL}{B+C \times ARI} i \quad \text{Equation 5}_1$$

Where: A = 1.555, B = 126.995, C = -18.174

$$c_{GA} = \frac{A+TL}{B+C \times ARI} i \quad \text{Equation 5\_2}$$

Where: A = 1.292, B = -9.77, C = 58.155

$$TL = \frac{BMD - AMD}{BMD} i \quad \text{Equation 5(a)}$$

$$ARI = \frac{AMD/BMD}{1-(AMD/BMD)^2} i \quad \text{Equation 5(b)}$$

where

i stands for an aggregate source. TL and ARI should be calculated separately for texture and angularity.

3b. Option 2—input:

- Texture measured using AIMS at t = 0 polishing time.
- Texture measured using AIMS at t = 105 minutes of polishing.
- Texture measured using AIMS at t = 180 minutes of polishing.

Use solver to fit Equation 2 to three data points and determine  $a_{Tx}$ ,  $b_{Tx}$ , and  $c_{Tx}$ :

$$\text{Texture } (t) = a_{Tx} + b_{Tx} \cdot \exp(-c_{Tx} \cdot t) i \quad \text{Equation 2\_1}$$

$$\text{Angularity } (t) = a_{GA} + b_{GA} \cdot \exp(-c_{GA} \cdot t) i \quad \text{Equation 2\_2}$$

**4. Calculate the weighted average  $a_{Tx}$ ,  $b_{Tx}$ ,  $c_{Tx}$ ,  $a_{GA}$ ,  $b_{GA}$ , and  $c_{GA}$  for all aggregate sources as follows:**

$$\overline{a_{Tx}} = \sum_{i=1}^n \alpha_i w_i a_{Tx}$$

$$\overline{b_{Tx}} = \sum_{i=1}^n \alpha_i w_i b_{Tx}$$

$$\overline{c_{Tx}} = \sum_{i=1}^n \alpha_i w_i c_{Tx}$$

$$\overline{a_{GA}} = \sum_{i=1}^n \alpha_i w_i a_{GA}$$

$$\overline{b_{GA}} = \sum_{i=1}^n \alpha_i w_i b_{GA}$$

$$\overline{c_{GA}} = \sum_{i=1}^n \alpha_i w_i c_{GA}$$

$$\alpha_i = \frac{\text{Percent retained on sieve \#4 in aggregate } i}{\text{Sum of the percent retained on sieve \#4 for all aggregates}}$$

$w_i$  = percent of aggregate  $i$  in the mix

- 5. Use the parameters obtained from the previous steps to calculate  $a_{mix}$ ,  $b_{mix}$ , and  $c_{mix}$  using Equation 6, 7, and 8.**

$$a_{mix} = \frac{40.493 + \lambda}{330 - 0.0011 \times (AMD_{Tx})^2} \quad \text{Equation 6}$$

$$a_{mix} + b_{mix} = 0.4 \ln \frac{(1.43757(a_{Tx} + b_{Tx}) + 46.8933\lambda + (3433.491k))}{(2.02031 \times (a_{GA} + b_{GA}))} \quad \text{Equation 7}$$

$$c_{mix} = (2.654c_{Tx} + 1.5c_{GA}) \quad \text{Equation 8}$$

- 6. Obtain the mixture MPD.**

6a. Option1: Enter the MPD values from experimental measurements.

6b. Estimate MPD from gradation parameters using Equation 9.

$$MPD = (\lambda/5.403) + (3.491/k) + (k^{0.104}) + N^{-0.47} - 2.594 \quad \text{Equation 9}$$

- 7. Input road information:**

Divided/Undivided, Number of lanes in each direction, Total AADT in both directions, Percent of truck traffic.

- 8. Calculate TMF using Equation 10a.**

The TMF is calculated using Equation 4.15.

$$TMF = \frac{\text{Number of days between construction and field testing} \times \text{adjusted traffic}}{1000} \quad (4.15)$$

The adjusted traffic is calculated using Equation 4.16.

$$\text{Adjusted traffic} = \frac{AADT \times (100 - PTT) \times DL_{AADT}}{100} + \frac{AADT \times PTT \times DL_{truck} \times 20}{100} \quad (4.16)$$

where:

AADT: average annual daily traffic for each section.

$DL_{AADT}$ : design lane factor of AADT (depends on number of lanes and urban/rural condition).

$DL_{truck}$ : design lane factor of trucks (depends on number of lanes and urban/rural condition).

PTT: percent truck traffic.

### Rural Highway

Number of Lanes in each direction	Undivided		Divided	
	$DL_{AADT}$	$DL_{truck}$	$DL_{AADT}$	$DL_{truck}$
1	0.50	0.50	N/A	N/A
2	0.40	0.45	0.80	0.90
3	0.30	0.40	0.40	0.50

### Urban Highway

Number of Lanes in each direction	Undivided		Divided	
	$DL_{AADT}$	$DL_{truck}$	$DL_{AADT}$	$DL_{truck}$
1	0.50	0.50	N/A	N/A
2	0.30	0.40	0.70	0.90
3	0.25	0.35	0.40	0.50
4	N/A	N/A	0.30	0.40

TMF: Traffic Multiplication Factor

### 9. Calculate equivalent number of polishing cycles N using Equation 10.

$$N = TMF \times 10^{\frac{1}{A + B \times c_{mix} + \frac{C}{c_{mix}}}} \quad \text{Equation 10}$$

Where: A = -0.452, B = -58.95, C =  $5.834 \times 10^{-6}$



**10. Calculation IFI as a function of equivalent number of polishing cycles using Equation 11.**

$$IFI(N) = a_{mix} + b_{mix} \times \exp(-c_{mix} \cdot N) \quad \text{Equation 11}$$

**11. Calculate SN as a function of vehicles using Equation 12.**

$$SN_{50}(N) = 4.81 + 140.32[IFI(N) - 0.045] \times e^{\frac{-20}{SP}} \quad \text{Equation 12}$$

$$S_p = 14.2 + 89.7MPD \quad \text{Equation 12(a)}$$

**12. Plot SN as a function N.**

**13. Input parameters for ranking a road section.**

Skid resistance service life before the road should be resurfaced, Skid resistance threshold values.

**14. Rank a road section based on the following skid number values.**

Example of a situation where user can define threshold values of skid number—what he/she thinks is acceptable (high), acceptable but requires frequent monitoring (medium), or not acceptable (low).

Aggregate Class	SN Threshold Value
High	$SN(50) \geq 30$
Medium	$21 \leq SN(50) < 30$
Low	$SN(50) < 21$

**15. Export input and output data files**

Input and output data are created in two separate Microsoft Excel files.

Example of a situation where user can define threshold values of skid number—what he/she thinks is acceptable (high), acceptable but requires frequent monitoring (medium), or not acceptable (low).

<b>Aggregate Class</b>	<b>SN Threshold Value</b>
High	$SN(50) \geq 30$
Medium	$21 \leq SN(50) < 30$
Low	$SN(50) < 21$